Selected Topics in

Advanced Experimental Physics

Markus Lippitz

November 20, 2025

Contents

Part I

Concept: Fourier Transformation

Chapter 1
Fourier transformation

Markus Lippitz
September 18, 2023

Overview

It is useful and helpful to have an intuitive approach to the Fourier transform. The bottom line is that in experimental physics one rarely needs to actually calculate a Fourier transform. Very often it is sufficient to know a few frequently occurring Fourier pairs and to combine them with simple rules. This is what I want to present here. A very nice and much more detailed presentation can be found in Butz, 2015. I will follow his notation here.

Before we get to Fourier pairs, however, we need to lay down some foundations.

Fourier series: a periodic function and its Fourier coefficients

We first consider everything here in one dimension in time or frequency space with the variables t and $\omega = 2\pi\nu$. Let the function $f(t)$ be periodic in time with period T, i.e.

$$f(t) = f(t + T) \quad . \tag{1.1}$$

Then this can be written as a Fourier series

$$f(t) = \sum_{k=-\infty}^{\infty} C_k \, e^{i\,\omega_k\,t} \quad \text{with} \quad \omega_k = \frac{2\pi\,k}{T} \tag{1.2}$$

and the Fourier coefficients

$$C_k = \frac{1}{T} \int_{-T/2}^{T/2} f(t) \, e^{-i\,\omega_k\,t} \, dt \quad . \tag{1.3}$$

Note the negative sign in the exponential function in contrast to the equation before. For reel-valued functions $f(t)$, 'opposite' C_k are conjugate-complex, so $C_k = C_{-k}^{\star}$. For $k < 0$ the frequencies ω_k are negative, but this is not a problem.[1] Thus, the zeroth coefficient C_0 is just the time average of the function $f(t)$.

[1] One could alternatively require $k \geq 0$ and apply a $\sin$ and $\cos$ series.

An arbitrary function and its Fourier transform

Now we remove the restriction to periodic functions $f(t)$ by letting the period T go to infinity. This turns the sum into an integral and the discrete ω_k become continuous. Thus

$$F(\omega) = \int_{-\infty}^{+\infty} f(t)\, e^{-i\omega t}\, dt \tag{1.4}$$

$$f(t) = \frac{1}{2\pi} \int_{-\infty}^{+\infty} F(\omega)\, e^{+i\omega t}\, d\omega \quad . \tag{1.5}$$

Here, the first equation is the forward transformation (minus sign in the exponent), and the second is the reverse transformation (plus sign in the exponent). The symmetry is broken by the 2π. But this is necessary if one wants to keep $F(\omega = 0)$ as mean[2]. Alternatively, we could formulate all this with ν instead of ω, but then we would have a 2π in many more places, though not before the integral.

[2] $F(0) = \int f(t)\, dt$ without $1/T$ in front of it is meant here by Butz as mean!

Sidenote: Delta Function

The delta function can be written as

$$\delta(x) = \lim_{a \to 0} f_a(x) \quad \text{with} \quad f_a(x) = \begin{cases} a & \text{if } |x| < \frac{1}{2a} \\ 0 & \text{other} \end{cases} \tag{1.6}$$

or as

$$\delta(x) = \frac{1}{2\pi} \int_{-\infty}^{+\infty} e^{+i x y}\, dy \quad . \tag{1.7}$$

An important property is that the delta function selects a value, i.e.

$$\int_{-\infty}^{+\infty} \delta(x)\, f(x)\, dx = f(0) \quad . \tag{1.8}$$

Important Fourier pairs

It is very often sufficient to know the following pairs of functions and their Fourier transforms. I write them here, following Butz, as pairs in t and ω (not $\nu = \omega/(2\pi)$). In the same way, one could have written pairs in x and k. The important question is whether a 2π appears in the exponential function of the plane wave or not. So

$$e^{i\omega t} \quad \text{and} \quad e^{ikx} \quad \text{, but} \quad e^{i2\pi\nu t} \quad . \tag{1.9}$$

Further, I follow here the convention made above about the asymmetric distribution of the 2π between forward and reverse transformations. If you distribute them differently, then of course the prefactors change. A good overview of many more Fourier pairs in various '2π' conventions can be found in the English Wikipedia under 'Fourier transform'. In their nomenclature, the Butz convention used here is 'non-unitary, angular frequency'.

constant and delta function $f(t) = a$ becomes $F(\omega) = a\, 2\pi\, \delta(\omega)$ and $f(t) = a\, \delta(t)$ becomes $F(\omega) = a$. This is again the asymmetric 2π.

rectangle and sinc   The rectangle function of width b becomes a sinc[3], the sinus cardinalis. So from

$$f(t) = \text{rect}_b(t) = \begin{cases} 1 & \text{for} \quad |t| < b/2 \\ 0 & \text{other} \end{cases} \tag{1.10}$$

we get

$$F(\omega) = b \,\frac{\sin \omega b/2}{\omega b/2} = b \,\text{sinc}(\omega b/2) \quad . \tag{1.11}$$

Gaussian   The Gaussian function is preserved under Fourier transform. Its width changes into the reciprocal value. So from a Gauss function of area one

$$f(t) = \frac{1}{\sigma\sqrt{2\pi}} \, e^{-\frac{1}{2}\left(\frac{t}{\sigma}\right)^2} \tag{1.12}$$

we get

$$F(\omega) = e^{-\frac{1}{2}(\sigma\,\omega)^2} \quad . \tag{1.13}$$

(two-sided) exponential decay and Lorentz curve   From a curve decaying exponentially at both positive and negative times

$$f(t) = e^{-|t|/\tau} \tag{1.14}$$

we obtain the Lorentz curve

$$F(\omega) = \frac{2\tau}{1 + \omega^2\,\tau^2} \quad . \tag{1.15}$$

one-sided exponential decay   As a side note, here the one-sided exponential decay

$$f(t) = \begin{cases} e^{-\lambda t} & \text{for} \quad t > 0 \\ 0 & \text{other} \end{cases} \quad . \tag{1.16}$$

It will become

$$F(\omega) = \frac{1}{\lambda + i\,\omega} \tag{1.17}$$

and it is therefore complex-valued. Its magnitude squared is again a Lorentz function

$$|F(\omega)|^2 = \frac{1}{\lambda^2 + \omega^2} \tag{1.18}$$

and the phase is $\phi = -\omega/\lambda$.

One-dimensional point lattice   An equidistant chain of points or delta functions remains an equidistant chain under Fourier transform. The distances take the reciprocal value. So from

$$f(t) = \sum_n \delta(t - \delta t\,n) \tag{1.19}$$

we get

$$F(\omega) = \frac{2\pi}{\delta t} \sum_n \delta\left(\omega - n\frac{2\pi}{\Delta t}\right) . \quad . \tag{1.20}$$

Three-dimensional cubic lattice   A three-dimensional primitive cubic lattice of side length a makes the transitions to a primitive cubic lattice of side length $2\pi/a$. A face-centered cubic lattice with lattice constant a of conventional unit cell is converted to a space-centered cubic lattice with lattice constant $4\pi/a$ and vice versa.

[3] sometimes $\text{sinc}(x) = \sin(\pi x)/(\pi x)$ is defined, especially when ν and not ω is used as conjugate variable.

Theorems and properties of the Fourier transform

In addition to the Fourier pairs, we need a few properties of the Fourier transform. In the following, let $f(t)$ and $F(\omega)$ be Fourier conjugates and likewise g and G.

linearity   The Fourier transform is linear

$$a\,f(t) + b\,g(t) \quad \leftrightarrow \quad a\,F(\omega) + b\,G(\omega) \quad . \tag{1.21}$$

shift   A shift in time implies a modulation in frequency and vice versa.

$$f(t - a) \quad \leftrightarrow \quad F(\omega)\,e^{-i\omega a} \tag{1.22}$$

$$f(t)\,e^{-i\omega_0 t} \quad \leftrightarrow \quad F(\omega + \omega_0) \quad . \tag{1.23}$$

scaling

$$f(a\,t) \quad \leftrightarrow \quad \frac{1}{|a|}\,F\left(\frac{\omega}{a}\right) \quad . \tag{1.24}$$

convolution and multiplication   Convolution is converted into a product, and vice versa

$$f(t) \otimes g(t) = \int f(\zeta)g(t - \zeta)d\zeta \quad \leftrightarrow \quad F(\omega)\,G(\omega) \tag{1.25}$$

and

$$f(t)\,g(t) \quad \leftrightarrow \quad \frac{1}{2\pi}\,F(\omega) \otimes G(\omega) \quad . \tag{1.26}$$

Parseval's Theorem   The total power is the same in both time and frequency domain

$$\int |f(t)|^2\,dt = \frac{1}{2\pi}\int |F(\omega)|^2\,d\omega \tag{1.27}$$

time derivatives

$$\frac{d\,f(t)}{dt} \quad \leftrightarrow \quad i\omega\,F(\omega) \quad . \tag{1.28}$$

Example: Diffraction at a double slit

As an example, we consider the Fourier transform of a double slit, which describes its diffraction pattern. The slits have a width b and a center distance d. Thus the slit is described by a convolution of the rectangular function with two delta functions at the distance d

$$f(x) = \text{rect}_b(x) \otimes (\delta(x - d/2) + \delta(x + d/2)) \quad . \tag{1.29}$$

The Fourier transform of the rectangular function is the sinc, that of the delta functions a constant. However, the shift in position causes a modulation in k-space. Thus, the sum of the two delta functions becomes

$$\mathcal{FT}\{\delta(x - d/2) + \delta(x + d/2)\} = e^{-ikd/2} + e^{+ikd/2} = 2\cos(kd/2) \quad . \tag{1.30}$$

The convolution with the rectangular function passes into a multiplication with the sinc. Together we get

$$\mathcal{FT}\{f(x)\} = b\frac{\sin(kb/2)}{kb/2}\, 2\cos(kd/2) = \frac{4}{k}\,\sin(kb/2)\,\cos(kd/2) \quad .$$

(1.31)

The intensity in direction k is then the squared magnitude of this.

Test yourself

1. *Temporal shift* Sketch the amplitude and phase of the FT of a temporal square pulse pulse centred on time zero! What changes if the pulse is shifted to positive times?

2. *Pulse sequence* You wonder what the Fourier transform (magnitude squared) of an infinite sequence of square pulses looks like and start searching for it on the internet. Your fellow student replies that you can "see" it immediately. Sketch the Fourier transform! Explain why you could derive it directly or why you should "see" it!

3. *Light pulse* Think of a "light pulse" as a mathematical construction of an infinitely long cosine oscillation corresponding to the frequency of light. The "pulse" is obtained by multiplying the wave by a time-limited Gaussian pulse envelope (e.g. half-width of 10 light oscillations). Sketch the construction of the Fourier transform in the spectral domain.

Two-dimensional Fourier transformation

We can extend the definition of the Fourier transform to two and more dimensions. The conjugated variables are (x, y) and (k_x, k_y) instead of t and ω. The wave vector $k_i = 2\pi/\lambda_i$ contains the factor 2π as in the angular frequency ω. We define

$$F(k_x, k_y) = \iint_{-\infty}^{+\infty} f(x, y)\, e^{-i(k_x\, x + k_y\, y)}\, dx\, dy$$

(1.32)

$$f(x, y) = \frac{1}{(2\pi)^2} \iint_{-\infty}^{+\infty} F(k_x, k_y)\, e^{+i(k_x\, x + k_y\, y)}\, dk_x\, dk_y \quad .$$

(1.33)

When we can separate the function $f(x, y)$ into a product of one-dimensional functions, then the Fourier transform is simply the product of the individual Fourier transforms

$$f(x, y) = g(x) \cdot h(y) \quad \leftrightarrow \quad F(k_x, k_y) = G(k_x) \cdot H(k_y) \quad .$$

(1.34)

A rectangle of size $a \times b$ is transformed into a product of sinc functions

$$(x, y) = \text{rect}_a(x) \cdot \text{rect}_b(y)$$

(1.35)

$$\leftrightarrow \quad F(k_x, k_y) = ab\, \text{sinc}(k_x a/2)\, \text{sinc}(k_y b/2) \quad .$$

(1.36)

A special case of this is the rotational symmetric two-dimensional Gaussian function

$$f(x, y) = \frac{1}{2\pi\sigma^2}\, e^{-\frac{x^2+y^2}{2\sigma^2}} \quad \leftrightarrow \quad F(k_x, k_y) = e^{-\frac{\sigma^2}{2}\left(k_x^2+k_y^2\right)} \quad .$$

(1.37)

One important function can not be separated into a product of one-dimensional functions: a disc of radius a

$$f(x, y) = \begin{cases} 1 & \text{for} \quad x^2 + y^2 < a \\ 0 & \text{other} \end{cases} \tag{1.38}$$

is transformed into

$$F(k_x, k_y) = a \frac{J_1(\pi a \rho)}{\rho} \quad \text{width} \quad \rho = \sqrt{k_x^2 + k_y^2} \tag{1.39}$$

and the (cylindrical) Bessel function of the first kind $J_1(x)$

$$J_1(x) = \frac{1}{\pi} \int_0^\pi \cos(\tau - x \sin \tau) \, d\tau \quad , \tag{1.40}$$

which is the cylindrical analogue of a sinc function.

Discrete FT: a periodic sequence of values

In particular, if one collects and evaluates measurement data with a computer, then one does not know the measured function $f(t)$ on a continuous axis t, but only at discrete times $t_k = k \, \delta t$, nor does one know the function from $t = -\infty$ to $t = +\infty$. So we have only a finite sequence of numbers f_k as a starting point. Because we do not know the sequence of numbers outside the measured interval we make the assumption that it is periodic. With N measured values the period is $T = N\Delta t$. For simplicity, we also define $f_k = f_{k+N}$ and thus $f_{-k} = f_{N-k}$ with $k = 0, 1, \ldots, N - 1$. Thus the Fourier transform becomes[4]

$$F_j = \frac{1}{N} \sum_{k=0}^{N-1} f_k \, e^{-k \, j \, 2\pi i / N} \tag{1.41}$$

and its inverse transform

$$f_k = \sum_{j=0}^{N-1} F_j \, e^{+k \, j \, 2\pi i / N} \quad . \tag{1.42}$$

The definition is again such that F_0 corresponds to the mean. Because of $f_{-k} = f_{N-k}$, the positive frequencies are in the first half of F_j as the frequency increases. After that come the negative frequencies, starting at the 'most negative' frequency and increasing to the last frequency before zero. So the maximum frequency that can be represented is the Nyquist (angular) frequency

$$\Omega_{\text{Nyquist}} = \frac{\pi}{\delta t} \quad . \tag{1.43}$$

This frequency is such that we take two samples per period of the oscillation. Faster oscillations or fewer samples per period cannot be represented. Even with f_{Nyquist} the imaginary part is always zero, because we always sample the sine at the zero crossing.

FFTW

The most used package for numerical Fourier transform is probably FFTW[5].

You have to pay attention to the details of the definition. In particular, the prefactors may differ between different packages. In FFTW, the prefactor $1/N$ changes from the forward to the backward transformation, i.e.

$$F_j = \sum_{k=0}^{N-1} f_k\, e^{-k\,j\,2\pi i/N} \tag{1.44}$$

and the inverse Fourier transform

$$f_k = \frac{1}{N} \sum_{j=0}^{N-1} F_j\, e^{+k\,j\,2\pi i/N} \quad . \tag{1.45}$$

In equations, I (and Butz) use mathematical indices (starting from zero). Some programming languages count from one (e.g., Julia).

One helpful thing of FFTW is that is supplies also a frequency axis. As mentioned above, first come the positive frequencies, starting from zero to the maximum, then the most negative frequency, again rising until just before zero. Depending wether the number of samples N is even or odd, it is a little bit of a hassle to calculate the respective frequencies, but FFTW does this for us:

```
fftfreq(5) # gives [0.0, 0.2, 0.4, -0.4, -0.2]
fftfreq(6) # gives [0.0, 0.166, 0.333, -0.5, -0.333, -0.1.66]
```

Test yourself

4. Try yourself the FFT in a language of your choice. The FFT of, say, $[1111]$ should give something like $[4000]$.

5. The inverse FFT is IFFT. Check that it inverts and test how the pre-factors are distributed.

Wrapping & fftshift

Now lets look at the Fourier transform of a cosine. We evaluate the cosine at 8 points:

$$x_n = n\frac{2\pi}{8} \quad \text{with} \quad n = 0\ldots 7 \tag{1.46}$$

$$f_n = \cos x_n \tag{1.47}$$

$$F = \mathcal{FT}(f) \quad . \tag{1.48}$$

We find that only F_1 and F_7 are different from zero and have the same, real value. Two values must be different from zero because

$$\cos(x) = \frac{1}{2}\left(e^{ix} + e^{-ix}\right) \quad . \tag{1.49}$$

In general, for real values f_n we have

$$F_{N-j} = F_j^{\star} \quad . \tag{1.50}$$

The position of these two non-zero values is a consequence of the definition of F_k: first come all positive frequencies and then all negative. For a nicer representation it is often better if the frequency zero is not the first element but in the middle between the positive and negative frequencies. frequencies. This we get by `fftshift` or backwards by `ifftshift`.

Test yourself

6. Convince yourself that you understand why it is element 1 and 7 that differs from zero in the example above.

7. Replace the cosine with a sine in this example and explain the result.

Sampling theorem

We need at least two samples per period to describe a function by its Fourier coefficients. The frequencies must be below the Nyquist frequency f_{Nyquist}

$$f_{\text{Nyquist}} = \frac{1}{2\Delta t} \quad . \tag{1.51}$$

The *sampling theorem* states that this is then also sufficient, i.e., we do not lose any detail by sampling. Let $f(t)$ be a bandwidth-limited function, i.e. $F(\omega)$ is different from zero only in the interval $|\omega| \leq \Omega_{\text{Nyquist}}$. Then the sampling theorem[6] applies and gives

$$f(t) \stackrel{!}{=} \sum_{k=-\infty}^{\infty} f(k\Delta t)\, \text{sinc}\left(\Omega_{\text{Nyquist}} \cdot [t - k\Delta t]\right) \quad . \tag{1.52}$$

So it is enough to sample f all Δt. At the times in between, f is completely described by the (infinitely long) sum of the neighbouring values times the sinc.

In measurement technology, therefore, all we need to do is ensure, for example by means of an electrical filter, that all the frequencies of a signal are below Ω_{Nyquist}, and then our digital acquisition of the signal will be is identical to the signal itself. However, if we sample too infrequently, or if there are higher frequencies present, then these too high frequency components will be reflected at the Nyquist frequency and end up at seemingly lower frequencies. This 'aliasing' distorts the signal.

Zero padding

We began with a repeating pattern of numerical values and their Fourier transform. We always picked the length of the sequence in the examples to match an integer multiple of the period. But of course, this isn't feasible in reality. We lack accurate knowledge of the signal's duration. Or sometimes, multiple signals with varying frequencies are important.

The problem is then a truncation error, which leads to artefacts in the Fourier transform. Fig. 1.1 shows an example. 12 data points of a cosine with period 8 are sampled. The FFT assumes periodic continuation (thick) which is not the 'true' signal (thin). In this case, the FFT of the data is far from a peak at the original frequencies. The real part is even spectrally constant (see below Fig. 1.2)

The way out is *zero-padding*. Let our actual measured signal sequence $f(t)$, which we know in the interval $[-T, T]$. Now we pretend that we measured instead
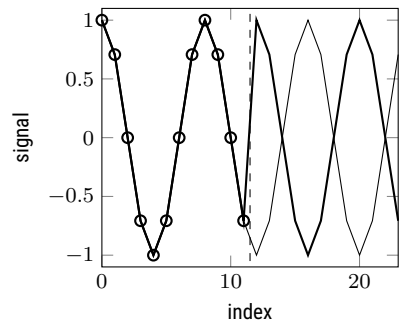
$$g(t) = f(t) \cdot w(t) \tag{1.53}$$

Figure 1.1: Clipping a cosine after 1.5 periods

with the window function $w(t)$

$$w(t) = 1 \quad \text{for} \quad -T < t < T \quad \text{other} = 0 \quad . \tag{1.54}$$

Thus we can 'measure' $g(t)$ over arbitrarily long times, because it is is quasi always zero. But the Fourier transform is

$$G(\omega) = F(\omega) \otimes W(\omega) \tag{1.55}$$

with

$$W(\omega) = 2T \frac{\sin \omega T}{\omega T} = 2T\, \text{sinc}(\omega T). \quad . \tag{1.56}$$

So we extend our data set on both sides with zeros. The effect is that we convolve the actual Fourier transform of our data set with a sinc whose characteristic width is determined by the actual measurement duration. The frequency resolution does not increase. Rather, a kind of interpolation in Fourier space occurs, which just eliminates the artefacts of the truncation error.

We consider the same data set as above, only we 'extend' it to 10 times the length. This means that the clipping error has less influence and the peak is always at 1 Hz in frequency space. But this does not give more resolution, of course. Peaks that are close to each other cannot be separated by zero-padding, only the position of a peak can be be determined better .

Windowing

The oscillations in the spectrum in the last example are still artefacts. Actually, one would expect two delta functions at ± 1Hz. They are a consequence of the rectangular window $w(t)$, which leads to the sinc in frequency space. The square-wave window is natural in the sense that we always start and stop measuring. Other window functions[7], however, may be better. They differ the width of the peak and the steepness of the slopes. Unfortunately one must trade one against the other. Interesting parameters are the width of the central peak in frequency space, measured as a -3dB bandwidth, as well as the sideband suppression in [8] dB or its drop in dB/octave.

Typical window functions are (with $|x| = |t/T| < 1/2$)

$$\text{cosine} = \cos \pi x \tag{1.57}$$

$$\text{triangle} = 1 - 2|x| \tag{1.58}$$

$$\text{Hanning} = \cos^2 \pi x \tag{1.59}$$

$$\text{Hamming} = a + (1 - a)\cos^2 \pi x \tag{1.60}$$

$$\text{Gauss} = \exp\left(-\frac{1}{2}\frac{x^2}{\sigma^2}\right) \tag{1.61}$$

$$\text{Kaiser-Bessel} = \frac{I_0(\pi\alpha\sqrt{1 - 4x^2})}{I_0(\pi\alpha)} \tag{1.62}$$

with the modified Bessel function I_0.

With a window, the measured values are reduced, but the Fourier transform is smoother, because the transition to the zero padding becomes smoother. This makes it possible to recognize in the example the peaks at ± 1Hz even with very few sampled points.
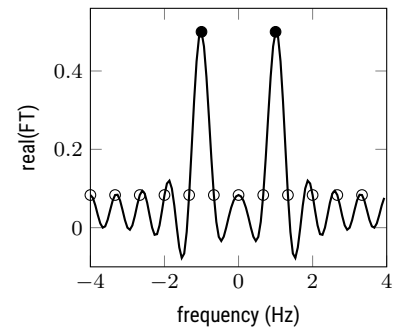

Figure 1.2: Zeropadding (line) approaches better the real spectrum (filled symbols) compared to the clipped FT (open symbols).

[7] https://en.wikipedia.org/wiki/Window_function

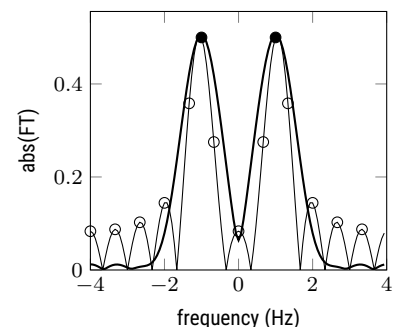[8] dB = decibel = $10 \log_1 0x$

Figure 1.3: Zeropadding after windowing (thick) removes the fringes of the un-windowed data (thin) and approaches the true spectrum (solid symbols).

We consider as example[9] a sum of 6 cosine functions with partly very different amplitudes A_l and frequencies f_l:

$$f(t) = \cos \omega t + 10^{-2} \cos 1.15 \omega t + 10^{-3} \cos 1.25 \omega t \qquad \text{(1.63)}$$
$$+ 10^{-3} \cos 2 \omega t + 10^{-4} \cos 2.75 \omega t + 10^{-5} \cos 3 \omega t$$

We sample 256 data points at intervals of $\Delta t = 1/8$, i.e. only $8/3 \approx 3$ data points per oscillation of the highest occurring frequency, which is 5 orders of magnitude weaker than the lowest frequency. Nevertheless, this peak can be found with a suitable window and zero-padding.

References

Butz, Tilman (2015). *Fourier Transformation for Pedestrians*. 2. ed. Springer. ⬀.

Horowitz, Paul and Winfield Hill (2015). *The art of electronics*. Third edition. New York, NY: Cambridge University Press.

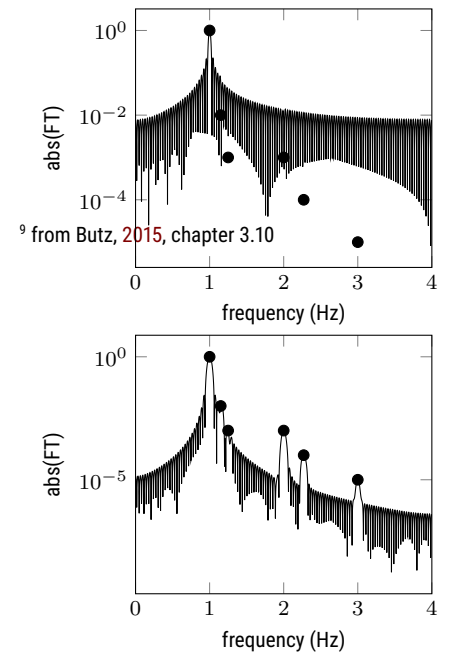
[9] from Butz, 2015, chapter 3.10

Figure 1.4: Without windowing (top), only the main signal component is recovered. A Hanning window (bottom) allows to find even signals 10^{-5} below the main component.

Chapter 2
X-Ray Scattering

Markus Lippitz
October 27, 2023

Overview

A classic application of Fourier transforms is X-ray scattering to determine a crystal structure, or similar experiments with electrons or neutrons. We will review the differences between the Bragg and Laue formalisms and then discuss the influence of a basis on the diffraction pattern.
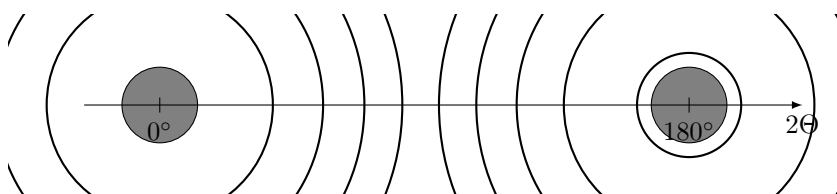
How to measure this?

Figure 2.1: Sketch of the diffraction pattern in a Debye-Scherrer powder diffractometer

.

In a Debye-Scherrer powder diffractometer, a monochromatic X-ray beam passes through a crystalline powder. The radiation that is diffracted is detected by a film that is placed in a ring around the sample. This is why there are notches in the film at $0°$ and $180°$ to allow the X-ray beam to pass through. Concentric elliptical lines are found, each of which has a constant angle of deflection called 2θ.

This method is simpler than the historically older Laue method, which uses a single homogeneous crystal as the diffractive element. The powder contains all the orientations of the crystal with respect to the incident beam. As we will see below with the Ewald sphere, it is rather unlikely that the combination of wavelength, incident direction and grating will lead to constructive interference. In the Laue method, therefore, the crystal must be appropriately oriented and/or broad spectrum X-rays must be used.

The formalism presented in this chapter is not restricted to the diffraction of X-rays. You can also diffract visible light, electrons or neutrons in a completely analogous way. The relationship between energy per particle and
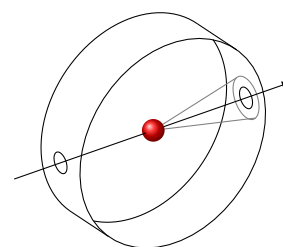
Figure 2.2: Sketch of a powder diffractometer according to Debye-Scherrer

.

wavelength is different. Short wavelengths can be obtained with massive particles at lower energies. The choice of beam also determines whether electrons (X-rays) or nuclei (neutrons) are studied.

Fundamental idea of scattering theory

How does a wave interact with a given arrangement of objects? This question is answered by the scattering theory. In this section, we remain general, specifying neither the type of wave (light, electrons, neutrons), nor the type of objects (slits, electrons, nuclei). The nomenclature follows Hunklinger, 2014.

A plane, here for simplicity scalar wave $A(t)$ thus

$$A(t) = A_0 \, e^{-i \, (\omega_0 t - \mathbf{k}_0 \cdot \mathbf{r})} \tag{2.1}$$

is described by the amplitude A_0, angular frequency ω_0 and wave vector $\mathbf{k}_0$. This wave falls on the point-like scattering center at the origin of the coordinate system and generates an outgoing spherical wave of the form

$$A_{sc}(t) = \frac{\tilde{A}}{R} \, e^{-i \, (\omega_0 t - k_0 R)} \tag{2.2}$$

where the spherical wave depends only on the distance $R = |\mathbf{R}|$ to the center of the sphere and the magnitude $k_0 = |\mathbf{k}_0|$ of the wave vector. The amplitude $\tilde{A}$ depends on the efficiency of the process.

An extended sample thus consists of many scattering centers over which one sums the amplitudes. However, one must consider the phase difference of the individual waves when integrating over many scattering centers. For two scattering centers, one at the origin, the other at $\mathbf{r}$, one finds by geometrical considerations the phase difference

$$\delta\phi = (\mathbf{k} - \mathbf{k}_0) \cdot \mathbf{r} \quad , \tag{2.3}$$

if $\mathbf{k}$ is the wave vector of the outgoing scattered plane wave.[1] So this gives

$$A_S(t) = \frac{\tilde{A}}{R} \, e^{-i \, (\omega_0 t - k_0 R)} \sum_j e^{-i \, (\mathbf{k} - \mathbf{k}_0) \cdot \mathbf{r}_j} \quad . \tag{2.4}$$

Here we made the assumption that the size of the sample, i.e., the differences between the $\mathbf{r}_j$ is small compared to the distance R to the screen. Thus, we are interested in the scattered wave only at a distance so large that, regardless of the location of the scattering center, all partial waves with wave vector $\mathbf{k}$ arrive at the same location. In Fourier optics we called this Fraunhofer approximation. Also, as virtually always in scattering theory, we assume that each wave is scattered only once. This is the Born approximation.

Now we go from single scattering centers at positions $\mathbf{r}_j$ to a *scattering density* $\rho(\mathbf{r})$, i.e., to the number of scattering centers in a volume element dV. Thus the sum becomes an integral and we obtain for the scattered wave

$$A_S(t) = \frac{\tilde{A}}{R} \, e^{-i \, (\omega_0 t - k_0 R)} \int_{V_{\text{sample}}} \rho(\mathbf{r}) \, e^{-i \, (\mathbf{k} - \mathbf{k}_0) \cdot \mathbf{r}} \, dV = \frac{\tilde{A}}{R} \, e^{-i \, (\omega_0 t - k_0 R)} \, \mathcal{A}(\mathbf{K}) \tag{2.5}$$
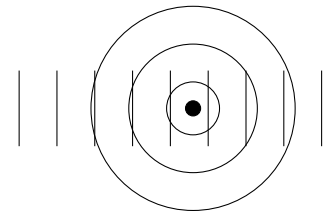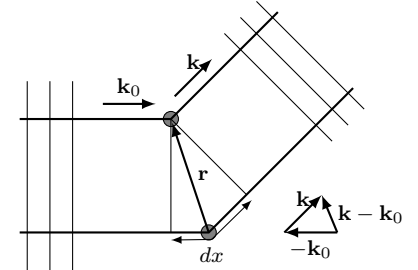

Figure 2.3: Scattering at a point

Figure 2.4: Sketch to path difference $dx = \delta\phi/|\mathbf{k}| = (\mathbf{k} - \mathbf{k}_0) \cdot \mathbf{r}/|\mathbf{k}|$ at two scattering centers.

[1] The spherical wave from above can be written as an integral over plane waves in all spatial directions

with the *scattering amplitude* as Fourier-transformed scattering density

$$\mathcal{A}(\mathbf{K}) = \int_{V_{\text{sample}}} \rho(\mathbf{r})\, e^{-i\,(\mathbf{k}-\mathbf{k}_0)\cdot\mathbf{r}}\, dV = \mathcal{FT}\{\rho(\mathbf{r})\} \qquad (2.6)$$

and the *scattering vector* $\mathbf{K} = \mathbf{k} - \mathbf{k}_0$. Thus, in scattering experiments, one measures the Fourier transform of the scattering density. This is valid for diffraction at double slit as well as for diffraction of X-rays at electron distribution in a crystal.

The reciprocal lattice

If the electron density in the crystal already gives the diffraction pattern as scattering amplitude via Fourier transform, then one can also look at the Fourier transform of, for example, the electron density right away.

The scattering density $\rho(\mathbf{r})$, like all properties of a crystal, is lattice-periodic, i.e.

$$\rho(\mathbf{r}) = \rho(\mathbf{r} + \mathbf{T}) = \rho(\mathbf{r} + n_1\mathbf{a}_1 + n_2\mathbf{a}_2 + n_3\mathbf{a}_3) \qquad (2.7)$$

with n_i integers and $\mathbf{a}_i$ primitive unit vectors. Thus $\rho(\mathbf{r})$ is representable as a Fourier series

$$\rho(\mathbf{r}) = \sum_{h,k,l} \rho_{hkl}\, e^{i\,\mathbf{G}_{hkl}\cdot\mathbf{r}} \qquad (2.8)$$

with h, k, l integers, the Fourier coefficient as integral over the primitive unit cell PUC

$$\rho_{hkl} = \frac{1}{V_{\text{PUC}}} \int_{\text{PUC}} \rho(\mathbf{r})\, e^{-i\,\mathbf{G}_{hkl}\cdot\mathbf{r}}\, dV \qquad (2.9)$$

and the *reciprocal lattice vectors*

$$\mathbf{G}_{hkl} = h\mathbf{b}_1 + k\mathbf{b}_2 + l\mathbf{b}_3 \quad . \qquad (2.10)$$

The $\mathbf{b}_i$ are the primitive unit vectors of the reciprocal lattice. $\mathbf{G}_{hkl}$ thus describes the set of all lattice points. Each of these lattice points is associated with exactly one Fourier coefficient ρ_{hkl} of the scattering density.

Bragg Theory of Diffraction

The scattering amplitude $\mathcal{A}(\mathbf{K})$, i.e. the amplitude of the scattered wave in the direction $\mathbf{K} = \mathbf{k} - \mathbf{k}_0$, is simply the Fourier transform of the scattering density $\rho(\mathbf{r})$ in real space. Bragg theory is another way of finding the conditions for constructive interference and hence peaks in the scattering image. Below we will merge the different ways.

In which direction $\mathbf{K} = \mathbf{k} - \mathbf{k}_0$ do strong peaks occur in scattering experiments with X-rays, electrons, or neutrons? Bragg theory assumes that atoms form planes at distance d. The (matter) waves are reflected at these planes. If the phase difference is suitable, then there is constructive interference and thus a peak.

From geometrical considerations one finds that constructive interference occurs exactly when the *Bragg condition* is satisfied
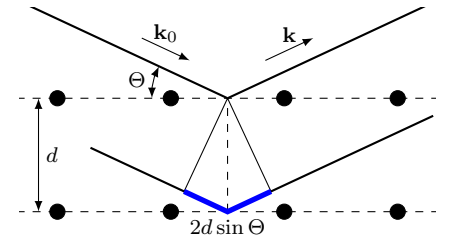
$$n\,\lambda = 2\,d\,\sin\Theta \quad . \qquad (2.11)$$

Figure 2.5: Phase difference in reflection at two planes
.

Here n denotes the diffraction order, λ the wavelength of the (matter) wave, d the distance of the planes and Θ the angle between incident ray and lattice plane. Of course, since specular reflection is involved, this is also the angle of the outgoing ray with the plane.[2] The difference $\mathbf{K}$ of the wave vectors is perpendicular to the reflecting lattice planes. For the magnitude we find

$$|\mathbf{K}| = |\mathbf{k} - \mathbf{k}_0| = 2|\mathbf{k}_0| \sin\theta \quad . \tag{2.12}$$

There are, of course, many ways to find planes in a crystal, and thus many directions that satisfy the Bragg condition, i.e., many scattering peaks.

Laue theory of diffraction

The Bragg condition only predicts whether there is a peak in a certain direction, but not its intensity. The Bragg theory uses only the lattice periodicity of the scattering density $\rho(\mathbf{r})$, not its exact form. Both changes with the Laue theory[3].

The intensity of a scattering peak is proportional to the square of the scattering amplitude. With Eq. 2.6 we get

$$I(\mathbf{K}) \propto |\mathcal{A}(\mathbf{K})|^2 = \left| \int_{V_{\text{sample}}} \rho(\mathbf{r})\, e^{-i\,\mathbf{K}\cdot\mathbf{r}}\, dV \right|^2 \quad . \tag{2.13}$$

We repeat again the steps from the beginning of the chapter and write the scattering density as a Fourier sum with the coefficients ρ_{hkl}

$$\rho(\mathbf{r}) = \sum_{h,k,l} \rho_{hkl}\, e^{i\,\mathbf{G}_{hkl}\cdot\mathbf{r}} \tag{2.14}$$

with h, k, l integers, the Fourier coefficients ρ_{hkl} and the reciprocal lattice vectors

$$\mathbf{G}_{hkl} = h\mathbf{b}_1 + k\mathbf{b}_2 + l\mathbf{b}_3 \quad . \tag{2.15}$$

In the following, I sometimes omit the indices at $\mathbf{G}$. Thus we obtain for the scattering intensity

$$I(\mathbf{K}) \propto |\mathcal{A}(\mathbf{K})|^2 = \left| \sum_{h,k,l} \rho_{hkl} \int_{V_{\text{sample}}} e^{i\,(\mathbf{G}-\mathbf{K})\cdot\mathbf{r}}\, dV \right|^2 \quad . \tag{2.16}$$

The integrand oscillates rapidly with $\mathbf{r}$ and averages away unless $\mathbf{G} = \mathbf{K}$. In this case, the integral just gives the sample volume V_{sample}.

Thus we have obtained the Laue scattering condition

$$\mathbf{G} = \mathbf{K} \quad . \tag{2.17}$$

The difference of the wave vectors must correspond to a lattice vector. Or the other way around: during diffraction at the lattice, a lattice vector is added to the incident wave vector. The scattering intensity in this case is

$$I(\mathbf{K} = \mathbf{G}_{hkl}) \propto |\mathcal{A}(\mathbf{K} = \mathbf{G}_{hkl})|^2 = |\rho_{hkl}|^2\, V_{\text{sample}}^2 \quad . \tag{2.18}$$

Thus, a single Fourier coefficient determines the intensity of the peak in the (hkl) direction.

A side note on the shape of the peaks in reciprocal space. The position is determined by $\mathbf{G}$. The width is finite, i.e. not delta-shaped, because the sample is finite in size. This is analogous to the width of the diffraction peaks at an optical line grating, which also drops as $1/N_\text{lines}$. Thus, in three dimensions, the width of the peak is $1/V_\text{sample}$. Since the height of the peak is proportional to V_sample^2, the integral over a peak is proportional to V_sample. This is very convenient, since the intensity of the effect should go linearly with the amount of matter, and not quadratically as Eq. 2.18 suggests.

Equivalence of the two conditions

We start from the Laue condition $\mathbf{G} = \mathbf{K}$ and derive the Bragg condition from it:

$$|\mathbf{K}| = |\mathbf{k} - \mathbf{k}_0| = 2|\mathbf{k}_0| \sin \Theta = \frac{4\pi}{\lambda} \sin \Theta = |\mathbf{G}| = n |\mathbf{G}| \quad . \tag{2.19}$$

The first steps are Eq. 2.12 and pure geometric considerations for reflection, so not yet the Bragg condition. In the last step, we exploited the fact that any integer multiple of a lattice vector is also a lattice vector again.[4]

Each lattice vector describes a plane wave and thus a set of planes at a distance of

$$d = \frac{2\pi}{|\mathbf{G}|} \quad . \tag{2.20}$$

All together this gives the Bragg condition

$$\frac{4\pi}{\lambda} \sin \Theta = n \frac{2\pi}{d} \tag{2.21}$$

$$2d \sin \Theta = n\lambda \quad . \tag{2.22}$$

Ewald sphere

Only a few orientations of a crystal relative to the incident beam produce any reflections at all. The construction of the Ewald sphere makes it possible to identify these orientations and the reflections that are then visible:

1. draw the lattice as a point lattice in reciprocal space

2. to draw the incident beam with the wave vector $\mathbf{k}_0$ so that the arrowhead ends at the lattice point (000). This defines the orientation of the beam relative to the crystal.

3. draw a circle / sphere around the start of $\mathbf{k}_0$ with radius $|\mathbf{k}_0|$. This gives all points that satisfy $|\mathbf{k}| = |\mathbf{k}_0|$.

4. All points of the reciprocal lattice that lie on the circle / sphere satisfy the scattering condition $\mathbf{G} = \mathbf{K}$.

In a finite crystal, the lattice points are not mathematical points, but extended by the Fourier uncertainty between real space and reciprocal space. Similarly, no (matter) wave is exactly delta-shaped in frequency space, because the Fourier uncertainty between time and frequency also comes into play. So for physical systems there exists points that lie on the circle.
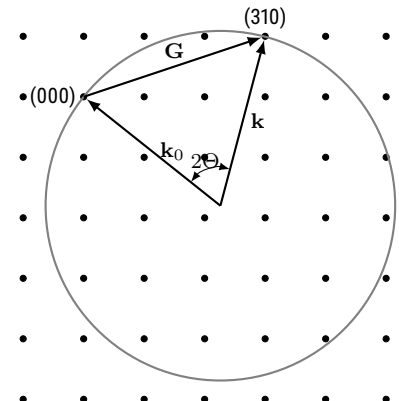
[4] $\mathbf{G}$ is, after all, fully named $\mathbf{G}_{hkl}$, i.e., a set of vectors

Figure 2.6: Construction of the Ewald sphere

But of course there are many Ewald spheres where only the point (000) lies on the sphere. So Laue diffraction does not always occur, or the crystal has to be oriented more precisely. The use of broadband radiation, e.g. Bremsstrahlung, makes this easier, but loses the possibility to measure the lattice constant.

Structure factor

So far we have considered only the mathematical lattice and its diffraction pattern. Now we also consider the basis, so especially if it contains more than one atom. The short version is: The lattice determines in which direction reflections can occur. The basis determines the intensity of these reflections, which in particular can be zero. This is due to destructive interference between diffracting atoms in one sublattice and those in the other.

At the same time the 'reciprocal' in the reciprocal space becomes clear here also once more. The mathematical lattice is 'larger' in real space in the sense that it is described by integer factors (i.e. ≥ 1) in front of the primitive unit vectors. The basis is described by factors between zero and one. In reciprocal space, everything goes with the reciprocal. The mathematical lattice is then 'smaller' than the Fourier transform of the basis. In units of the primitive reciprocal vector of the lattice, the basis is now responsible for effects not between zero and one, but for those at integers ≥ 1, i.e. the modulation of the amplitude of the diffraction peaks.

We start from Eq. 2.6 and insert the definition of the Fourier components Eq. 2.9. Thus we obtain

$$\mathcal{A}(\mathbf{K} = \mathbf{G}_{hkl}) = \rho_{hkl} V_{\mathsf{sample}} = N_{\mathsf{PUC}} \int_{\mathsf{PUC}} \rho(\mathbf{r})\, e^{-i\,\mathbf{G}_{hkl}\cdot\mathbf{r}}\, dV \qquad (2.23)$$

with the number of primitive unit cells $N_{\mathsf{PUC}} = V_{\mathsf{sample}}/V_{\mathsf{PUC}}$. We now divide the integral over the primitive unit cell into a sum over the atoms of the unit cell and an integral over the direct environment of the atoms. In the end, we integrate over the whole unit cell again. The old spatial coordinate $\mathbf{r} = \mathbf{r}' + \mathbf{r}_\alpha$ we write as the sum of the position of the atom $\mathbf{r}_\alpha$ and the local coordinate $\mathbf{r}'$ in its vicinity. Thus we obtain

$$\mathcal{A}(\mathbf{K} = \mathbf{G}_{hkl}) = N_{\mathsf{PUC}} \sum_{\alpha} e^{-i\,\mathbf{G}_{hkl}\cdot\mathbf{r}_\alpha} \int_{V_\alpha} \rho_\alpha(\mathbf{r}')\, e^{-i\,\mathbf{G}_{hkl}\cdot\mathbf{r}'}\, dV' \quad .$$
$$(2.24)$$

The integral over the scattering density in the vicinity of the atom α is a Fourier transform and atom-specific. Therefore one defines an *atomic scattering factor* (or also *atomic form factor*) $f_\alpha(\mathbf{G})$ as a Fourier transform of the atomic scattering density

$$f_\alpha(\mathbf{G}) = \mathcal{FT}(\rho_\alpha(\mathbf{r})) \qquad (2.25)$$

and receives

$$\mathcal{A}(\mathbf{K} = \mathbf{G}_{hkl}) = N_{\mathsf{PUC}} \sum_{\alpha} f_\alpha(\mathbf{G}_{hkl})\, e^{-i\,\mathbf{G}_{hkl}\cdot\mathbf{r}_\alpha} \quad . \qquad (2.26)$$

The coordinates $\mathbf{r}_\alpha$ of the atomic positions depend only on the crystal structure, i.e., the Bravais lattice. We write the position in the primitive unit

vectors $\mathbf{a}_i$ as

$$\mathbf{r}_\alpha = u_\alpha\,\mathbf{a}_1 + v_\alpha\,\mathbf{a}_2 + w_\alpha\,\mathbf{a}_3 \tag{2.27}$$

with $0 \le u, v, w \le 1$. Together with the definition of $\mathbf{G}$ we then get

$$\mathcal{A}(\mathbf{K} = \mathbf{G}_{hkl}) = N_{\mathsf{PUC}} \sum_\alpha f_\alpha(\mathbf{G}_{hkl})\,e^{-2\pi\,i\,(hu_\alpha + kv_\alpha + lw_\alpha)} \tag{2.28}$$

$$= N_{\mathsf{PUC}}\,\mathcal{S}_{hkl} = \rho_{hkl}\,V_{\mathsf{sample}} \tag{2.29}$$

with the *structure factor* $\mathcal{S}_{hkl}$

$$\mathcal{S}_{hkl} = \rho_{hkl}\,V_{\mathsf{PUC}} = \sum_\alpha f_\alpha(\mathbf{G}_{hkl})\,e^{-2\pi\,i\,(hu_\alpha + kv_\alpha + lw_\alpha)} \quad. \tag{2.30}$$

Example: CsCl

Caesium chloride (CsCl) forms a cubic-primitive lattice with a diatomic basis, for example with the Cs atom at the origin and the Cl atom at the center of the space diagonal. Thus the structure factor is

$$\mathcal{S}_{hkl} = f_{\mathsf{Cs}}\,e^{-2\pi\,i\,\mathbf{G}\cdot\mathbf{0}} + f_{\mathsf{Cl}}\,e^{-2\pi\,i\,\frac{1}{2}(h+k+l)} \quad. \tag{2.31}$$

The first exponential function is always 1, the second is $+1$ if the sum $h + k + l$ is even, and -1 otherwise. This results in

$$\mathcal{S}_{hkl} = \begin{cases} f_{\mathsf{Cs}} + f_{\mathsf{Cl}} & \text{if } h + k + l \text{ even} \\ f_{\mathsf{Cs}} - f_{\mathsf{Cl}} & \text{if } h + k + l \text{ odd} \end{cases} \quad. \tag{2.32}$$

In X-ray scattering $f_{\mathsf{Cs}} \approx f_{\mathsf{Cl}}$, so only every second reflection can be seen. In neutron scattering, on the other hand, the atomic structure factors are clearly different and all peaks can be seen.

Example: bcc monatomic and sc diatomic

A cubic body-centred lattice can be seen as a cubic primitive lattice with a diatomic basis. Both describe the same position of the atoms in space. However, they are different mathematical lattices and therefore different $\mathbf{G}_{hkl}$. This apparently results in different peaks in the diffraction pattern, which of course should not be the case.

The resolution is again found in the structure factor. The basis needed to turn a cubic primitive into a cubic body-centred lattice is again half the space diagonal, as in the last section. However, unlike in the last section, both positions are now occupied by the same atoms. So all the peaks at odd $h+k+l$ disappear. These are just the ones that make the difference between $\mathbf{G}_{bcc}$ and $\mathbf{G}_{sc}$. There is a similar condition for the face-centred cubic lattice.

Evaluation of powder diffractometry

The experiment gives the position of the peaks as a function of the double scattering angle 2Θ with known wavelength λ of the radiation. From this one would like to determine the possible values of the length of the lattice
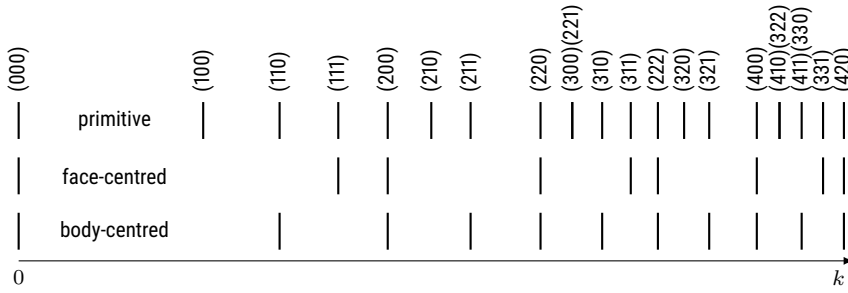
Figure 2.7: If peaks are indexed according to the conventional unit cell, then some are not visible in the centred lattices.

vector $|\mathbf{G}|$ and thus make a statement about the Bravais lattice, the basis and the lattice constant. In general this is not trivial. In simple cases, like the example at the beginning of the chapter, one can proceed as follows:

We consider the reciprocal distance of the lattice planes

$$\frac{1}{d} = \frac{|\mathbf{G}|}{2\pi} = \frac{2\sin\Theta}{\lambda} \quad . \tag{2.33}$$

In cubic lattices this is

$$\sqrt{h^2 + k^2 + l^2} = \frac{2a\,\sin\Theta}{\lambda} \tag{2.34}$$

with the lattice constant a of the conventional unit cell in real space, thus

$$h^2 + k^2 + l^2 = \left(\frac{2a}{\lambda}\right)^2 \sin^2\Theta \quad . \tag{2.35}$$

So one tries to describe the position of all peaks by a single choice of a/λ and a set of integers (hkl) each. Thus one obtains the lattice constant a and from the presence or absence of the peaks the structure factor and thus the lattice.

References

Hunklinger, Siegfried (2014). *Festkörperphysik*. 4. aktualisierte Auflage. München: De Gruyter. ☐.

Chapter 3
Fourier Optics

Markus Lippitz
October 23, 2024

Overview

Fourier transformation simplifies the description of light, especially when it passes through obstacles, as in diffraction. The action of a lens also involves a Fourier transform. This is the field of *Fourier optics*. I will follow chapter 4 of Saleh and Teich, 1991 here. Another good source is Goodman, 2005. Note that books (as Saleh & Teich) from the engineering side of optics use $j = -i = -\sqrt{-1}$ instead of i. Sometimes this j is even written as i, so engineering is the complex conjugate of physics.

   We will briefly lay the foundations of Fourier optics and then discuss diffraction and optical Fourier transform through a lens. For our purposes it is sufficient to consider scalar waves, i.e. we ignore the vectorial nature of the electric (or magnetic) field of light and use only a complex scalar value at each point in space to describe light.

Spatial frequencies

Let us start with a plane wave

$$U(\boldsymbol{r}) = A e^{i \boldsymbol{k} \cdot \boldsymbol{r}} \quad \text{with} \quad k = |\boldsymbol{k}| = \frac{2\pi}{\lambda} \quad . \tag{3.1}$$

We assume that all three components of $\boldsymbol{k}$ are real (*far-field optics* in contrast to *near-field optics*), but the amplitude A might be complex. The wave vector $\boldsymbol{k}$ makes the angles $\Theta_{x,y}$ with the $x-z$ and the $y-z$ plane, respectively, with

$$\sin \Theta_x = \frac{k_x}{k} \quad . \tag{3.2}$$

In the $z = 0$ plane, the field is

$$U(x, y, 0) = f(x, y) = A\, e^{2\pi\, i(\nu_x x + \nu_y y)} \tag{3.3}$$

with the *spatial frequencies* ν_x and ν_y

$$\nu_{x,y} = \frac{k_{x,y}}{2\pi} = \frac{1}{\Lambda_{x,y}} \tag{3.4}$$

and the period of the field $\Lambda_{x,y}$ in the x and y direction. And of course all this is related, i.e.,

$$\sin \Theta_x = \frac{k_x}{k} = \lambda \nu_x = \frac{\lambda}{\Lambda_x} \tag{3.5}$$

and similar for the y direction. The assumption of all-real $\mathbf{k}$ components makes sure that for all combinations of k_x,k_y, k_z an angle Θ can be found, i.e., the right side of the equation is real and below one in absolute value.

We will almost always make the *paraxial approximation* assuming that the wave vector is roughly parallel to the z-direction, the angles $\Theta_{x,y}$ are thus small, and $k_{x,y} \ll k$. Then we can omit the sine in the last equation and get

$$\Theta_x \approx \frac{k_x}{k} = \lambda \nu_x = \frac{\lambda}{\Lambda_x} \quad . \tag{3.6}$$

What happened here? The combination of all-real $\mathbf{k}$ components, i.e., optical far-field, and fixed wavelength λ removes one degree of freedom in the three components of the wave vector. As long as we know the wavelength and we know that the plane wave is nicely propagating, only two real values are enough to fully describe it. These two values could be the angles $\Theta_{x,y}$, or the spatial frequencies $\nu_{x,y}$ or the $\Lambda_{x,y}$.

Transmittance function

A plane wave of amplitude one is traveling in $+z$ direction. At $z = 0$ it is transmitted through a thin optical element with the complex transmittance function $f(x,y)$ with

$$f(x,y) = e^{2\pi i (\nu_x x + \nu_y y)} \quad . \tag{3.7}$$

Directly after this plate, the optical field is $U(x,y,0) = f(x,y)$, i.e., the field is modulated by the transmittance function. We know from above that such a field is traveling in the direction given by the $\Theta_{x,y}$ or equally by the spatial frequencies $\nu_{x,y}$. The field is thus diffracted in this direction.[1]

In general, if the transmittance function f would have an arbitrary shape, it could be decomposed into a sum of harmonic functions. Each harmonic component would diffract a part of the plane wave into its direction. So when we express f by its Fourier transform F

$$f(x,y) = \mathcal{FT}\{F(\nu_x,\nu_y)\} = \iint F(\nu_x,\nu_y)\, e^{2\pi i (\nu_x x + \nu_y y)}\, d\nu_x d\nu_y \tag{3.8}$$

then we get

$$U(x,y,0) = \iint F(\nu_x,\nu_y)\, e^{2\pi i (\nu_x x + \nu_y y)}\, d\nu_x d\nu_y \quad . \tag{3.9}$$

This becomes useful when calculating the field *at any point in space*, i.e., by including the z coordinate:

$$U(x,y,z) = \iint F(\nu_x,\nu_y)\, e^{2\pi i (\nu_x x + \nu_y y)}\, e^{i k_z z}\, d\nu_x d\nu_y \quad , \tag{3.10}$$

where k_z now depends on the integrating variables

$$k_z = \sqrt{k^2 - k_x^2 - k_y^2} = 2\pi \sqrt{\frac{1}{\lambda^2} - \nu_x^2 - \nu_y^2} \quad . \tag{3.11}$$

Again the requirement of propagating waves entails $\nu_x^2 + \nu_y^2 < 1/\lambda^2$, so not all Fourier components of F play a role.

[1] This is not an optical grating yet, as this would change the amplitudes only, i.e., have a real-valued tranmittance function.

Transfer function and impulse response

Let us first introduce the concepts with electric circuits such as an RC-filter. One can define a transfer function $H(\omega)$ that relates the frequency spectrum $F(\omega)$ at the input (of the filter) with that at the output

$$G(\omega) = F(\omega) \cdot H(\omega) \quad . \tag{3.12}$$

In time domain, the impulse response $h(t)$ is another description. The signal $f(t)$ at the input results in an output $g(t)$

$$g(t) = \int h(\tau) f(t - \tau) d\tau \quad , \tag{3.13}$$

where causality requires that $h(t)$ is zero for $t < 0$. The interesting point is that not only the signals f and g are connected to their Fourier transforms F and G, but also the transfer function H is the Fourier transform of the impulse response h. A Fourier transform converts a product into a convolution, and vice versa.

Transfer function of free space

We now apply this scheme to spatial frequencies describing a superposition of plane waves. Letting the wave propagate by a distance d from a source plane $f(x, y) = U(x, y, 0)$ to a target plane $g(x, y) = U(x, y, d)$, how do the spatial amplitudes F and G relate? Looking at eq. 3.10, we see that it is just the last exponential function that depends on z, but we need to take eq. 3.11 into account. Together we find

$$H(\nu_x, \nu_y) = \exp\left(2\pi\, i\, d\, \sqrt{\frac{1}{\lambda^2} - \nu_x^2 - \nu_y^2}\right) \quad . \tag{3.14}$$

For spatial frequencies $\nu_x^2 + \nu_y^2 < 1/\lambda^2$, i.e., within a circle of radius $1/\lambda$, the magnitude does not change ($|H| = 1$), only the phase changes. Outside this circle, the magnitude drops exponentially width d, as the square-root becomes imaginary. These waves are called *evanescent waves*, as they do not propagate and only exist in the near-field.

High spatial frequencies ν near $1/\lambda$ are far away from the paraxial approximation. In most cases it is sufficient to restrict ourself to low spatial frequencies $\ll 1/\lambda$. In this case, we can use the *Fresnel approximation* of the transfer function

$$H(\nu_x, \nu_y)_{\text{Fresnel}} = H_0 \exp\left(-\pi\, i\, d\lambda \left(\nu_x^2 + \nu_y^2\right)\right) \quad \text{with} \quad H_0 = e^{ikd} \quad . \tag{3.15}$$

The term H_0 factors out the trivial phase evolution due to propagation along the optical axis.

When we know the spatial frequency amplitudes F at $z = 0$, then we obtain G at $z = d$ by

$$G(\nu_x, \nu_y) = F(\nu_x, \nu_y) \cdot H(\nu_x, \nu_y) \quad . \tag{3.16}$$

We can Fourier transform the equation to obtain

$$g(x, y) = f(x, y) \otimes h(x, y) \tag{3.17}$$

where $\otimes$ signals a convolution. The impulse response of free space is in the Fresnel approximation

$$h(x,y)_{\mathsf{Fresnel}} \approx h_0 \, \exp\left(ik\frac{x^2 + y^2}{2d}\right) \quad \text{with} \quad h_0 = -\frac{i}{\lambda d}\, e^{ikd} \quad . \qquad \text{(3.18)}$$

Eq. 3.17 means that we get from one plane to the other by convolving each source point with a wave of shape h. This is equivalent to the Huygens principle, where each point should be a source of a spherical wave. When we take the paraxial approximation of a spherical wave we obtain $h(x,y)_{\mathsf{Fresnel}}$.

Optical Fourier transform by propagation

Up to now we used the Fourier transform to simplify description of optical fields. In this section, we will show that the propagation of an optical field by a long enough distance allows to optically 'compute' the Fourier transform. We will find that the field in the target plane $g(x,y)$ is proportional to the Fourier transform F of the field in the source plane.

The Fourier components F of the field f in the source plane determine the direction of travel of the plane waves, as we have seen above. The problem is that a plane wave is everywhere in space. We need thus to find a condition for 'far enough' so that the individual pieces of the plane wave have separated enough. We do not only employ the paraxial approximation, i.e., that the wave vectors are not too inclined on the optical axis. The key point is that we also require the size of the source plane to be limited. This leads to the two conditions of the Fraunhofer approximation

Figure 3.1: Fraunhofer condition

$$N_F = \frac{a^2}{\lambda d} \ll 1 \quad \text{and} \quad N_F' = \frac{b^2}{\lambda d} \ll 1 \qquad \text{(3.19)}$$

where the two N_F are the Fresnel numbers, and a,b are the radius of the relevant and allowed regions in the target and source planes, respectively. d is again the distance between the planes. The Fraunhofer approximation is a more severe restriction than the Fresnel approximation.

We start by writing down the convolution integral of eq. 3.17 in the Fresnel approximation

$$g(x,y) = f(x,y) \otimes h(x,y)_{\mathsf{Fresnel}} \qquad \text{(3.20)}$$

$$= h_0 \iint f(x',y') \exp\left(ik\frac{(x-x')^2 + (y-y')^2}{2d}\right) dx'dy' \quad . $$

$$\text{(3.21)}$$

The term $(x - x')^2$ in the exponent of the exponential function is multiplied out into three terms. We keep the mixed terms. Both squared terms can be neglected due to the Fraunhofer approximation. For example we get

$$\exp\left(i\pi\frac{x'^2 + y'^2}{\lambda d}\right) \approx 1 \qquad \text{(3.22)}$$

as $N_F' \ll 1$. The terms without prime vanish due to $N_F \ll 1$. So we have

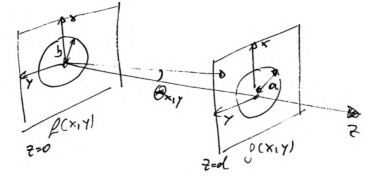$$g(x,y) \approx h_0 \iint f(x',y') \exp\left(-i2\pi\frac{xx' + yy'}{\lambda d}\right) dx'dy' \quad . \qquad \text{(3.23)}$$

We now identify the factor $x/\lambda d$ with the spatial frequency ν_x (y similar) and write

$$g(x,y) \approx h_0 F\left(\nu_x, \nu_y\right) = h_0 F\left(\frac{x}{\lambda d}, \frac{y}{\lambda d}\right) \quad . \qquad (3.24)$$

When we place a screen g at a distance fulfilling the Fraunhofer condition after a diffracting obstacle f, the interference pattern visible on the screen will be described by the Fourier transform F of f. This simplifies a lot the calculation of single slit, double slit and grating, as typically presented in the introductory optics lecture.

Test yourself

1. Convince yourself that the textbook solution, for example in Demtröder, can be obtained by a Fourier transform.

2. Estimate the required distance so that a typical diffraction grating fulfils the Fraunhofer condition.

Optical Fourier transform by a lens

The distance d required to stay within the Fraunhofer approximation can be prohibitively large. We will see here that a lens is able to shorten the distance between the grating and the screen and still keep the Fourier relation. This explains why spectrometers are not too long, but contain a lens or curved mirror.

From geometrical optics in the paraxial approximation we know already that a lens focuses a beam (angles Θ_x, Θ_y to the optical axis) on a point

$$(x,y) = (f\Theta_x, f\Theta_y) \qquad (3.25)$$

Figure 3.2: Optical Fourier transform by a lens

in the focal plane, where f describes the focal length of the lens. A lens thus separates plane waves by their propagation direction. As in the beginning of the chapter, we can convert angles into optical frequencies and thus find that the field in the target plane g is proportional the the Fourier amplitude F

$$g(x,y) = \tilde{h}\, F\left(\nu_x, \nu_y\right) = \tilde{h}\, F\left(\frac{x}{\lambda d}, \frac{y}{\lambda d}\right) \quad . \qquad (3.26)$$

The remaining question is the prefactor $\tilde{h}$. If it would depend of the spatial coordinates x and y, this would destroy the Fourier transform. To obtain $\tilde{h}$, we multiply the transfer functions of free space for the distance source plane to lens (length d) and lens to target plane (length f). And we need to multiply a transfer function for the lens, as the lens has a thickness profile $t(x,y)$ of a material with a certain index of refraction. All together one obtains[2]

[2] details in Saleh and Teich, 1991, chapter 4

$$\tilde{h}(x,y) = \tilde{h}_0 \exp\left(-i\pi\frac{(x^2+y^2)(d-f)}{\lambda f^2}\right) \quad \text{with} \quad \tilde{h}_0 = \frac{-i}{\lambda f}\, e^{ik(d+f)} \quad .$$
$$(3.27)$$

This factor becomes spatially constant when the condition $d = f$ is met. A lens thus performs an optical Fourier transform between is two focal planes. In a spectrometer, the grating sits in the front focal plane of the curved mirror (acting as a lens), the detector in its back focal plane.
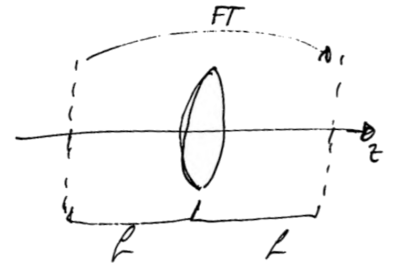
Spatial filter

In addition to spectrometers, the spatial filter is another important application of a lens as a Fourier transform device. We consider a so-called 4f-system, see Saleh and Teich, 1991. All components are separated by one focal length f: a source plane f, a first lens, a filter plane p, a second lens and a target plane g. Both lenses are identical.

Let the transfer function p of the filter plane be $p(x, y) = 1$ for the beginning. Then the first lens Fourier transforms f into F in the filter plane. The filter does nothing and the second lens transforms back F into f, so that we get in the target plane what we started with , i.e., $f = g$. Of course this make the assumption that all plane waves nicely propagate, i.e., the spatial frequencies in f are small enough to cause only propagating plane waves.

The filter plane can be used to modify the Fourier components F. At position x in the p plane, only the Fourier component $\nu_x = x/(\lambda f)$ is present. We can put a mask $p(x, y)$, either just absorbing or with a complex transfer function in the filter plane. The overall transfer function of the 4f-system is then

$$H(\nu_x, \nu_y) = p(\lambda f \nu_x, \lambda f \nu_y) \quad , \tag{3.28}$$

ignoring an overall phase factor for the propagation.

An often used transfer function is a circular aperture. It removes all spatial frequencies above a certain threshold. In this way, one can clean up a laser beam, so that is follows the expected Gaussian profile even after transmission though many non-ideal optical elements.

The inverse filter, i.e. a opaque disc, acts as high-pass filter, increasing the edges in an optical image. A vertical slit lets only pass horizontal features in the image.
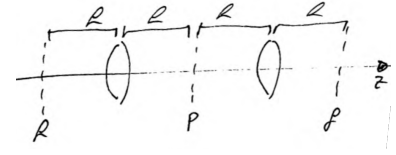

Figure 3.3: A $4f$ system can be used as spatial filter.

Resolution of a microscope

In an optical microscope, a sample is imaged on a detector by a system of lenses. Not all spatial frequencies are transmitted equally well. A fundamental limit is the transfer function of free space (eq. **??**), which limits the spatial frequencies to $\nu_{x,y} \leq n/\lambda_0$. A short vacuum wavelength λ_0, i.e. blue or ultraviolet light, or a high refractive index n, i.e. immersion oil instead of air, shifts the limit to higher spatial frequencies. The highest observable spatial frequency is the wavelength of light in the medium.

A technical limitation sets in earlier. High spatial frequencies correspond to plane waves with a large angle θ to the optical axis. In the limiting case, the plane wave propagates perpendicular to the optical axes, i.e. parallel to the sample surface. The microscope objective has to capture as many of these rays as possible, i.e. it has to have a large aperture angle $\theta_{\text{objective}}$. This is quantified in the *numerical aperture*

$$NA = n \sin \theta_{\text{objective}} \tag{3.29}$$

so that the maximum spatial frequencies are $\nu_{x,y} \leq NA/\lambda_0$. Numerical apertures greater than one require the use of an immersion medium. Glycerin ($n = 1.47$) allows to obtain NA $\approx 1.3 \ldots 1.45$.

Another approach to the resolution of a microscope is the *point spread function* (PSF). It is the impulse response of the imaging system, i.e., the image of a point source in the sample plane. Diffraction at the circular aperture of the microscope objective leads to the Airy-pattern of the Bessel function J_1 (see **??**)

$$PSF(\rho) = \left(\frac{J_1(k_0\, NA\, \rho)}{k_0\, NA\, \rho} \right)^2 \tag{3.30}$$

where ρ is the radial coordinate in the sample plane, i.e., the point placed there appears to be larger. Two points are said to be resolvable if they are separated so that the image of one point falls into the first zero of the PSF of the second point. This results in the value

$$\Delta x = 0.61 \frac{\lambda_0}{NA} \quad . \tag{3.31}$$

References

Goodman, Joseph W. (2005). *Introduction to Fourier optics*. 3. ed. Roberts.
Saleh, Bahaa E. A. and Malvin C. Teich (1991). *Fundamentals of photonics*. New York, NY [u.a.]: Wiley. 🔗.

Chapter 4

Spatial Light Modulator

Markus Lippitz, Christoph Schnupfhagn
October 27, 2023

Overview

In optics, we not only Fourier transform between the two focal planes of a
lens, but we can also Fourier transform between energy and time. A spatial
light modulator (SLM) spatially modulates light (in the image plane of a
grating spectrometer) to shape the temporal evolution of ultrafast (≈ 10 fs)
laser pulses. We follow the formalism of Träger, 2012.

Generation and properties of ultrashort laser pulses

To build a laser we need at least a cavity, an active medium and a pump
source. The cavity has longitudinal modes if multiples of the half wavelength
fit into the cavity length l. For integer n and wavelength λ this standing-wave
condition reads $l = n\lambda/2$. Consequently, the resonances are equidistant in
frequency space at $\omega_n = n\pi c/l$, where c is the speed of light. In general, the
electric field $E(x, t)$ results from a superposition of all cavity modes ω_n with
individual amplitudes $A(\omega_n)$ and relative phases ϕ_n

$$E(x, t) = \Re \left[\sum_i A(\omega_i) e^{i(\omega_i t - kx + \phi_i)} \right] \quad . \tag{4.1}$$

The wave vector k is given by the dispersion relation $k = \omega/c$. The spatial
dependence is dropped for simplicity. The electric field in time domain is
linked to its counterpart in frequency domain by Fourier transform

$$E(\omega) = \mathcal{F}[E(t)] = \int_{-\infty}^{\infty} E(t) e^{-i\omega t} dt \quad . \tag{4.2}$$

Since $E(\omega)$ is complex-valued while $E(t)$ is a real function, it follows
$E(\omega) = E^*(-\omega)$. Therefore, it is sufficient to look only at the positive
frequencies $E^+(\omega)$ and one separates them by writing

$$E(\omega) = E^+(\omega) + E^-(\omega) \quad , \tag{4.3}$$

where

$$E^+(\omega) = \begin{cases} E(\omega) & \text{if } \omega \geq 0 \\ 0 & \text{if } \omega < 0 \end{cases} \quad \text{and} \quad E^-(\omega) = (E^+(-\omega))^* \quad . \tag{4.4}$$

The Fourier transform of $E^+(\omega)$ is then

$$E^+(t) = \frac{1}{2\pi} \int E^+(\omega) e^{i\omega t} d\omega \quad . \tag{4.5}$$

And of course we can decompose the complex $E^+(\omega)$ into phase and amplitude

$$E^+(\omega) = |E^+(\omega)| \, e^{-i\phi(\omega)} \quad . \tag{4.6}$$

In order to generate short laser pulses, the phase relation $\phi(\omega)$ between the laser modes needs to be fixed in time. This is called *mode locking*. Additionally, to generate confined pulses in time domain Fourier's theorem requires a broad distribution in the frequency domain, i.e., an active medium with a broad gain spectrum. This is expressed by the product of temporal width Δt (full width at half maximum, FWHM) and spectral width $\Delta \nu$ (FWHM), which can not be smaller than a minimum value TBP$_{\text{min}}$

$$\Delta t \cdot \Delta \nu \geq \text{TBP}_{\text{min}} \quad . \tag{4.7}$$

This minimum *time-bandwidth product* (TBP) depends on the temporal shape of the pulse. In case of a Gaussian shape the value is TBP$_{\text{min}} = 0.441$, i.e., 7 fs pulses centered at 800 nm require a minimum spectral width of approximately 135 nm.

Test yourself

1. Superimpose in increasing number of harmonic functions with equidistant frequencies to synthesis a laser pulse.

2. Vary the phase relation between these modes to simulate a light field that is not 'mode locked'

Spectral phase

The actual pulse duration for a given spectrum strongly depends on the spectral phase $\phi(\omega)$. In general, the first derivative of the phase with respect to frequency is called *group delay* (GD) while the second derivative is called *group delay dispersion* (GDD). Expanding the phase in a Taylor series around the central frequency ω_0 yields

$$\begin{aligned} \phi(\omega) =&\phi(\omega_0) + \phi'(\omega_0)(\omega - \omega_0) + \frac{1}{2}\phi''(\omega_0)(\omega - \omega_0)^2 \\ &+ \frac{1}{6}\phi'''(\omega_0)(\omega - \omega_0)^3 + ... \quad , \end{aligned} \tag{4.8}$$

where

$$\phi^{(n)} = \left. \frac{\partial^n \phi}{\partial \omega^n} \right|_{\omega=\omega_0} \quad . \tag{4.9}$$

The propagation of laser pulses is determined by the optical properties of the materials, in particular the dispersion of the refractive index $n(\omega)$. As the refractive index in general varies with the frequency, the spectral colors gather different phase shifts during propagation. The variations are most pronounced in the vicinity of material resonances, affecting also higher orders in the Taylor expansion of the phase. To illustrate this, the influence
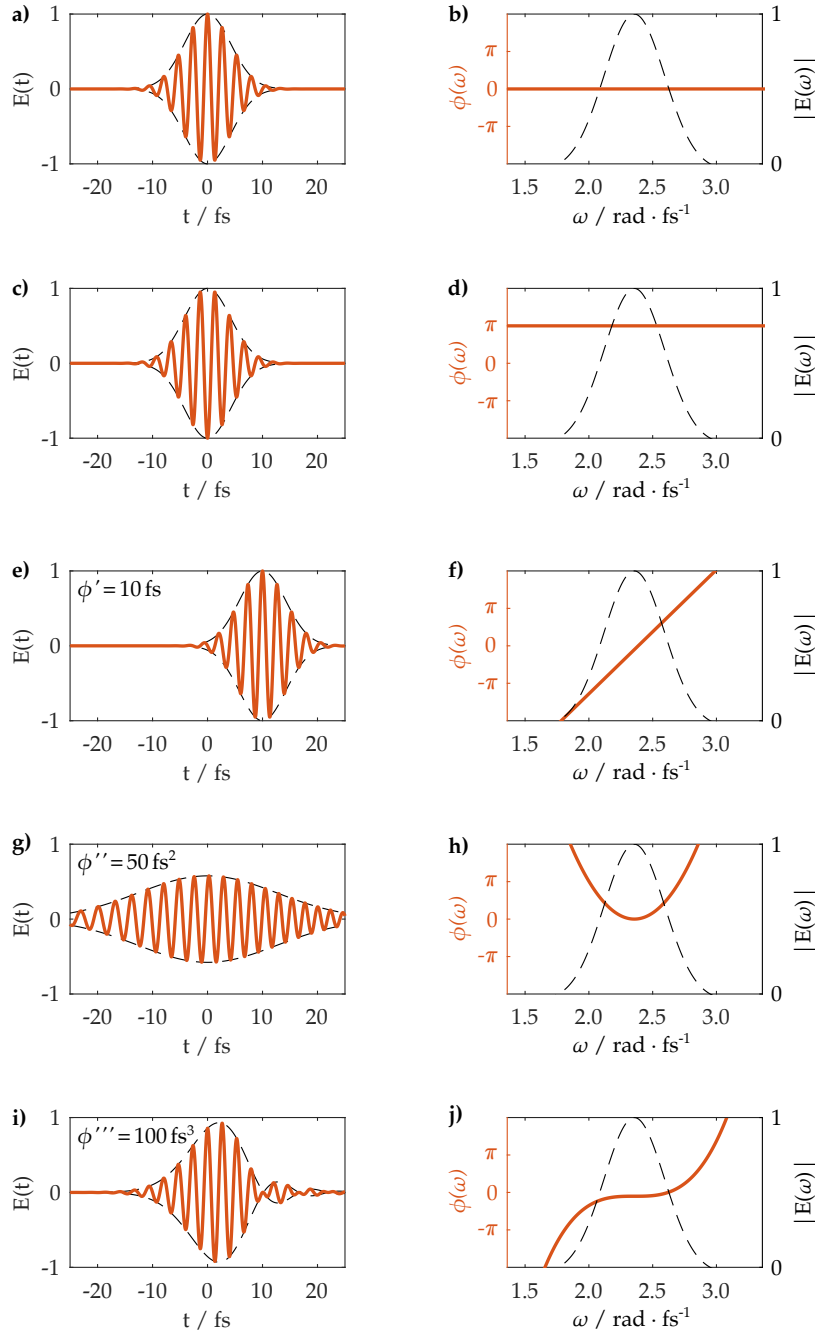
Figure 4.1: Dependence of the temporal pulse shape on different orders in the Taylor expansion of $\phi(\omega)$. The Gaussian shaped pulses have a bandwidth limit of 7 fs and are centered at 800 nm.

of the different orders in the Taylor expansion on the temporal shape of bandwidth-limited 7 fs pulses is shown in Figure 4.1.

A constant phase term defines the phase difference between the carrier wave and the envelope, known as the carrier-envelope phase (CEP) without altering the pulse shape. Similarly, a linear phase term shifts the pulse in time without any distortions, where the value of ϕ' is equivalent to the introduced time offset.

In contrast, applying a quadratic phase term, also called *linear chirp*, stretches the pulse in time. Energy conservation then requires the peak intensity to decrease. Furthermore, the different frequencies do not arrive simultaneously: The red colors arrive before the blue in case of $\phi'' > 0$, which is typical for most materials. Ultrashort pulses are exceptionally affected by temporal broadening since the large spectral bandwidth allows for large spectral variations of the refractive index.

The figure shows a pulse broadening from 7 fs to 21 fs (FWHM) at $\phi'' = 50$ fs^2, corresponding to a transmission through 1.2 mm SiO$_2$ glass at 800 nm. This small propagation length already increases the TBP by a factor of 3 from 0.441 to 1.323. At the same time the peak intensity is reduced by 67 %. Other glasses yield even higher GDD values[1], e.g., $\phi'' \approx 143$ fs^2 in SF10.

[1] Träger, 2012.

Applying even higher orders in the phase expansion creates increasingly complex pulse shapes; a cubic phase term for instance generates multi-pulse sequences which are asymmetric in time.

In an experiment, one usually needs the shortest possible laser pulse at the sample. Optical elements between laser and sample can contribute a complex optical phase. It is one task of the spatial light modulator to compensate these phase differences.

Pulse shaping with spatial light modulators

Since both the intensity spectrum and the spectral phase determine the pulse shape in time domain, it is desirable to control both parameter sets in the experiment. This can be achieved with a spatial light modulator which directly addresses the frequency domain in a $4f$ setup as illustrated in Figure 4.2: The spectral colors of incident pulses with electric field $E_\text{in}(\omega)$ are spatially separated by a diffraction grating. A lens with focal length f focuses each color into its Fourier plane, which is again located in a distance f. In this plane a complex transfer function $H(\omega) = A(\omega)\,e^{i\phi(\omega)}$, consisting of amplitude and phase term $A(\omega)$ and $\phi(\omega)$, can be applied. This could, e.g., be realized with a glass plate having a spatially varying thickness to generate a frequency-dependent phase function. An additional metallic coating might, similar to a filter wheel with variable optical density, create the amplitude mask. However, a more sophisticated way to shape pulses is to use liquid crystal masks instead of static masks where each pixel controls a different frequency. After the spectral modifications, the colors are recombined and collimated with an additional lens-grating combination in distance f, yielding the output electric field distribution

$$E_\text{out}^+(\omega) = H(\omega)\,E_\text{in}^+(\omega) \quad .\tag{4.10}$$

A multiplication in frequency domain corresponds to a convolution in time domain, therefore

$$E_{\text{out}}^+(t) = \mathcal{F}\left[H(\omega)\right] \otimes E_{\text{in}}^+(t) \quad ,$$

(4.11)

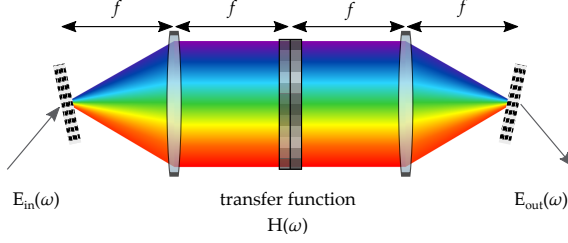where $\otimes$ denotes the convolution.

Figure 4.2: Sketch of a $4f$ setup consisting of two gratings and lenses. The incoming electric field $E_{\text{in}}(\omega)$ is manipulated by a transfer function $H(\omega)$ in the Fourier plane of the lens, resulting in an outgoing field $E_{\text{out}}(\omega)$.

Typical masks

A *linear phase*

$$\phi(\omega) = \tau(\omega - \omega_0)$$

(4.12)

translates the laser pulse by the τ in time, without any further spectral modification. The maximum accessible value of τ depends on the maximum phase change of the SLM. Values around 1 ps are typical, corresponding to 300 μm travel.

A *polynomial phase mask*

$$\phi(\omega) = \sum_n \frac{a_n}{n!}(\omega - \omega_0)^n$$

(4.13)

will be used frequently in order to compensate the group delay dispersion of optical elements. Its parameters a_n correspond the the Taylor coefficients of the phase dispersion.

The *sinusoidal phase mask*

$$\phi(\omega) = a \cos\left[\tau(\omega - \omega_0) - \Delta\phi\right] \quad .$$

(4.14)

generates a train of a few pulses[2], separated by τ in time. The amplitude of the n-th puls is controlled by the modulation amplitude a and is proportional to the Bessel function of first kind $J_n(a)$.

A *V-shaped phase mask* splits the spectrum at ω_s

$$\phi(\omega) = \begin{cases} -\tau_-(\omega - \omega_s) & \text{for} \quad \omega < \omega_s \\ +\tau_+(\omega - \omega_s) & \text{for} \quad \omega \geq \omega_s \end{cases}$$

(4.15)

and separates both spectral components by $\tau_+ + \tau_-$ in time. This is similar to pump-probe spectroscopy, where two laser pulses interact with the sample.

The *sinusoidal amplitude mask*

$$A(\omega) = \cos\left[\frac{\tau}{2}(\omega - \omega_0) - \Delta\phi\right] \quad .$$

(4.16)

creates two identical copies of the pulse separated by a time delay τ. The carrier-envelope phase of both pulses is the same unless $\Delta\phi \neq 0$. This amplitude mask can be used to measure the autocorrelation of a laser pulse. Note that here A changes sign. Depending on the implementation, one might want to leave $A > 0$ and include a π phase shift.

[2] Renard et al., 2004.

Realization by liquid crystals

How could one change amplitude A and phase ϕ of the optical field at each pixel? A variation in phase is obtained from a variation of the index of refraction that is experienced by the light field. The amplitude is modified by rotating the direction of linear polarization of the field, and then letting it pass through a linear polarizer, which removes the unwanted fraction of the amplitude. So we need to briefly look into polarization optics and birefringence to understand the working of the spatial light modulator.

First we need a birefringent material as used in polarization optics, but the amount of birefringence should be controllable from the outside. This we find in liquid crystals. Uniaxial liquid crystals are anisotropic materials which can be approximated by an ellipsoidal molecular shape. The anisotropic shape results in an index of refraction that depends not only on the polarization direction, but also on the angle Θ between the wave vector $\boldsymbol{k}$ and the symmetry axis of the molecule. The latter is called 'optic axis' in polarization optics, not to be confused[3] with the 'optical axis'. Light is decomposed into ordinary and extraordinary rays with refractive indices n_{o} and $n_{\mathsf{eo}}(\theta)$, respectively. While n_{o} does not depend on Θ, we have for n_{eo}

[3] in German, *both* is 'optische Achse' !

$$\frac{1}{n_{\mathsf{eo}}^2(\theta)} = \frac{\cos^2\theta}{n_{\mathsf{0}}^2} + \frac{\sin^2\theta}{n_{\mathsf{eo}}^2(90°)} \quad .$$

(4.17)

By the manufacturing process of the electrodes a preferential direction, called *director*, is given. Without external electric field, the molecules align in this direction. Applying an electric field, the molecules orient in this field and turn. The angle Θ thus changes and so does the index of refraction. The phase difference $\Delta\phi$ between light polarized parallel and perpendicular to the director depends thus on the applied voltage U

$$\Delta\phi(\omega, U) = \frac{\omega d}{c_0}\left[n_{\mathsf{eo}}(\omega, U) - n_{\mathsf{o}}(\omega)\right] \quad .$$

(4.18)

The exact relation has no analytical solution and needs to be calibrated.

This gives only one degree of freedom. In the devices, two liquid crystal panels (A,B) are put directly after each other, but with directors rotated by 90 degrees. Before and after the SLM two linear and crossed polarizers are placed. The two directors are under ± 45 degrees to them. The transmitted electric field is then

$$E^+ = E_0^+ \sin\left(\frac{\Delta\phi_{\mathsf{A}} - \Delta\phi_{\mathsf{B}}}{2}\right)\exp\left[i\left(\frac{\Delta\phi_{\mathsf{A}} + \Delta\phi_{\mathsf{B}} + \pi}{2}\right)\right].$$

(4.19)

It is apparent that this setup imposes an amplitude and phase term to the electric field, depending on the sum and difference of ϕ_{A} and ϕ_{B}, respectively. Therefore, by varying the voltages U_{A} and U_{B} amplitude and phase of the transmitted field can be independently tuned. Since the SLM is positioned in the Fourier plane, this allows to shape the pulses over the complete spectral bandwidth.

a)

liquid crystal

640 px

glass
substrate

97 µm   3 µm I 10 µm

ITO electrodes

b)

ITO
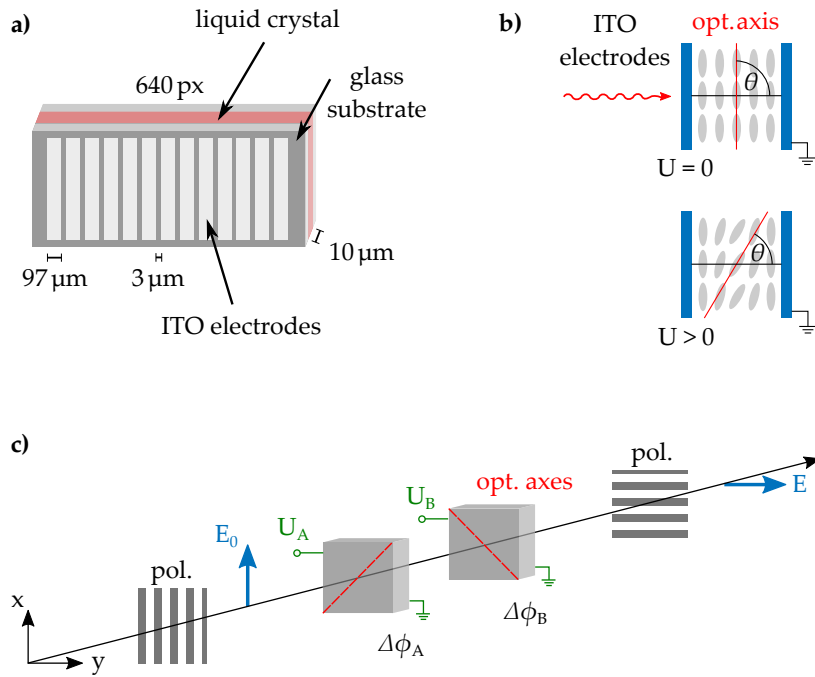electrodes   opt. axis

θ

U = 0

θ

U > 0

Figure 4.3: (a) Sketch of a single liquid crystal mask. (b) The liquid crystal molecules (gray) are aligned along the electrode surface (blue) if no voltage is applied. For voltages $U > 0$ the tilting angle θ of the molecules changes. (c) In the experiment, two liquid crystal masks are placed between crossed polarizer.

c)

pol.

opt. axes

E_0 U_A U_B E

pol.

x

y

$\Delta\phi_A$ $\Delta\phi_B$

References

Renard, M. et al. (2004). "Pulse trains produced by phase-modulation of ultrashort optical pulses: tailoring and characterization". In: *Opt. Express* 12.3, pp. 473–482. ✇.

Träger, Frank, ed. (2012). *Springer Handbook of Lasers and Optics*. Berlin, Heidelberg: Springer. ✇.

Chapter 5
Mössbauer Spectroscopy

Markus Lippitz
November 20, 2025

Overview

We close the part on oscillations and Fourier transforms by the Mössbauer effect, which describes the recoil-less emission and absorption of a gamma photon by an atomic nucleus. It leads to very narrow spectral lines with $\Delta E/E \approx 10^{-15}$ (Potzel et al., 1992).

During his PhD thesis work in Munich and Heidelberg in the years 1955 – 1958, Rudolf Mössbauer investigated the emission and reabsorption of gamma radiation by ^{191}Ir. He discovered an unexpected increase in absorption when cooling both the emitter and the absorber material. This observation and its explanation led to his receiving the Nobel Prize in 1961 at the age of 32. Today, Mössbauer spectroscopy is a common tool used to study materials. One example is the Mars rovers, which use Mössbauer spectroscopy to search for water (Klingelhöfer et al., 2006).

The structure of this chapter follows that of the Nobel Prize lecture by Rudolf Mössbauer (see Mössbauer, 1961, reprinted in Kalvius and Kienle, 2012). Other good sources are Schatz, Weidinger, and Deicher, 2010 and Wegener, 1966.

Resonance fluorescence

At room temperature, the fluorescence emission peak of dye molecules is displaced from the absorption peak due to the Stokes shift. The molecules lose energy between absorption and emission, for example, through the reorientation of the surrounding solvent or matrix molecules.

This is different for atoms in the gas phase. When yellow light from a sodium lamp shines on sodium vapor, the atoms in the vapor absorb the light and re-emit it a few nanoseconds later. The emission of photons by the sodium atoms in the lamp and the absorption of photons by the sodium atoms in the vapor occur at the same energy or wavelength. This process is called resonance fluorescence. It is fluorescence, not scattering, because an excited state is populated.

The natural linewidth of a transition in emission or and absorption is

given by the decay rate to the ground state via Fourier transform. This is the ultimate limit. The line can be broadened by other processes, for example by collisions with other atoms, by Doppler shifts due to thermal motion, or by saturation due to high excitation rate. A typical relative linewidth of atomic lines in the visible is $\Delta E/E \approx 5 \cdot 10^5$ with $E \approx 2$ eV and ΔE given by a decay rate of 1 ns^{-1}.

Recoil in resonance absorption

When a photon of frequency ν is emitted, it carries a momentum $\hbar k = h\nu/c$ with it. If the atom was at rest before emission, then momentum conservation requires that also the atom must move afterwards. This movement carries kinetic energy ΔE_{recoil}, which has to be taken from the transitions energy E_0. We find

$$\Delta E_{\text{recoil}} = \frac{|p_{\text{atom}}|^2}{2M} = \frac{E_0^2}{2Mc^2} \quad , \tag{5.1}$$

with the mass of the atom M and c the velocity of light. For the D-line of sodium, this is about $\Delta E_{\text{recoil}} \approx 0.1$ neV. This corresponds to 25 kHz linewidth and is much smaller than the natural linewidth of the transition. For an optical transition involving atoms or molecules, the recoil effect can be neglected.

This is different for atomic nuclei that emit gamma radiation. After a nuclear reaction such as an alpha- oder beta-decay, the nucleus will most likely end up in an excited state. It can decay to its ground state by emission of a gamma photon with an energy in the range of a few keV to MeV. E_0 and thus ΔE_{recoil} are much larger than for visible light emission. Since metastable nuclear states have lifetimes of nanoseconds or longer, the natural linewidth is comparable to that of dye molecules

The recoil acts twice. First, the spectrum of the emitted gamma photon shifts to lower energies because some energy remains at the emitting nucleus. Second, absorption requires an additional amount of energy, equal to the recoil energy, because the absorbed photon must supply the energy necessary for the nucleus to move afterward. Thus, there is a $2\Delta E_{\text{recoil}}$ mismatch between the emitted photon and gamma absorption. Depending on thermal broadening, some overlap is found (Fig. 5.1). Unlike resonance fluorescence in the visible spectrum, resonance absorption of gamma radiation should not or only extremely weakly occur when source and absorber are identical.

Doppler shifting of transitions

Things changed in 1951 when P. B. Moon published[1] an experiment, in which he supplied the missing energy of $2\Delta E_{\text{recoil}}$ through a Doppler shift:

$$\Delta E_{\text{doppler}} = E_0 \frac{v}{c} \quad . \tag{5.2}$$

For this to work, one needs an excited nuclear state that decays in the emitter by gamma radiation to the ground state. In the absorber, all nuclei are
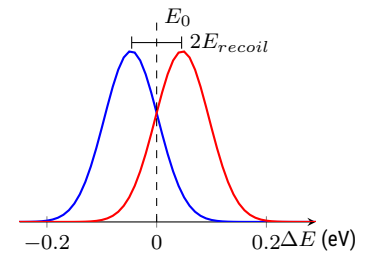
Figure 5.1: Thermal motion causes emission (blue) and absorption (red) lines to broaden. Recoil leads to a relative shift. Only the overlapping region contributes to resonance absorption. The sketch is to scale for the 129 keV transition of ^{191}Ir at room temperature.

[1] Moon, 1951.

in the ground state and thus able to absorb a gamma photon when the recoil mismatch is compensated. In Moons experiment, the tips of a high-speed rotor were coated with gold that had been treated in a nuclear reactor. The ^{198}Au isotope decays into an excited ^{198}Hg which in turn decays by gamma emission of 412 keV into the ^{198}Hg ground state. At a speed of $v = 630$ m/s of the gold tip toward the mercury absorber, the Doppler shift should compensate for $2\Delta E_{\mathrm{recoil}}$. Moon found the expected increase in absorption.

Temperature tuning of transitions

Mössbauer investigated[2] the isotope ^{191}Ir, which decays by emitting a 129-keV gamma photon to the ground state. This choice simplifies resonance absorption because the nucleus is heavy and the photon has low energy. One can learn something about the linewidth by tuning the temperature of either the emitter or the absorber. In both cases, the overlap region in Fig. 5.1 changes. Mössbauer kept the absorber at room temperature and switched the emitter temperature between 88 K and 303 K. From the difference in absorption he derived a line with in terms of excited state lifetime of $\tau = 360$ ps.

In a second series of experiments, he kept the absorber at 88 K and adjusted the temperature of the source from 370 K to 88 K. One might expect a significant decrease in resonance absorption when both the emission and absorption lines narrow and the recoil remains constant. However, this is not what Mössbauer found. The absorption increased by about a factor of 10. Initially, he considered this to be an experimental flaw, as he mentioned in his Nobel Lecture.
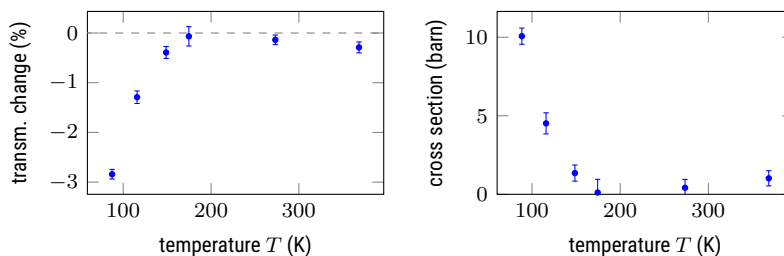
Figure 5.2: Left: Transmission reduction when the source and absorber are both cooled. Right: Absorption cross section calculated from the data on the left. Data from Mössbauer, 1958b

Simple model

How can this observation be explained? The key point is that the atoms are not in a gaseous state. Above, we implicitly assumed a gas phase because the recoil momentum is taken over by just one atom. Additionally, the thermal broadening was calculated assuming a Maxwell velocity distribution. This is not the case in a solid. In a solid, the atoms (and thus the nuclei) are bound by an energy of about 10 eV, which is much stronger than the recoil energy. The atoms vibrate around their equilibrium position. Their vibrational frequencies are described by the photon dispersion relation.

Let's assume the simplest photon dispersion relation: the Einstein model. The only allowed vibrational frequency is Ω. The vibration can absorb en-

ergies in integer multiples of $E_{\text{phonon}} = \hbar\Omega$. If the recoil energy, E_{recoil}, is much larger than Ω, this quantization has only a minor effect. However, when $E_{\text{recoil}} \ll \hbar\Omega$, no phonon is emitted when a gamma photon is emitted. This is the Mössbauer effect, the recoilless emission (and absorption) of gamma radiation.

In the following, we will first stay with the Einstein model and examine the emission probabilities for different numbers of phonons. Next, we introduce the full phonon dispersion. This leads us to the Debye-Waller factor, which also describes the blurring of spots in X-ray diffraction.

Classical model of the Debye Waller factor

We use the classical model of a vibrating atom that continuously emits gamma radiation (Schatz, Weidinger, and Deicher, 2010). A quantum mechanical approach can be found in Czycholl, 2016. The position of the atom oscillates with an amplitude of a.

$$x(t) = a \sin \Omega t \qquad (5.3)$$

so that the emitted field at frequency ω_0 is ($k = 2\pi/\lambda$)

$$E(t) = E_0 e^{-i(\omega_0 t + k x(t))} \qquad (5.4)$$

$$= E_0 e^{-i\omega_0 t} \left(1 - ika \sin \Omega t - \frac{k^2 a^2}{2} \sin^2 \Omega t + \dots \right) \qquad . \qquad (5.5)$$

The $\sin^n$ terms lead to new[3] frequencies in the gamma emission spectrum at $\omega_0 \pm n\Omega$ and the fundamental line at ω_0 is reduced in amplitude. For its amplitude A one finds

[3] this is very similar to Raman scattering

$$A = 1 - \frac{k^2 a^2}{4} + \dots = J_0(ka) \simeq \exp\left(-\frac{k^2 a^2}{4} \right) \qquad , \qquad (5.6)$$

with J_0 the zeroth order Bessel function. The *Debye Waller factor* f describes the intensity, i.e. the square of the amplitude

$$f = |A|^2 = J_0(ka)^2 \simeq \exp\left(-\frac{k^2 a^2}{2} \right) \qquad . \qquad (5.7)$$

In a real system (and in quantum mechanics) the amplitude a would not be constant. It is thus convenient to express a by the mean square displacement $\langle x^2 \rangle$ of a 1d or 3d ($\langle u^2 \rangle$) oscillation

$$\langle x^2 \rangle = \frac{a^2}{2} \quad \text{and} \quad \langle u^2 \rangle = 3 \langle x^2 \rangle \qquad (5.8)$$

so that we get all together[4]

[4] the $\simeq$ vanishes in quantum mechancis

$$f = \exp\left(-\frac{k^2 \langle u^2 \rangle}{3} \right) \qquad . \qquad (5.9)$$

Debye model

To find the mean square displacement $\langle x^2 \rangle$ (or $\langle u^2 \rangle$) we start from a single-frequency oscillator at frequency Ω and mass M. Its mean potential energy,

i.e., potential energy at the mean square displacement, is half the total energy

$$\frac{1}{2} M \Omega^2 \langle x^2 \rangle_n = \frac{1}{2} \hbar \Omega \left(n + \frac{1}{2} \right) \tag{5.10}$$

when the oscillator is in quantum state n. Thus

$$\langle x^2 \rangle_n = \frac{\hbar}{M\Omega} \left(\frac{1}{2} + n \right) \tag{5.11}$$

and averaging over all possible states n occupied with the probability P_n we get in the Einstein model for the phonon dispersion

$$\langle x^2 \rangle_E = \frac{\hbar}{M\Omega} \left(\frac{1}{2} + \sum n P_n \right) = \frac{\hbar}{2M\Omega} \left(1 + \frac{2}{\exp(\hbar\Omega/k_B T) - 1} \right) \quad . \tag{5.12}$$

In the Debye model (i.e. constant velocity of sound), the density of states is

$$D(\Omega) d\Omega = \frac{9 N \hbar^3 \Omega^2}{k_B^3 \Theta_D^3} d\Omega \quad , \tag{5.13}$$

with the Debye temperature Θ_D and N the number of unit cells and 3 vibrational degrees of freedom. We now weight $\langle x^2 \rangle_E$ with $D(\Omega)$ to plug in the Debye model

$$\langle x^2 \rangle = \frac{1}{3N} \int_0^{\Omega_D} D(\Omega) \langle x^2 \rangle_E \, d\Omega \quad . \tag{5.14}$$

Without going further into the details here (see, e.g. Schatz, Weidinger, and Deicher, 2010), we get $\langle x^2 \rangle \propto T$ for $T \gg \Theta_D$. At zero temperature, $\langle x^2 \rangle$ remains finite due to the quantum mechanical zero point motion. With increasing temperature, it increases quadratically. In this limit, one can compute the integral and get for the Debye-Waller factor in the Debye approximation

$$f_D(T) = \exp \left\{ - \frac{3 E_0^2}{4 M c^2 k_B \Theta_D} \left[1 + \frac{2\pi^2}{3} \left(\frac{T}{\Theta_D} \right)^2 \right] \right\} \quad , \tag{5.15}$$

where we have used $\hbar k = E_0/c$ with the energy E_0 of the gamma quant.

Interpretation

At all temperatures, a fraction $f(T)$ of all emission and absorption events occur without recoil. This fraction increases exponentially as the temperature decreases, but it does not approach one even at $T = 0$. It also increases with the Debye temperature; that is, the Mössbauer effect is more pronounced in harder, stiffer crystals. A lower gamma energy E_0 increases the effect as well.

Fig. 5.3 shows an example for 3 different materials. Soft materials with high gamma energy have a low Debye-Waller factor. Iron is much better suited for Mössbauer spectroscopy.

Although the Mössbauer effect is called "recoilless", momentum must still be conserved. The recoil momentum must remain somewhere. If a phonon does not absorb the momentum, then the crystal as a whole does. The entire crystal then moves slightly in the direction opposite the gamma quantum emission. However, since the crystal is much heavier than an atom, this movement is not observable.
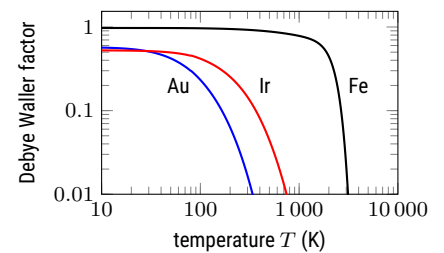

Figure 5.3: Debye Waller factors for the elementary crystals of ^{57}Fe, ^{197}Au and ^{192}Ir with transition energies of 14.3, 77 and 129 keV. Data from Friedrich, 2020.
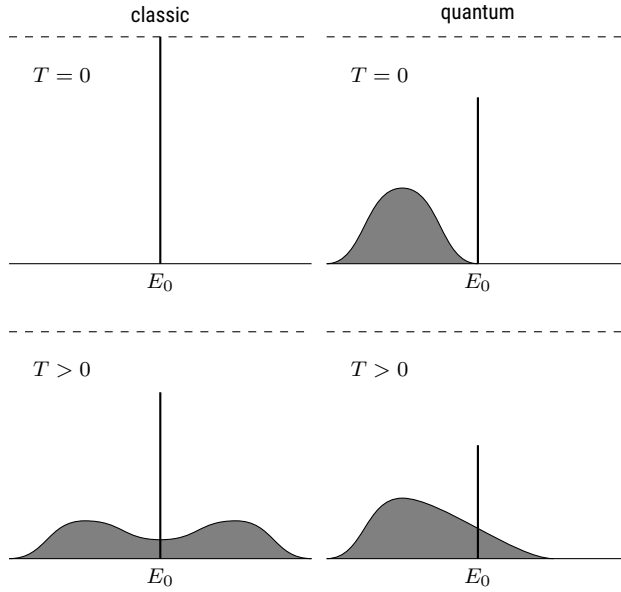
Figure 5.4: Sketch of the classical and quantum mechanical gamma spectrum. Inspired by Fig. 2.2 of Wegener, 1966

In a classical model without zero-point motion, the spectrum of emitted gamma radiation would be a sharp Lorentzian at the nuclear transition energy. This is depicted as a delta function in Figure 5.4. As temperature increases, crystal vibrations lead to the formation of symmetric sidebands above and below this frequency: the $\omega_0 \pm n\Omega$ terms above. Quantum mechanics introduces two changes. First, the spectrum at $T = 0$ contains a phonon band at a lower energy due to zero-point motion. This is because all "+" operations in the above equations and thus $f(T = 0) < 1$ trace back to the "$n + 1/2$" of the harmonic oscillator. At higher temperatures, the spectrum remains asymmetric because the emission of a phonon is always possible. However, absorption of a phonon, which leads to $E > E_0$, requires a populated phonon state.

The first Mössbauer spectrum

So far, our discussion has covered the situation of Walter Mössbauer when he submitted his first article, Mössbauer, 1958b. Only upon rereading his own article in the journal, he realized that measuring the gamma emission spectrum as sketched in Fig. 5.4 would be both convincing and technically feasible (Mössbauer, 2000). The idea is to use the Doppler shifting technique to scan an isotope's emission line against its own absorption line. Unlike the original experiment discussed above, the energy scale is no longer $E_{\text{recoil}} \approx 0.1$ eV, but rather the lifetime-limited linewidth of about 10 µeV. Thus, the velocity of the source can be about four orders of magnitude slower. Fearing that his competitors would realize this as well, Mössbauer set out to conduct the experiment himself, using toy mechanical gears to rotate the source at a speed of a few centimeters per second. Figure 5.5 shows the data.

This is the first observation of a recoilless transition, i.e. nuclear resonance absorption. The transition has an energy of 129 keV and a line width of just 4.6 µeV. The ratio or relative accuracy is about 10^{10}. In modern experiments, a relative linewidth of 10^{15} can be observed (Potzel et al., 1992).
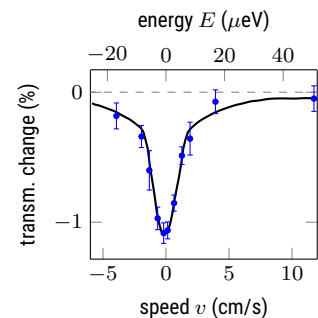

Figure 5.5: First spectrum of the Mössbauer line of ^{192}Ir. Data form Mössbauer, 1958a

Effects influencing the gamma energy

Several effects influence the position of the gamma absorption line or cause line splitting in high-resolution Mössbauer spectroscopy. In the following discussion, we will examine some of these effects using ^{57}Fe as an example. This isotope is relatively abundant (about 2.5%) and stable in natural iron. Therefore, it is easy to produce gamma absorbers containing ^{57}Fe.
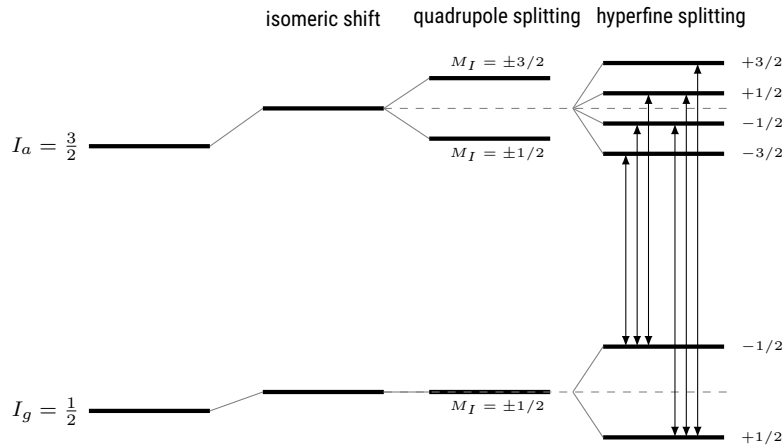

Figure 5.6: Splitting of the nuclear levels in iron.

Figure 5.6 shows the level scheme. The transition to the ground state has an energy of 14.41 keV and a lifetime of 97.8 ns. The ground state has a nuclear spin of $I = 1/2$, while the excited state has $I = 3/2$. We will discuss three effects.

isomeric shift The electron density at the nucleus, combined with the different sizes of nuclei in various isomers (metastable, excited nuclear states), causes a shift. This shift is also called a "chemical shift."

electric quadrupole splitting Line splitting occurs when an electric field gradient is combined with a nuclear quadrupole moment.

magentic hyperfine splitting In a ferromagnetic material, such as ^{57}Fe, the 'external' magnetic field splits the degenerate lines similar to the Zeeman effect.

The first two have the same origin. Electrons generate an electric potential at the nucleus's position, resulting in Coulomb energy. This potential can be expressed[5] as a Taylor series and in terms of the electron wave function Ψ. The lowest order contains two contributions: the isomeric shift and the electric quadrupole splitting.

The isomeric shift is

[5] Schatz, Weidinger, and Deicher, 2010.

$$E_I = \frac{e}{6\epsilon_0} \left|\Psi(0)\right|^2 \int \rho(\boldsymbol{r}) r^2 d\boldsymbol{r} = \frac{Ze^2}{6\epsilon_0} \left|\Psi(0)\right|^2 \left\langle r^2 \right\rangle \quad , \qquad (5.16)$$

where ρ is the nuclear charge distribution and $\left\langle r^2 \right\rangle$ the mean square nuclear radius. The energy E_I depends on the state (via $\left\langle r^2 \right\rangle$) and the chemical environment of the atom (via $\Psi(0)$). This term allows us to distinguish between chemical environments when source and absorber contain the same isotope.

The example Fig. 5.7 shows tin (Sn), which has the electron configuration [Kr] $4d^{10}$ $5s^2$ $5p^2$. In ionic crystals, two to four electrons leave. This modifies the electron density at the nucleus and leads to an isomeric shift in the Mössbauer spectrum.

The electric quadrupole splitting can be written as

$$E_Q = \frac{e}{6} \sum_{i=x,y,z} V_{ii} Q_{ii} = \left(3m_I^2 - I(I+1)\right) \hbar\omega_Q \quad , \tag{5.17}$$

with the tensor of the electric field gradient V_{ii} and the nuclear quadrupole moment Q_{ii}. This field gradient vanishes when the crystal structure is cubic. The quadrupole moment vanishes when the nucleus is spherical, i.e. for $I = 1/2$. At higher nuclear spin values, one finds a splitting according to $|m_I|$, i.e. into $m_I = \pm 1/2$ and $m_I = \pm 5/2$ in the case of ^{57}Fe.

The magnetic hyperfine splitting results from the energy of the nuclear magnetic moment I in an external magnetic field $\boldsymbol{B}$, which can also be produced by a magnetized sample. As usual we have

$$E_{HF} = -\boldsymbol{\mu} \cdot \boldsymbol{B} = -g_I\,\mu_N\,m_I\,B_z \tag{5.18}$$

with the nuclear magneton $\mu_N = e\hbar/(2m_p) \approx 3 \cdot 10^{-8}$ eV/T (proton mass m_p). g_I is the corresponding g-factor.

In the case of ^{57}Fe, the hyperfine splitting leads to 6 lines, see sketch 5.6, as shown in Fig. 5.8. One finds a strong internal magnetic field ($B_z = -33$ T), which results from the influence of the 3d-electrons on the 4s-electrons (Schatz, Weidinger, and Deicher, 2010).

Figure 5.7: Isomeric shift of Sn indifferent environments relative to BaSnO$_3$. Data from Schatz, Weidinger, and Deicher, 2010.
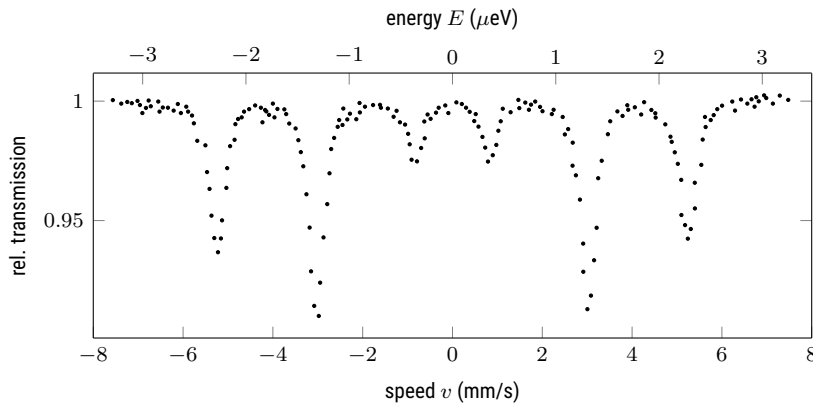
Figure 5.8: Mössbauer spectrum of ^{57}Fe relative to a ^{57}Co source that emits only a single line. The ratio of the peak amplitudes depends on the direction of magnetization by an external magnetic field relative to that of the gamma beam (here, 90 degrees). Data from Gonser, 1975
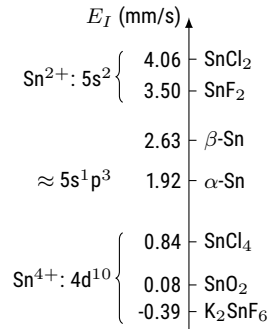
References

Czycholl, Gerd (2016). *Theoretische Festkörperphysik, Band 1*. 4. Aufl. Springer. ☑.

Friedrich, Thomas (2020). *Root-mean square parametrization*. ☑.

Gonser, Uli (1975). "From a strange effect to Mössbauer spectroscopy". In: *Mössbauer Spectroscopy*. Ed. by Uli Gonser. Topics in Applied Physics. Springer, pp. 1–50. ☑.

Kalvius, Michael and Paul Kienle, eds. (2012). *The Rudolf Mössbauer Story*. Springer. ☑.

Klingelhöfer, G. et al. (2006). "Two earth years of Mössbauer studies of the surface of Mars with MIMOS II". In: *Hyperfine Interact.* 170.1-3, pp. 169–177. ☑.

Moon, PB (1951). "Resonant nuclear scattering of gamma-rays: Theory and preliminary experiments". In: *Proceedings of the Physical Society. Section A* 64.1, p. 76. ☑.

Mössbauer, Rudolf L (1958a). "Kernresonanzabsorption von Gammastrahlung in Ir191". In: *Naturwissenschaften* 45.22, pp. 538–539. ☑.

– (1958b). "Kernresonanzfluoreszenz von Gammastrahlung in Ir191". In: *Zeitschrift für Physik* 151.2, pp. 124–143. ☑.

– (1961). "Recoilless nuclear resonance absorption". In: *Nobel Lecture*. ☑.

– (2000). "The discovery of the Mössbauer effect." In: *Hyperfine Interact.* 126. ☑.

Potzel, W et al. (1992). "Gravitational redshift experiments with the high-resolution Mössbauer resonance in^{67}Zn". In: *Hyperfine Interact.* 72. ☑.

Schatz, Günter, Alois Weidinger, and Manfred Deicher (2010). *Nukleare Fest-körperphysik*. 4., überarb. Aufl. Wiesbaden: Vieweg + Teubner.

Wegener, Horst (1966). *Der Mössbauer-Effekt und seine Anwendungen in Physik und Chemie*. Mannheim: Bibliogr. Inst.

Part II

Concept: Hybridization

Chapter 6
Hybridization in classical systems

Markus Lippitz
November 8, 2023

Overview

'Hybridization' is, according to the Cambridge dictionary, 'the process of producing a plant or animal from two different types of plant or animal'. In chemistry, 'orbital hybridization' plays an important role in describing hydrocarbons, for example. Here we want to broaden the view and describe various coupling phenomena from the point of view of hybridization. When two systems couple, they lose their original individual properties, and combined properties emerge. In this chapter we discuss systems of classical physics without quantum mechanics, namely classical mechanical pendulums, phonons in crystals, and Rayleigh scattering of assemblies of nanoparticles.

Coupled Pendulum

A mathematical pendulum of point mass m and rod length L is governed by the differential equation of its angular displacement ϕ in the approximation of small angles $|\phi| \ll 1$

$$\ddot{\phi} + \frac{g}{L}\,\phi = 0 \quad \text{with} \quad \omega^2 = \frac{g}{L} \quad , \tag{6.1}$$

where g is the acceleration due to gravity and ω its angular eigen-frequency. When two of such pendulums are coupled by a spring between the two masses, we get a coupled system of differential equations

$$\ddot{\phi}_1 + \frac{g}{L_1}\,\phi_1 + \frac{k}{m_1}\,(\phi_1 - \phi_2) \;=\; 0 \tag{6.2}$$

$$\ddot{\phi}_2 + \frac{g}{L_2}\,\phi_2 - \frac{k}{m_2}\,(\phi_1 - \phi_2) \;=\; 0 \tag{6.3}$$

with the spring constant k. For the moment, we assume that the pendulums are identical, i.e., $L = L_1 = L_2$ and $m = m_1 = m_2$. The eigen-frequencies are then

$$\omega_+^2 = \frac{g}{L} \quad \text{and} \quad \omega_-^2 = \frac{g}{L} + 2\frac{k}{m} \quad , \tag{6.4}$$

where in the mode with frequency ω_+ both masses move to the same direction, in the ω_- in opposite directions. Only in the latter case the coupling spring comes into play.

To investigate the general case, we assume harmonic oscillations, i.e. $\phi(t) = \phi_0 \, \exp(i\omega t)$ and write the differential equation as matrix

$$\boldsymbol{M}\,\boldsymbol{\phi} = \begin{pmatrix} \frac{g}{L_1} + \frac{k}{m_1} & -\frac{k}{m_1} \\ -\frac{k}{m_2} & \frac{g}{L_2} + \frac{k}{m_2} \end{pmatrix} \boldsymbol{\phi} = \omega^2 \, \boldsymbol{\phi} \quad . \tag{6.5}$$

We thus search eigen-values and eigen-vectors of $\boldsymbol{M}$. Assuming individual lengths, but identical masses, we get

$$\omega_\pm^2 = \left(\frac{\omega_1^2 + \omega_2^2}{2} + \frac{k}{m} \right) \pm \sqrt{ \left(\frac{\omega_1^2 - \omega_2^2}{2} \right)^2 + \left(\frac{k}{m} \right)^2 } \quad . \tag{6.6}$$

For identical lengths, i.e., identical eigen-frequencies $\omega_1 = \omega_2$, this recovers the results from above.

We see here already the common theme of hybridization: two systems couple. Depending on the ratio of coupling constant (here k/m) and energy difference (here $\omega_1^2 - \omega_2^2$), the new eigen-frequencies (or eigen-energies) are closer to the original ones, or split around some kind of average value.

Two coupled oscillators

Lets do the same with two springs of spring constant K. Each spring connects a mass $m_{1,2}$ to the wall, and the masses are connect by a third (coupling) spring of constant κ. The differential equation in matrix form for harmonic motion along x reads

$$\boldsymbol{M}\,\boldsymbol{x} = \begin{pmatrix} \frac{K+\kappa}{m_1} & -\frac{\kappa}{m_1} \\ -\frac{\kappa}{m_2} & \frac{K+\kappa}{m_2} \end{pmatrix} \boldsymbol{x} = \omega^2 \, \boldsymbol{x} \quad . \tag{6.7}$$

The solutions look very similar to above. For equal masses we get

$$\omega_+^2 = \frac{K}{m} \quad \text{and} \quad \omega_-^2 = \frac{K + 2\kappa}{m} \quad . \tag{6.8}$$

Normal modes

How does one handle a system of N masses, all connected by more or less harmonic potentials? This is a problem of classical mechanics and leads to the normal modes.[1]

We use mass-weighted generalized coordinates $q_i = \sqrt{m_i}\Delta\tilde{q}_i$, where the index i runs over all atoms and all spatial directions, i.e., from 1 to $3N$. m_i is the mass of the associated atom and $\Delta\tilde{q}_i$ is the deviation from the equilibrium position. Thus, the kinetic energy T is

$$T = \frac{1}{2} \sum_{i=1}^{3N} \dot{q}_i^2 \quad . \tag{6.9}$$

For the potential we use a Taylor expansion in q_i. We set the zero of the energy scale to the minimum of the potential. Thus the first two terms of the

[1] see for example chapter 6.3 in Demtröder, 2013

Taylor series disappear and we keep only the next one:

$$V \approx \frac{1}{2} \sum_{i,k=1}^{3N} \frac{\partial V}{\partial q_i \partial q_k} \, q_i \, q_k = \cdot \frac{1}{2} \sum_{i,k=1}^{3N} b_{ik} \, q_i \, q_k \quad . \qquad (6.10)$$

Thus we can write the Lagrangian function $L = T - V$ and obtain in this formalism the equations of motion

$$\ddot{q}_i + \sum_{k=1}^{3N} b_{ik} \, q_k = 0 \quad \text{for} \quad i = 1 \ldots 3N \qquad (6.11)$$

or as a matrix with $\tilde{\mathbf{B}} = (b_{ik})$ and $\mathbf{q} = (q_i)$

$$\ddot{\mathbf{q}} + \tilde{\mathbf{B}} \cdot \mathbf{q} = 0 \quad . \qquad (6.12)$$

This is a system of $3N$ coupled differential equations. To decouple them we diagonalize $\tilde{\mathbf{B}}$, and find $3N$ eigenvectors $\mathbf{q}_n^0$ and (potentially degenerate) eigenvalues λ_n so that

$$\tilde{\mathbf{B}} \cdot \mathbf{q}_n^0 = \lambda_n \mathbf{q}_n^0 \quad \text{and thus} \quad \mathbf{q}_n(t) = \mathbf{q}_n^0 \, e^{i \, t \, \sqrt{\lambda_n}} \quad . \qquad (6.13)$$

The eigenvectors $\mathbf{q}_n^0$ are called *normal modes*. Thus, they describe the simultaneous motion of all nuclei in all spatial directions at normal mode n with frequency[2] $\omega_n = \sqrt{\lambda_n}$. Since the b_{ik} are real-valued, in the normal mode all atoms oscillate in phase, thus making the zero crossing simultaneously, and of course at the same frequency. In the basis of normal modes the potential simplifies: it has only quadratic forms of the kind $\frac{1}{2} k q_i^2$ but no bi-linear ones of the kind $\frac{1}{2} k q_i q_k$, otherwise $\tilde{\mathbf{B}}$ would not be diagonalized.

[2] some λ_n must be zero, since there can be only $3N - 5$ (or 6) normal modes

Chain of coupled masses

As an example, lets look at the classical chain of coupled masses. We assume all N masses and springs to be equal and take only a movement along the chain into account. The potential then reads

$$U = \frac{1}{2} \kappa \sum_{n=1}^{N-1} (\tilde{q}_n - \tilde{q}_{n+1})^2 \qquad (6.14)$$

or

$$U = \frac{1}{2} \frac{\kappa}{m} \sum_{n=1}^{N-1} (q_n - q_{n+1})^2 \quad . \qquad (6.15)$$

When multiplied out, we get the squared terms q_n^2 twice, except for the first and last mass in the chain. And we get terms of neighboring masses $-2q_n q_{n+1}$. The cross-terms end up in the sub- and super-diagonals, and we get the matrix B as

$$B = \frac{\kappa}{m} \begin{pmatrix} 1 & -1 & 0 & 0 & \cdots & 0 \\ -1 & 2 & -1 & 0 & \cdots & 0 \\ 0 & -1 & 2 & -1 & \cdots & 0 \\ 0 & 0 & -1 & 2 & \cdots & 0 \\ \vdots & & & & & \vdots \\ 0 & & \cdots & & -1 & 1 \end{pmatrix} \quad . \qquad (6.16)$$

We determine the eigenvalues λ_n and from them the eigen-frequencies $\omega_n = \sqrt{\lambda_n}$. We find that

$$\omega_n^2 = \frac{2\kappa}{m}\left[1 - \cos\left(\frac{n-1}{N}\pi\right)\right]$$

(6.17)

and the eigenvectors describe oscillatory patterns.

What happened here? We coupled oscillators, and the new hybridized system has new eigenfrequencies. If we use many oscillators, we get a continuous band of eigenfrequencies that spans symmetrically around $\omega = \sqrt{2\kappa/m}$, which is what we would get if a single mass were attached to a wall by two springs.

Analytic approach

Matrix diagonalization is fine, but tedious for large matrices. Even the derivation of eq. 6.17 is beyond my capabilities. I only knew the end of this section. So let us take a different approach.

We now *assume* that the deviation of the masses from their rest position follows a harmonic pattern, which we describe by a wave vector $k = 2\pi/\lambda$. This way we know what all the masses are doing and we can use an analytical approach. Let u_s be the deviation of the mass s from its equilibrium position. The force on the mass s is then

$$F_s = \sum_p \kappa_p \left(u_{s+p} - u_s\right)$$

(6.18)

with the spring constant κ_p, which describes how the mass under consideration is linked to another mass p lattice sites away. Thus, only the relative displacement of the masses with respect to each other enters. The equation of motion thus becomes

$$m\frac{d^2 u_s}{dt^2} = \sum_p \kappa_p \left(u_{s+p} - u_s\right)$$

(6.19)

where we have used that all masses are equal. With the ansatz of a plane wave the deviation of the mass with the index $s + p$ becomes

$$u_{s+p} = U_0\, e^{-i(\omega t - k\, a\, (s+p))}$$

(6.20)

with the length k of the wave vector in reciprocal space and the distance a of the lattice points in real space. The term $a(s + p)$ thus describes the equilibrium position of the mass under consideration in real space. If we insert this ansatz into the equation of motion we get

$$-\omega^2 m = \sum_p \kappa_p \left(e^{ik\, a\, p} - 1\right) \quad .$$

(6.21)

Since all masses are identical, $\kappa_p = \kappa_{-p}$ is reasonable and therefore

$$\omega^2 = \frac{2}{m}\sum_{p=1}^{\infty} \kappa_p \left(1 - \cos(k\, a\, p)\right) \quad .$$

(6.22)

Such a relation between frequency ω and wave vector k is called *dispersion relation*. It is equivalent to a relation between energy and momentum.

Now we make the additional assumption that only nearest neighbors interact with each other, as in the last section. Thus only $\kappa_{\pm 1} = \kappa$ are different from zero and the sum is omitted. We now also take the root and get

$$\omega = \sqrt{\frac{4\,\kappa}{m}}\left|\sin\left(\frac{1}{2}\,k\,a\right)\right|\quad.\tag{6.23}$$

Three dimensions

In three dimensions, we do the same, just keeping track of all neighbors becomes a bit more demanding. Lets discuss the example of copper. It has a face-centered cubic (fcc) crystal structure with a monatomic basis. The reciprocal lattice is thus body-centered cubic (bcc). The lattice constant is 3.6 Å.

Our ansatz for the deviation $\mathbf{u}$ from the equilibrium position now contains vectors, $\mathbf{u}_0$ for the amplitude and direction, and $\mathbf{k}$ for the wave vector:

$$\mathbf{u} = \mathbf{u}_0\, e^{i(\mathbf{k}\mathbf{r}-\omega t)}\quad.\tag{6.24}$$

We take only displacements of the masses in the direction $\hat{\mathbf{n}}_i$ of the spring into account and sum over all $i = 1\ldots 12$ nearest neighbors. In an fcc-lattice, the neighbors are along the diagonal of each cartesian plane. The sum reads

$$m\frac{d^2\mathbf{u}}{dt^2} = \sum \kappa_i\left[(\mathbf{u}(\mathbf{r}_i) - \mathbf{u}(0))\cdot\hat{\mathbf{n}}_i\right]\hat{\mathbf{n}}_i\quad.\tag{6.25}$$

We insert our ansatz for $\mathbf{u}$ and get

$$-\omega^2 m\,\mathbf{u}_0 = \sum \kappa_i\,(e^{i\mathbf{k}\mathbf{r}_i} - 1)[\mathbf{u}_0\cdot\hat{\mathbf{n}}_i]\,\hat{\mathbf{n}}_i\quad.\tag{6.26}$$

This is again an eigen-value equation

$$\mathbf{A}\mathbf{u}_0 = -\omega^2 m\mathbf{u}_0\tag{6.27}$$

with

$$\mathbf{A}_{uv} = \sum C_i\,(e^{i\mathbf{k}\mathbf{r}_i} - 1)\,\hat{\mathbf{n}}_{i,u}\,\hat{\mathbf{n}}_{i,v}\tag{6.28}$$

where $\hat{\mathbf{n}}_{i,v}$ is the v-th cartesian component of the normal vector in direction of atom i.

For each value of $\mathbf{k}$, we construct the 3×3 matrix $\mathbf{A}$ and calculate its eigen-values. We thus obtain a function $\omega(\mathbf{k})$ that has at each point three solutions that are potentially degenerate (see also Pluto script[3]). This is the dispersion relation. This simple model fits rather nicely the measured data (Fig.6.3). The entire figure represents the frequency of phonons along a path in reciprocal space shown in Figure 6.2. One can take advantage of the fact that reciprocal lattice vectors $\mathbf{G}$ can be added without changing anything. There are only acoustic branches because there is only one atom in the base. The transverse modes are doubly degenerate along the highly symmetric directions. In the [110] direction, the degeneracy is removed.
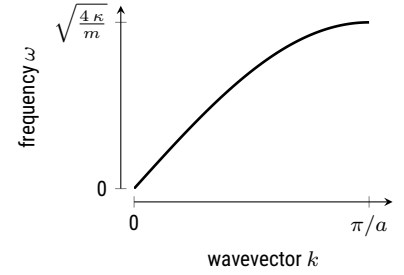
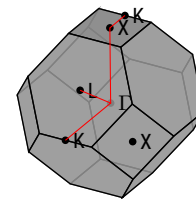Figure 6.1: Dispersion relation of a chain of identical masses and springs.

Figure 6.2: Points of high symmetry in the Brillouin zone are marked by large letters. the Γ point is the center of the BZ, so $k = 0$. The path Γ–X–K–Γ–L takes advantage of the symmetry of the Brillouin zone.
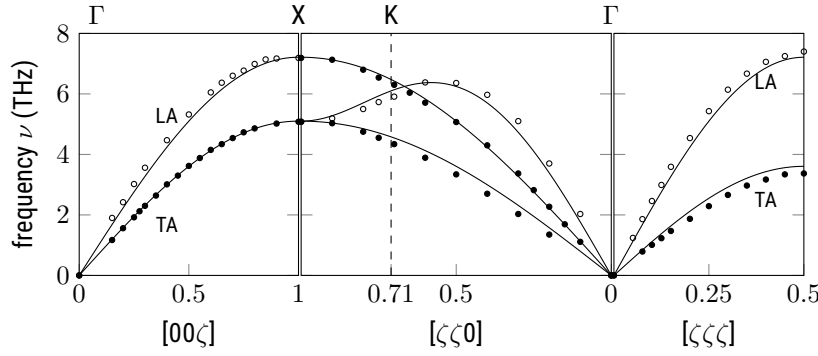
[3] download   run on binder

Figure 6.3: Phonon dispersion in copper (data from Svensson, Brockhouse, and Rowe, 1967) compared to the spring model. The only scaling parameter is the maximum frequency.

Rayleigh scattering of small spheres

And now to something completely different. As oscillators, we use now the collective oscillation of conduction electrons in small metal spheres. These oscillators couple with each other, as each oscillating sphere radiates an electromagnetic wave that interacts with the electrons of the other spheres. We will again find hybridized states with new eigen-frequencies, now in the visible spectral range.

A sphere of radius R and dielectric constant ϵ_{in} is embedded in a medium of dielectric constant ϵ_{out}. We assume that the radius R is much smaller than the wavelength λ of the electromagnetic light field. This means that the phase is constant across the sphere and that we can employ the quasi-static approximation. One solves the Laplace equation taking boundary conditions and symmetry into account.[4,5,6] The sphere responds to the light field with a polarization of

$$\mathbf{p}(t) = \epsilon_0\,\epsilon_{out}\,\alpha\,\mathbf{E}(t) \tag{6.29}$$

with the polarizability

$$\alpha = 4\pi\,R^3\,\frac{\epsilon_{in} - \epsilon_{out}}{\epsilon_{in} + 2\epsilon_{out}} \quad . \tag{6.30}$$

We find a resonance when $\epsilon_{in}(\omega) + 2\epsilon_{out}(\omega) = 0$, which requires one dielectric function to be negative, as it is the case in metals. Small metal particles show thus exceptional strong interaction with light in a certain spectral range. This is the particle plasmon resonance.

As the electric field oscillates $E(t) = E_0\,e^{-i\omega t}$, also the polarization p oscillates and radiates a secondary, scattered electromagnetic field

$$\mathbf{E}_S = \frac{e^{i\,kr}}{4\pi\epsilon_0\,\epsilon_{out}}\frac{1}{r^3}\left\{(kr)^2\,(\hat{\mathbf{r}}\times\mathbf{p})\times\hat{\mathbf{r}} + (1 - ikr)\,(3\hat{\mathbf{r}}\,[\hat{\mathbf{r}}\cdot\mathbf{p}] - \mathbf{p})\right\} \quad , \tag{6.31}$$

where $k = 2\pi/\lambda$ is the length of the wave vector in the medium. In a driven oscillator, we need a 90 degree phase difference between driving force and oscillator to transfer energy. The power that is absorbed by the dipole[7] is thus

$$P_{abs} = \frac{\omega}{c}\,\Im\left(\mathbf{p}\,\mathbf{E}^\star\right) \quad , \tag{6.32}$$

so that we get the absorption cross section

$$\sigma_{abs} = k\,\Im(\alpha) = 4\pi\,k\,R^3\,\Im\left(\frac{\epsilon_{in} - \epsilon_{out}}{\epsilon_{in} + 2\epsilon_{out}}\right) \quad . \tag{6.33}$$

[4] Jackson, 1999.

[5] Nolting, 2016, excercise 2.4.2.

[6] Bohren and Huffman, 2007, chapter 5.2.

[7] Novotny and Hecht, 2012, Chapter 8.

We assume that the surrounding medium is a transparent dielectric, i.e., ϵ_{out} is real-valued. The material of the nanosphere should be described by the Drude model of metals. This is often the case when one is far enough away from inter-band transitions that lead to the color of metals, i.e., when one is far enough in the infrared. The dielectric function then reads

$$\epsilon_{in}(\omega) = \epsilon_{\infty} - \frac{\omega_P^2}{\omega\,(\omega\,+\,i\,\gamma)} \quad , \tag{6.34}$$

where ϵ_{∞} is the high-frequency limit, $\gamma = 1/\tau_{\text{coll}}$ the damping parameter of the plasma oscillation, and ω_P the plasma frequency

$$\omega_P = \sqrt{\frac{n\,e^2}{m^\star \epsilon_0}} \quad . \tag{6.35}$$

The plasma frequency depends on the effective electron mass $m^\star$ and number density n.

The polarizability α has a resonance when its denominator equals zero, i.e., at $\epsilon_{in}(\omega_{res}) = -2\epsilon_{out}$. For a Drude metal with low damping this happens at

$$\omega_{res} = \frac{\omega_P}{\sqrt{2\epsilon_{out} + \epsilon_{\infty}}} \quad . \tag{6.36}$$

The resonance wavelength in the absorption spectrum thus depends on the plasma frequency of the metal and the dielectric function of the environment.

Plasmon hybridization

Now we hybridize two particle plasmons. We investigate the optical properties of two small Rayleigh particles which are brought close to each other. The optical response of each particle is described by a dipole $\mathbf{p}_i(t)$, where $i = 1, 2$. Each dipole experiences the incident field $\mathbf{E}^{\text{inc}}(\mathbf{r}_i)$ and the field scattered from the other dipole. The sum of these two fields multiplied by the dipole's polarizability α_i has to give in a self-consistent way the dipole moment (see, for example, Myroshnychenko et al., 2008)

$$\begin{aligned}
\mathbf{p}_1 &= \epsilon_0\,\epsilon_{out}\,\alpha_1\left[\mathbf{E}^{\text{inc}}(\mathbf{r}_1) + \mathbf{E}_2^{\text{scat}}(\mathbf{r}_1)\right] \\
\mathbf{p}_2 &= \epsilon_0\,\epsilon_{out}\,\alpha_2\left[\mathbf{E}^{\text{inc}}(\mathbf{r}_2) + \mathbf{E}_1^{\text{scat}}(\mathbf{r}_2)\right] \quad .
\end{aligned} \tag{6.37}$$

The scattered electrical near-field $\mathbf{E}^{\text{scat}}$ of the dipole i at position of the dipole j is given by eq. 6.31 above. As we aim for a large influence of this scattered field, we will need short distances between the dipoles and thus can focus on the near-field contribution of the scattered field

$$\mathbf{E}_i^{\text{scat, nf}}(\mathbf{r}_j) = \frac{1}{4\pi\epsilon_0\,\epsilon_{out}}\frac{1}{d^3}\left(3\hat{\mathbf{r}}_{ij}\left[\hat{\mathbf{r}}_{ij}\cdot\mathbf{p}_i\right] - \mathbf{p}_i\right) \quad , \tag{6.38}$$

where $\hat{\mathbf{r}}_{ij} = \mathbf{r}_j - \mathbf{r}_i$ is a vector of length one pointing from the dipole to the point where the field is evaluated, and d is the distance between the particles.

For simplicity, we assume that both particles have the same dielectric function and are of course embedded in the same medium. We can chose the polarization direction of the incoming electric field $\mathbf{E}^{\text{inc}}$. Things become
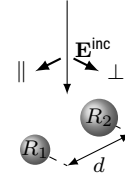

Figure 6.4: Sketch of the light field shining on two small particles

simple when we chose it to be either parallel or perpendicular to the connecting axis of the particles. In both cases, the scattered near-field at particle j has the direction of the dipole i, which is not the case for other polarization directions. This allows us to use scalar dipole amplitudes p_i and a simplified scattered field amplitude

$$E_i^{\text{scat, nf}}(\mathbf{r}_j) = \frac{1}{4\pi\epsilon_0\,\epsilon_{out}}\frac{v}{d^3}\,p_i \quad , \tag{6.39}$$

where the factor v is -1 for perpendicular and $+2$ for parallel polarization.

We solve the equation system for $p_{1,2}$, which we write as effective polarizabilities $\alpha_{1,2}^{\text{eff}}$

$$\alpha_1^{\text{eff}} = \frac{p_1}{\epsilon_0\epsilon_{out}E^{\text{inc}}} = \frac{\alpha_1 - v\frac{\alpha_1\,\alpha_2}{4\pi d^3}}{1 - v^2\frac{\alpha_1\,\alpha_2}{16\pi^2 d^6}} \tag{6.40}$$

and vice versa. The total polarizability[8] is then the sum of α_1^{eff} and α_2^{eff}

$$\alpha^{\text{eff}} = \frac{\alpha_1 + \alpha_2 - v\frac{\alpha_1\,\alpha_2}{2\pi d^3}}{1 - v^2\frac{\alpha_1\,\alpha_2}{16\pi^2 d^6}} \quad . \tag{6.41}$$

We are interested in resonance frequencies of α^{eff}. As both particles are of the same material, the individual polarizability α_i only differ in amplitude due to the factor R_i^3. The spectral shape is the same. The effective polarizability comes to resonance when the denominator vanishes, i.e.

$$R_1^3\,R_2^3\left(\frac{\epsilon_{in}-\epsilon_{out}}{\epsilon_{in}+2\epsilon_{out}}\right)^2 v^2 = d^6 \tag{6.42}$$

or,

$$\frac{\epsilon_{in}-\epsilon_{out}}{\epsilon_{in}+2\epsilon_{out}}\,v = \pm\left(\frac{d}{\sqrt{R_1 R_2}}\right)^3 \quad . \tag{6.43}$$

In total, we obtain the resonance frequency ω_{res} of the coupled two-particle system[9]

$$\omega_{\text{res}} = \frac{\omega_P}{\sqrt{2\epsilon_{out}+\epsilon_\infty}}\sqrt{\frac{1+g}{1+\eta\,g}} \tag{6.44}$$

with

$$\eta = \frac{\epsilon_\infty - \epsilon_{out}}{\epsilon_\infty + 2\epsilon_{out}} \quad \text{and} \quad g = m\left(\frac{\sqrt{R_1\,R_2}}{d}\right)^3 \quad . \tag{6.45}$$

Figure 6.5: Level scheme

In the case of gold particles in vacuum, the factor η takes a value of about $8/11 \approx 0.73$. For the electric field being parallel to the pair axis, the index m assumes the value -2 for parallel dipoles (head to tail) and 2 for anti-parallel dipoles (head-to-head). When the electric field is perpendicular to the pair-axis, m is $+1$ for the parallel configuration and -1 for the anti-parallel configuration.

Finally, lets have a look at the amplitudes of the resonance. We evaluate the enumerator of eq. 6.41 at the resonance condition (eq. 6.42).[10] It becomes

$$\alpha^{\text{eff, peak}} \propto \alpha_1 + \alpha_2 \pm 2\sqrt{\alpha_1\alpha_2} = \left(\sqrt{\alpha_1} \pm \sqrt{\alpha_2}\right)^2 \quad . \tag{6.46}$$

The absorption cross-section is $\sigma_{\text{abs}} = k\Im\alpha$. Two independent particles would just shown an absorption proportional to $\alpha_1 + \alpha_2$. The near-field coupling leads to the term $\pm 2\sqrt{\alpha_1\alpha_2}$. The total absorption is thus redistributed on the two new hybridized states, but in sum remains unchanged. For two equal particles $(R_1 = R_2)$, the symmetric mode caries twice the absorption strength of a single particle and the antisymmetric mode does not show up in the absorption spectrum, as its α_{eff} vanishes.
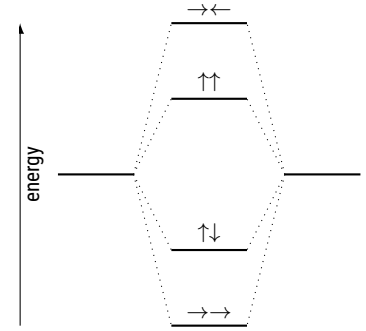
Test yourself

1. Use the Pluto script[11] to investigate the mode splitting in small Rayleigh particles. Compare the absorption spectrum with the analytic equations for resonance position and amplitude. Discuss differences.

Real metals

In the last section, we assumed a Drude metal for both particles. This allowed us to give analytical expressions for peak positions and amplitude. But of course plasmon hybridization also exists for real metals. In stead of the Drude formula (eq. 6.34) we use measured dielectric functions ϵ_{in}, for example from Johnson and Christy[12]. We assume an incoming polarization direction $\mathbf{E}^{inc}$ and wavelength λ. Then we solve the equation system given by eqs. 6.37 to obtain the dipole amplitudes and directions $\mathbf{p}_i$. With this we can calculate the absorption cross section. To get the full absorption spectrum we iterate over the wavelength λ.

[12] Johnson and Christy, 1972.

The effect of a real metal is additional damping due to interband absorption. For gold this happens at wavelengths below about 520 nm, leading to the color of gold. With $\omega_P = 9eV$, $\epsilon_\infty = 9$ and vacuum as medium ($\epsilon_{out} = 1$), the plasmon resonance would appear in the Drude model at $\omega_{res} \approx 2.7$ eV or $\lambda = 460$ nm. The interband absorption shifts the resonance position to about 530 nm wavelength, just at the rim of the absorption band. Plasmon hybridization the splits the peak. The lower wavelength / higher frequency peak overlaps more with interband absorption and will be damped out. Splitting of peaks is thus difficult to observe for small gold nanoparticles.
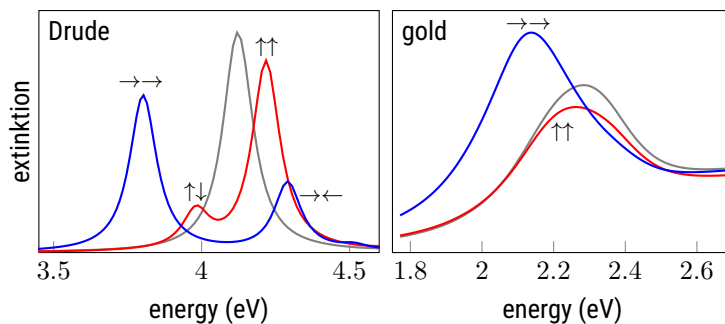

Figure 6.6: Comparison of plasmon hybridization in a Drude metal and in gold. The d-band absorption shifts the resonance and suppresses half of the modes. The simulations assume two spheres of 50 and 90 nm diameter with a gap of 10 nm. They go beyond the Rayleigh approximation and use Doicu, Wriedt, and Eremin, 2006.

Test yourself

2. Use the Pluto script[13] to investigate difference between the Drude model and the measured dielectric function of gold.

3. Plot the hybridized absorption spectrum in the Rayleigh approximation using the measured dielectric function of gold and silver.

References

Aizpurua, Javier and Rainer Hillenbrand (2012). "Localized Surface Plasmons: Basics and Applications in Field-Enhanced Spectroscopy". In: *Plasmonics*. Ed. by Stefan Enoch and Nicolas Bonod. Vol. 167. Springer series in optical sciences. ⬀.

Bohren, Craig F. and Donald R. Huffman (2007). *Absorption and Scattering of Light by Small Particles*. John Wiley & Sons, Ltd. ⬀.

Demtröder, Wolfgang (2013). *Molekülphysik. theoretische Grundlagen und experimentelle Methoden*. 2., überarb. und erw. Aufl. München: Oldenbourg, XVI, 487 S. ⬀.

Doicu, Adrian, Thomas Wriedt, and Yuri Eremin (2006). *Light Scattering by Systems of Particles-Null-Field Method with Discrete Sources-Theory and Programs*. Vol. 124. Springer series in optical sciences. Springer. ⬀.

Jackson, John David (1999). *Classical electrodynamics*. 3. ed. New York [u.a.]: Wiley.

Johnson, Peter B and R.W. Christy (1972). "Optical constants of the noble metals". In: *Physical review B* 6.12, p. 4370. ⬀.

Myroshnychenko, V et al. (2008). "Modelling the Optical Response of Gold Nanoparticles". In: *Chem. Soc. Rev.* 39.49. ⬀.

Nolting, Wolfgang (2016). *Theoretical Physics 3 Electrodynamics*. Springer. ⬀.

Novotny, Lukas and Bert Hecht (2012). *Principles of nano-optics*. 2. ed. Cambridge Univ. Press. ⬀.

Svensson, E. C., B. N. Brockhouse, and J. M. Rowe (1967). "Crystal dynamics of copper". In: *Physical Review* 155.3, p. 619. ⬀.

Chapter 7

Hybridization of quantum mechanical systems

Markus Lippitz
November 25, 2024

Overview

In this chapter we discuss the coupling of systems to be described by quantum mechanics. We start with a toy model to get used to the formalism, and then come to the Hückl method, which is close to the chemical hybridization of atomic orbitals. Here the coupling comes from the overlap of the atomic wave functions. As a second example, we will consider coupling due to the interaction of optical transition dipole moments, leading to so-called molecular H- and J-aggregates. This is the quantum mechanical analog of the interaction of scattering particles presented in the previous chapter.

Variational principle

The Schrödinger equation

$$\hat{H} \left| \Phi \right\rangle = E_0 \left| \Phi \right\rangle \tag{7.1}$$

is a differential equation and not always easy to solve. This is where the variational principle comes in. It says that for an arbitrary wave function $\left| \Psi \right\rangle$ we always have

$$E = \frac{\langle \Psi | H | \Psi \rangle}{\langle \Psi | \Psi \rangle} \geq E_0 \quad . \tag{7.2}$$

E becomes minimal if $\left| \Psi \right\rangle$ solves Schrödinger's equation. But even if $\left| \Psi \right\rangle$ is not a solution of the Schrödinger equation, one can easily calculate Eq. 7.2. So we try different test functions and try to minimise the energy according to Eq. 7.2. This way we get closer and closer to the true eigenfunction, which is the solution of the Schrödinger equation. Unfortunately, we do not know if we could get even smaller values of E by using even better test functions.

We want to investigate what happens when we couple quantum mechanical systems. We already know the solutions ϕ_i of the individual system, so we try to express the new coupled system by a linear combination of the known individual parts:

$$\left| \Psi \right\rangle = \sum_i c_i \left| \phi_i \right\rangle \tag{7.3}$$

with normalized $|\phi_i\rangle$ and real-valued coefficients c_i. This gives

$$\langle\Psi|\Psi\rangle \;=\; \sum_i c_i^2 + \sum_{i,j} c_i c_j \underbrace{\langle\phi_i|\phi_j\rangle}_{=S_{ij}} \tag{7.4}$$

$$\langle\Psi|H|\Psi\rangle \;=\; \sum_i c_i^2 \underbrace{\langle\phi_i|H|\phi_i\rangle}_{=H_{ii}} + \sum_{i,j} c_i c_j \underbrace{\langle\phi_i|H|\phi_j\rangle}_{=H_{ij}} \quad. \tag{7.5}$$

S_{ij} are the respective overlap integrals of the two wavefunctions and H_{ij} the matrix elements of the Hamilton operator. The diagonal elements H_{ii} give the Coulomb energy, and the off-diagonal elements H_{ij} the exchange energy. With these abbreviations, the self-energy can be written as

$$E = \frac{\sum_i c_i^2 H_{ii} + \sum_{i,j} c_i c_j H_{ij}}{1 + \sum_{i,j} c_i c_j S_{ij}} \quad. \tag{7.6}$$

For a minimum self-energy E, the partial derivatives to c_i must both be zero. This can be written as

$$|\mathbf{H} - E\mathbf{S}| = 0 \quad. \tag{7.7}$$

The eigen-energies E are solutions to this equation.

Two coupled states

Let us start with only two states ψ_1 and ψ_2. For simplicity, we label the diagonal entries of $\mathbf{H}$ as E_i and the off-diagonal entries as $H_{ij} = J$, i.e. we assume that both are identical. Without coupling ($J = 0$), the Hamiltonian reads as a matrix

$$\hat{H}_0 = \begin{pmatrix} E_1 & 0 \\ 0 & E_2 \end{pmatrix} \quad. \tag{7.8}$$

When the two states are coupled, then the energy of one state somehow depends on the other. In the matrix this results in an off-diagonal element J

$$\hat{H}_{coupled} = \begin{pmatrix} E_1 & J \\ J & E_2 \end{pmatrix} \quad. \tag{7.9}$$

As a consequence, the original eigen-functions ψ_i are no longer eigen-functions of this coupled Hamilton operator. We find new eigen-functions and eigen-values by diagonalizing $\hat{H}_{coupled}$, so that the diagonal elements become

$$E_\pm = \frac{E_1 + E_2}{2} \pm \sqrt{\left(\frac{E_1 - E_2}{2}\right)^2 + J^2} \tag{7.10}$$

and the new eigen-functions are[1]

$$\psi_\pm = \sqrt{\frac{1 \pm s}{2}}\,\psi_1 \;\pm\; \sqrt{\frac{1 \mp s}{2}}\,\psi_2 \quad, \tag{7.11}$$

with

$$s = \frac{E_1 - E_2}{\sqrt{(E_1 - E_2)^2 + (2J)^2}} \quad. \tag{7.12}$$

[1] Parson, 2015, eq. 8.10.

We can distinguish two limiting cases. The coupling energy J can be larger than the energy difference between the two states, i.e. $|J| \gg |E_1 - E_2|/2$. Then then new eigen-energies are split up by $\pm J$ around the average of the

old eigen-energies $(E_1 + E_2)/2$. The eigen-functions in this situation are symmetric and anti-symmetric combinations of the old eigen-function, i.e. $\psi_\pm = \pm\psi_1 + \psi_2$. When the coupling energy is small, i.e. $|J| \ll |E_1 - E_2|/2$, then the new eigen-energies and eigen-functions are close to the old ones.
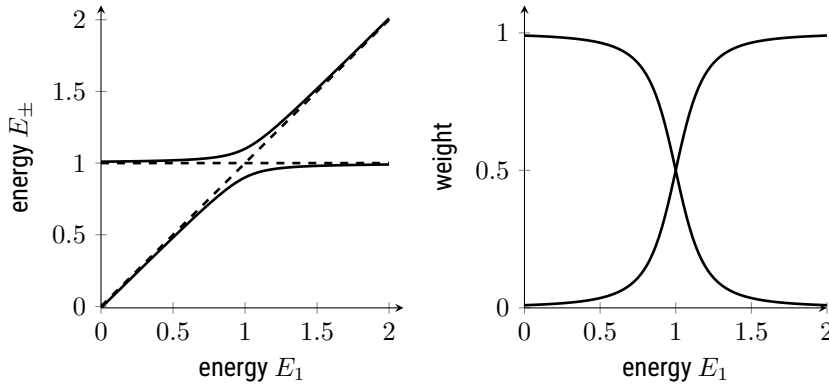

Figure 7.1: Eigen-energies and weights of the eigen-functions as function of the unperturbed energies ($E_2 = 1$).

The Hückel method

A classic example of hybridized quantum mechanical wave functions is the Hückel method for describing aromatic hydrocarbons. In conjugated molecules, the mechanical framework is formed by σ bonds between carbon atoms. A chain of carbon atoms is further linked by alternating σ and π bonds. The electrons involved in these bonds are then delocalised throughout the chain. The Hückel approximation can be used to calculate these extended π orbitals.

Thus, we consider only a subset of all atomic orbitals, only the π orbitals that also participate in the π bond. We assume that

- the atomic orbitals overlap only with themselves, so $S_{ij} = \delta_{ij}$

- all atoms are identical, so $H_{ii} = \alpha$

- exchange takes place only between adjacent orbitals, so $H_{ij} = \beta < 0$ if atoms i and j are adjacent, otherwise 0.

Analogous to equation 7.6 above, we calculate the self-energy according to the variation principle

$$E = \frac{\sum_{i,j} c_i\, c_j\, H_{i,j}}{\sum_{i,j} c_i\, c_j\, S_{i,j}} \quad . \tag{7.13}$$

The minimum self-energy E is obtained when all partial derivatives to the c_i are zero, or when

$$|\mathbf{H} - E\,\mathbf{S}| = 0 \quad . \tag{7.14}$$

Since we have assumed $S_{ij} = \delta_{ij}$, this simplifies to

$$|\mathbf{H} - E\,\mathbb{1}| = 0 \quad . \tag{7.15}$$

So we have to determine the eigenvalues and eigenvectors of $H_{i,j}$. The eigenvalues indicate the energy of the state, the eigenvectors the corresponding linear combination of the atomic orbitals.

As an example we consider benzene (C_6H_6). The 6 carbon atoms are sp^2 hybridized. σ bonds connect the carbon atoms with each other and with the hydrogen atoms. One non-hybridized p-orbital is perpendicular to each ring. These orbitals are considered in the Hückel approximation. The Hamiltonian matrix H_{ij} then has the form (zeros omitted)

$$\mathbf{H} = \begin{pmatrix} \alpha & \beta & & & & \beta \\ \beta & \alpha & \beta & & & \\ & \beta & \alpha & \beta & & \\ & & \beta & \alpha & \beta & \\ & & & \beta & \alpha & \beta \\ \beta & & & & \beta & \alpha \end{pmatrix} \quad . \tag{7.16}$$

The β in the corners close the ring. If we assume $E = \alpha + x\beta$, then the eigenvalue equation simplifies to

$$x^6 - 6x^4 + 9x^2 - 4 = 0 \quad \text{or} \quad x = \pm 1, \pm 1, \pm 2 \quad . \tag{7.17}$$

How to do this numerically you can see in the Pluto script[2].

Since we have to fill a total of 6 electrons into these orbitals, and each orbital can be occupied by 2 electrons (spin up and down), the orbitals with $E = \alpha + 2\beta$ and the two orbitals with $E = \alpha + \beta$ are occupied[3]. Thus, these orbitals also contribute to the binding, since they reduce the total energy by 8β overall. Considering the eigenfunctions, we see that the orbital with $E = \alpha + 2\beta$ is delocalized over the whole ring, the two with $E = \alpha \pm \beta$ over two atoms.

The Hückel approximation in molecular physics corresponds to the *tight binding* method for calculating the band structure of electrons in solid state physics. In solid state physics, one makes the transition from here $N = 6$ atoms to $N = 6 \cdot 10^{23}$ atoms, which then gives rise to $6 \cdot 10^{23}$ closely spaced states for electrons, all described by wave functions similar to Figure 7.2.

Test yourself

1. Compare the electron eigenfunctions of benzene in the Hückel approximation with those of a (possibly annular) box.

Tight binding model

Let us thus repeat the Hückel method, but with the solid state in mind, i.e. many atoms and using plane waves to describe everything. In the following, the tilde denotes variables that apply to a single atom. Let $\tilde{V}$ be the Coulomb-like potential of an atom. We know the solutions $\tilde{\psi}$ of the Schrödinger equation

$$H_A \tilde{\psi} = \left(-\frac{\hbar^2}{2m} \nabla^2 + \tilde{V} \right) \tilde{\psi} = \tilde{E} \tilde{\psi} \quad . \tag{7.18}$$

In the crystal there are now atomic nuclei at the lattice points $\mathbf{R}_m$, which cause an additional perturbation term in the Hamilton operator

$$H_S = \sum_{m \neq n} \tilde{V}(\mathbf{r} - \mathbf{R}_m) \quad , \tag{7.19}$$
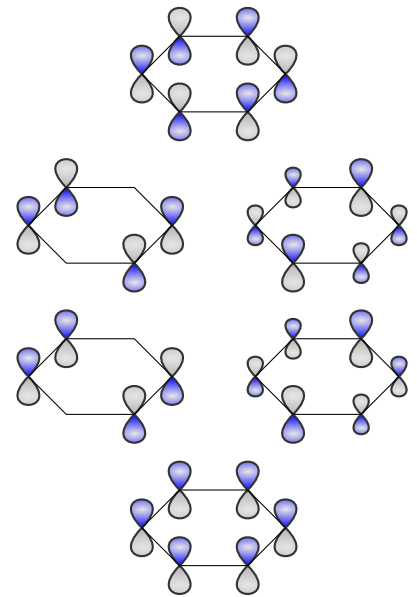
[2] download run on binder

Figure 7.2: Molecular orbitals of benzene in the Hückel approximation. The colors encode the sign of the wave function. The arrangement corresponds to the self-energy.

[3] $\beta < 0$

where the atom at $\mathbf{R}_n$ is already considered in the unperturbed operator. As an ansatz for the wave function, we choose a superposition of atom eigenfunctions at the locations $\mathbf{R}_m$ as in the Hückel method, i.e.

$$\psi = \sum_m a_m \tilde{\psi}(\mathbf{r} - \mathbf{R}_m) \quad . \tag{7.20}$$

Now we use the Bloch theorem[4]: the lattice-periodic part $u_\mathbf{k}$ is provided by the wave functions $\tilde{\psi}(\mathbf{r} - \mathbf{R}_m)$, so the plane wave must be in the coefficients a_m, i.e.

$$a_m \propto e^{i\mathbf{k}\cdot\mathbf{R}_m} \tag{7.21}$$

[4] It would also work without, but makes it easier here

with suitable normalization. This means that the wave function is

$$\psi = \frac{1}{\sqrt{N}} \sum_m \tilde{\psi}(\mathbf{r} - \mathbf{R}_m)\, e^{i\mathbf{k}\cdot\mathbf{R}_m} \quad . \tag{7.22}$$

The self-energy is as always

$$E = \frac{\int \psi^\star\, H\, \psi\, dV}{\int \psi^\star\, \psi\, dV} \quad . \tag{7.23}$$

The denominator is close to one because the atomic wave functions overlap very little. The numerator is more interesting. We can draw the sums over the atomic positions in front of the integral

$$E = \frac{1}{N} \sum_{m,n} e^{i\mathbf{k}\cdot(\mathbf{R}_m - \mathbf{R}_n)} \int \tilde{\psi}^\star(\mathbf{r} - \mathbf{R}_n)\, [H_A + H_S(\mathbf{r} - \mathbf{R}_m)]\, \tilde{\psi}(\mathbf{r} - \mathbf{R}_m) \quad . \tag{7.24}$$

We can distinguish three contributions

- Integrands of the form $\tilde{\psi}_n^\star\, H_A\, \tilde{\psi}_n$. These are the eigen-energies of the atoms that we already know.

- Integrands of the form $\tilde{\psi}_n^\star\, H_S\, \tilde{\psi}_n$. This is the influence of the potentials of the other atoms (in H_S) on 'our' atom n. We abbreviate this Coulomb integral with $-\alpha$.

- integrands of the form $\tilde{\psi}_n^\star\, H_S\, \tilde{\psi}_m$. This is the influence of the overlap with the other wave functions. We abbreviate this transfer integral with $-\beta_m$.

In total, we thus have[5].

$$E = \tilde{E} - \alpha - \sum_m \beta_m\, e^{i\mathbf{k}\cdot(\mathbf{R}_m - \mathbf{R}_n)} \quad . \tag{7.25}$$

[5] The sums over $\tilde{E}$ and α provide an N, which is canceled by the normalization

The Coulomb integral α causes a decrease in energy because the neighboring atoms also contribute some attractive Coulomb potential. The transfer integral β can be both positive and negative, and also direction-dependent, as in the case of covalent bonding in molecular physics. There, too, we saw that s and p orbitals can provide attractive or repulsive energy contributions depending on their arrangement. Exactly the same thing happens here. This integral provides the dependence on the wave vector $\mathbf{k}$ and thus the dispersion relation.

Example: cubic-primitive lattice

As an example, we consider a cubic-primitive lattice, only allow interaction between nearest neighbors, and assume the interaction to be direction-independent, as it would be for atomic s-orbitals. For the term $\mathbf{R}_m - \mathbf{R}_n$, only the three (Cartesian) lattice vectors of length a, each with both signs, can be considered. Multiplying out the scalar product results in

$$E = \tilde{E} - \alpha - 2\beta \left[\cos(k_x a) + \cos(k_y a) + \cos(k_z a)\right] \quad . \tag{7.26}$$

In total, this covers a band of width $\tilde{E} - \alpha \pm 6\beta$. The band is cosine-shaped. At the Γ point and at the boundary of the Brillouin zone, it therefore corresponds to the parabolic shape of the empty lattice approximation.

Interaction of light with atoms

I would like to discuss how the coupling between two quantum mechanical systems affects their optical absorption spectrum. Before doing so, we need to set the terms for how quantum mechanics describes light-matter interaction.

Fermi's Golden Rule gives the transition rate from the initial state $|i\rangle$ to the final state $|f\rangle$ caused by any time-dependent perturbation H' to the stationary Hamilton operator H_0 as

Figure 7.3: A light beam induces a transition from $|i\rangle$ to the $|f\rangle$.

$$\Gamma_{i\to f} = \frac{2\pi}{\hbar} \left|\langle f| H' |i\rangle\right|^2 \rho(E) \quad , \tag{7.27}$$

where $\rho(E) = dn/dE = \rho(\omega)/\hbar$ is the density of final states. The idea is that the initial state $|i\rangle$ is well known, but the outcome of the interaction $|f\rangle$ might have free parameters, for example the direction of the emitted electron or the mode of the absorbed photon. The density of states $\rho(E)$ thus can describe either electronic or photonic states, or both.

In general, the interaction of a charged particle with an electromagnetic vector potential $\mathbf{A}$ is described by the perturbation

$$H' = -\frac{i\hbar e}{m} \mathbf{A} \cdot \nabla \quad . \tag{7.28}$$

As the spatial extent of our wavefunctions is small compared to the wavelength of light, we employ the dipole approximation and assume $\exp(i\mathbf{k} \cdot \mathbf{r}) \approx 1$ in the plane-wave description of the vector potential. In this way, the perturbation operator H' simplifies to[6]

[6] see Bransden and Joachain (1996) for details

$$H' = e\,\mathbf{E}(t)\cdot \mathbf{r} = e\,E_0\,\hat{\mathbf{x}} \cdot \mathbf{r}\,\cos(\omega t) \quad , \tag{7.29}$$

where $\hat{\mathbf{x}}$ is a unit vector defining the polarization direction of the light field. We simplify further by using the rotating-wave approximation and keeping only co-rotating parts

$$\cos(\omega t) = \frac{1}{2}\left(e^{i\omega t} + e^{-i\omega t}\right) \approx \frac{1}{2}e^{i\omega t} \tag{7.30}$$

so that

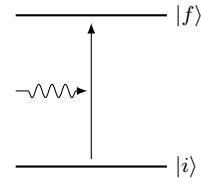$$H' = \frac{e\,E_0}{2}\,\hat{\mathbf{x}} \cdot \mathbf{r}\,e^{i\omega t} \quad . \tag{7.31}$$

We introduce the transition dipole matrix element μ_{if} as

$$\mu_{if} = -e \, \langle f | \, \mathbf{r} \, | i \rangle \quad . \tag{7.32}$$

It has the units of an electric dipole moment, i.e., charge times distance, and is the central element of an optical transition in quantum mechanics. For practical reasons, one uses the unit of 1 Debye = 1 electron displaced by 0.208 Å. With this the matrix element becomes

$$|\langle f | \, H' \, | i \rangle|^2 = \frac{1}{4} E_0^2 \, |\hat{\mathbf{x}} \cdot \mu_{if}|^2 \quad . \tag{7.33}$$

Plugging everything into Fermi's Golden Rule, we get

$$\Gamma_{i \to f} = \frac{\pi}{2\hbar^2} \, E_0^2 \, |\hat{\mathbf{x}} \cdot \mu_{if}|^2 \, \rho(\omega) \quad . \tag{7.34}$$

Now we have to take into account that we use a incoherent multimode light source. The electric field E is here an incoherent superposition of modes with the spectral energy density $u(\omega)$.[7] The total power is thus

[7] see Cohen-Tannoudji, Diu, and Laloë (1977) and Fox (2007) for details

$$\frac{1}{2}\epsilon_0 \, E_0^2 = \int u(\omega) \, d\omega \quad . \tag{7.35}$$

The transition rate is thus

$$\Gamma_{i \to f} = \frac{\pi}{\hbar^2 \epsilon_0} \, |\hat{\mathbf{x}} \cdot \mu_{if}|^2 \int u(\omega)\rho(\omega) d\omega \quad . \tag{7.36}$$

As the atomic transition is narrow compared with the light spectrum, the density of states $\rho(\omega)$ selects the transition frequency ω_{if}

$$\Gamma_{i \to f} = \frac{\pi}{\hbar^2 \epsilon_0} \, |\hat{\mathbf{x}} \cdot \mu_{if}|^2 \, u(\omega_{if}) \quad . \tag{7.37}$$

Both the absorption and the emission spectrum of an atom or a molecule is connected to the transition rate $\Gamma_{i \to f}$ via the Einstein coefficients, but with different pre-factors:

$$\text{absorption} \propto \omega_{if} \, |\mu_{if}|^2 \tag{7.38}$$

$$\text{emission} \propto \omega_{if}^3 \, |\mu_{if}|^2 \quad . \tag{7.39}$$

Transfer of excitation from one molecule to another

In a coupled pendulum, energy is transferred from one pendulum to the other (and back again). Here we will investigate this transfer of excitation for a quantum mechanical system[8]. We have two molecules and each molecule has a wave function of the ground state (a, b) and of an excited state ($a^\star$, $b^\star$). Two electrons (1,2) are involved, but we can not distinguish them, so that we need to construct the usual anti-symmetric wavefunctions. Initially, molecule a should be excited and b in the ground state. The initial wavefunction is thus

[8] More in Köhler and Bässler, 2015 and Valeur and Berberan-Santos, 2012

$$\psi_i = \frac{1}{\sqrt{2}} \left(\psi_{a^\star}(1) \, \psi_b(2) - \psi_{a^\star}(2) \, \psi_b(1) \right) \quad . \tag{7.40}$$

In the final state, the excitation should have swapped, i.e.

$$\psi_f = \frac{1}{\sqrt{2}} \left(\psi_a(1) \, \psi_{b^\star}(2) - \psi_a(2) \, \psi_{b^\star}(1) \right) \quad . \tag{7.41}$$

The two electrons will interact by their Coulomb potential. This is sufficient, as we will see, to swap the excitation. The transition matrix element or interaction energy J is

$$J = \frac{1}{4\pi\epsilon_0} \left\langle \psi_f \left| \frac{e^2}{r_{12}} \right| \psi_i \right\rangle \quad, \tag{7.42}$$

where r_{12} is the distance of the electrons. Multiplying this out, we get two pairs of terms. In each pair, electron 1 and 2 change role. One pair has the form

$$J^C = \frac{2}{4\pi\epsilon_0} \left\langle \psi_{a^\star}(1)\,\psi_b(2) \left| \frac{e^2}{r_{12}} \right| \psi_a(1)\,\psi_{b^\star}(2) \right\rangle \quad, \tag{7.43}$$

i.e., the electrons stay on 'their' molecule but change between excited and ground state. This is called the Coulomb term. In the second pair

$$J^E = \frac{2}{4\pi\epsilon_0} \left\langle \psi_{a^\star}(1)\,\psi_b(2) \left| \frac{e^2}{r_{12}} \right| \psi_a(2)\,\psi_{b^\star}(1) \right\rangle \tag{7.44}$$

the electrons change molecule and take their state (ground vs excited) with them. This is the exchange term. It requires a bond between the molecules for the electrons to move. In the following, we will only look at the first term, the Coulomb term, that acts 'via the air' and drop the C in J^C.

Coupling of two transition dipole moments

The transition matrix element J^C is similar to two charge densities that interact. It was the work of Dexter and Förster to apply a multipole-multipole expansion to simplify things. We keep only the lowest term, the dipole-dipole contribution. The dipoles are transition dipole moments of the form

$$\boldsymbol{\mu}_a = \langle \psi_{a^\star}(1) | e\,\boldsymbol{r} | \psi_a(1) \rangle \tag{7.45}$$

i.e., an electron changes from ground to excited state. The coupling energy J depends on the distance $\boldsymbol{r}_{ab}$ and the relative orientation of the transition dipoles $\boldsymbol{\mu}_{a,b}$. It can be thought of as the energy of one dipole in the field of another.

$$\begin{aligned} J \;&=\; \frac{1}{4\pi\epsilon_0}\left(\frac{\boldsymbol{\mu}_a\cdot\boldsymbol{\mu}_b}{|\boldsymbol{r}_{ab}|^3} - 3\frac{(\boldsymbol{\mu}_a\cdot\boldsymbol{r}_{ab})(\boldsymbol{\mu}_b\cdot\boldsymbol{r}_{ab})}{|\boldsymbol{r}_{ab}|^5}\right) \tag{7.46}\\[4pt] &=\; \frac{\mu_a\mu_b}{4\pi\epsilon_0\,r_{ab}^3}\left(\cos\theta - 3\cos\alpha\,\cos\beta\right) = \frac{\mu_a\mu_b}{4\pi\epsilon_0\,r_{ab}^3}\,\kappa \tag{7.47} \end{aligned}$$

where the angles are defined in the sketch.

We now consider three states: both molecules in the ground state, molecule a excited (ψ_i of last section), and molecule b excited (ψ_f). In matrix form, the Hamilton operator reads

$$\hat{H} = \begin{pmatrix} 0 & \mu_a\mathcal{E} & \mu_b\mathcal{E} \\ \mu_a^\star\mathcal{E}^\star & \hbar\omega_a & J \\ \mu_b^\star\mathcal{E}^\star & J^\star & \hbar\omega_b \end{pmatrix} \quad. \tag{7.48}$$

The transition dipole moments together with an external optical field $\mathcal{E}$ couple the ground state to the excited states. The excited states are coupled by dipole-dipole interaction without the need for an external field. For example, by measuring an absorption spectrum starting from the ground state,
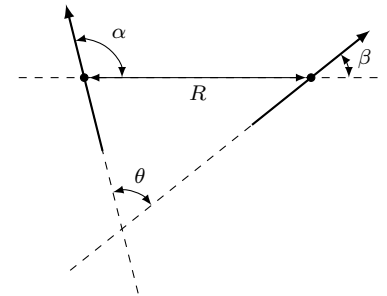

Figure 7.4: Sketch showing The angles used to calculate the coupling factor κ.

we can determine the energies of the excited states, which we can find by diagonalizing the lower 2×2 matrix as discussed above.

The coupling results in new states, which can be written as linear combinations of the uncoupled states. This has an effect on the observables. When $|\psi\rangle$ is a linear combination of ψ_a and ψ_b, then also the transition dipole moment from the ground state to $|\psi\rangle$ is a linear combination of μ_a and μ_b with the same weights. When $J \gg |E_a - E_b|/2$ then we get (see Fig. 7.1)

$$\boldsymbol{\mu}_\pm = \sqrt{1/2} \left(\boldsymbol{\mu}_a \pm \boldsymbol{\mu}_b \right) \quad . \tag{7.49}$$

The brightness of the absorption line is for identical molecules, i.e. $\mu = \mu_a = \mu_b$

$$I \propto |\boldsymbol{\mu}_\pm|^2 = (1/2) \left| \boldsymbol{\mu}_a \pm \boldsymbol{\mu}_b \right|^2 = (1 \pm \cos\theta) \left| \boldsymbol{\mu} \right|^2 \quad , \tag{7.50}$$

where θ is as above the angle between the transition dipole moments.

The spectroscopic signature of coherent coupling between two molecules is thus a splitting of the absorption line into two lines separated by twice the coupling energy J. The sum of the line amplitudes remains unchanged, but in some cases (H- and J-aggregates, see below) one transition takes up the whole amplitude and the other remains dark. In these cases there is no splitting but a shift of the absorption line. The coupling disappears when both dipoles are perpendicular to each other ($\theta = 90°$).

H- and J-aggregates

Two important limiting cases are the H- and J-aggregates.[9] In a J-aggregate the dipoles are oriented parallel and head-to-tail, i.e. $\alpha = \beta = \theta = 0$ and therefore $\kappa = -2$. A negative κ implies that the coupling constant J is negative. The state Ψ_+, which carries all the oscillator strength, has an energy $E_+ = (E_a + E_b)/2 + J$, which is lower than the average energy of the uncoupled states. The absorption line therefore shifts towards the red. The same applies to the fluorescence emission spectrum.

In an H-aggregate the dipoles are also parallel, but side by side, i.e. $\alpha = \beta = 90°$ and $\theta = 0$. In this case $\kappa = 1$ and J is positive. The absorption line shifts to blue when aggregates form, as the Ψ_+ state again gets all the oscillator power. However, as fluorescence emission is slow compared to other relaxation processes, this high energy state does not emit light. H-aggregates appear dark in the emission.

The width of the absorption line of a dye at room temperature is determined by dephasing, i.e. fluctuations in the environment that are fast compared to the lifetime of the excited state, and by static differences in the environment of different chromophores. The spectral position of the absorption line in a molecular aggregate is the average of two single chromophore transitions. As in the propagation of uncertainties in an experiment, the width of the new distribution, generated as an average over two values from the old distribution, is reduced by a factor of $\sqrt{2}$. This applies more generally[10], so that an aggregate of N chromophores is expected to have a spectral line width reduced[11] by $\sqrt{N}$.
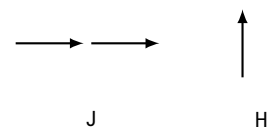

Figure 7.5: J- and H aggregates.

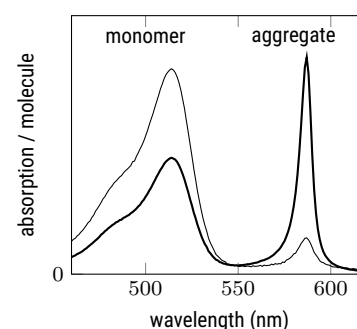[9] Köhler and Bässler, 2015, chapters 2.1.4.3, 2.2.5.3.

Figure 7.6: Absorption spectrum of TDBC dye in solution. When increasing the concentration (thick), more monomers aggregate. (Data by T. Kroh, 2014)

[10] Knapp, 1984.

[11] This is the same physics as motion narrowing in NMR.

References

Bransden, B. H. and C. J. Joachain (1996). *Physics of atoms and molecules*. Longman.

Cohen-Tannoudji, Claude, Bernard Diu, and Franck Laloë (1977). *Quantum Mechanics*. Wiley.

Fox, Mark (2007). *Quantum optics*. Oxford University Press.

Knapp, E.W. (1984). "Lineshapes of molecular aggregates, exchange narrowing and intersite correlation". In: *Chemical Physics* 85.1, pp. 73–82. ☑.

Köhler, Anna and Heinz Bässler (2015). *Electronic processes in organic semiconductors*. Weinheim: Wiley-VCH. ☑.

Parson, William W. (2015). *Modern optical spectroscopy*. Springer. ☑.

Valeur, Bernard and Mario Nuno Berberan-Santos (2012). *Molecular fluorescence*. 2. ed. Weinheim: Wiley-VCH. ☑.

Chapter 8

Hybridization of quantum optical systems

Markus Lippitz
November 28, 2024

Overview

In the previous chapter, it was the electron that was quantized and described by quantum mechanics. The light field was taken as a classical field, continuous in its amplitude. Now we also quantize the optical field into photons, the so-called second quantization. We let an atom, or better an emitter as described by quantum mechanics, interact with a light field that contains so few photons that every single photon counts. This is the field of quantum optics. Again, the two systems 'atom' and 'light field' couple and hybridize, creating a new system. We will no longer be able to say where the quantum of energy is at any given moment, in the atom or in a cavity photon.

Quantization of the light field

We now take the quantized nature of light into account. In quantum mechanics this is often called 'second quantization' and we will briefly have a look at the main results.

The principle idea is very similar to a quantum mechanical harmonic oscillator, i.e. a series of equidistant states that has a bottom boundary. We describe the states by a quantum number n, starting from $n = 0$. The Hamiltonian reads

$$\hat{H}\ket{n} = E_n \ket{n} = \left(n + \frac{1}{2} \right) \hbar\omega \ket{n} \quad , \tag{8.1}$$

where $\hbar\omega$ is the energy distance between the states.

It is convenient to use ladder operators for the creation ($\hat{a}^\dagger$) and annihilation ($\hat{a}$) of a quantum of energy, i.e.

$$\hat{a}^\dagger \ket{n} = \sqrt{n+1} \ket{n+1} \quad \text{and} \quad \hat{a}\ket{n} = \sqrt{n}\ket{n-1} \quad . \tag{8.2}$$

Useful properties are

$$\hat{a}\ket{0} = 0\ket{-1} = 0 \quad \text{and} \quad \hat{a}^\dagger\hat{a}\ket{n} = n\ket{n} \quad . \tag{8.3}$$

Now this needs to be connected to classical electrodynamics. We assume a single optical mode in a small optical resonator, similar to a laser cavity.

In the dark, i.e. in the state $|0\rangle$, quantum mechanics gives an eigen-energy $E_0 = 1/2\,\hbar\omega$. This is what we require also from classical electrodynamics[1]

$$E_0 = \int_{\text{cavity}} \frac{1}{2} \left(\boldsymbol{H} \cdot \boldsymbol{B} + \boldsymbol{E} \cdot \boldsymbol{D} \right) d\boldsymbol{r} = \int_{\text{cavity}} \epsilon_0 \boldsymbol{E}^2 \, d\boldsymbol{r} = \frac{1}{2}\,\hbar\omega \qquad (8.4)$$

so that

$$E_{vac} = \sqrt{\frac{\hbar\omega}{2\epsilon_0\,V}} \qquad (8.5)$$

is the amplitude of the field in the dark vacuum, with V being the volume of the cavity.[2] One obtains the volume by integrating over full space, weighted by the local intensity

$$V = \frac{1}{\max(\boldsymbol{E}_c)^2} \int_{\text{cavity}} \boldsymbol{E}_c^2 \, d\boldsymbol{r} \quad , \qquad (8.6)$$

where $\boldsymbol{E}_c$ can be a field of any amplitude inside the cavity. It just defines the spatial distribution of the optical mode. The vacuum field in total is thus

$$\boldsymbol{E}(\boldsymbol{r}) = \frac{E_{vac}}{\max(\boldsymbol{E}_c)} \, \boldsymbol{E}_c(\boldsymbol{r}) \qquad (8.7)$$

The electrical field of a single optical mode in a cavity then becomes[3,4]

$$\hat{\boldsymbol{E}}(z,t) = \hat{\boldsymbol{x}}\, E_{vac} \left(\hat{a}\, e^{i(kz-\omega t)} + \hat{a}^\dagger\, e^{-i(kz-\omega t)} \right) \quad , \qquad (8.8)$$

where $\hat{\boldsymbol{x}}$ is a unit vector defining the direction of polarization.

Test yourself

1. Two flat perfect mirrors of diameter d and separation L form a resonator. Calculate its mode volume at an eigenfrequency, assuming that no field leaks out of the cylinder formed by the mirrors. How would the refractive index of a medium between the mirrors enter?

2. In an elevator cabin, two opposing walls are covered by mirrors. Calculate the amplitude of the electric field in the dark cabin.

Pauli matrices for atoms

The two-level system representing our atom is a spin $1/2$ system, i.e., a Fermion, not a Boson as the photons in the cavity. We can use operators similar to the ladder operators to excite ($\hat{\sigma}_+$) or relax ($\hat{\sigma}_-$) the two-level system

$$\hat{\sigma}_+ = |e\rangle \langle g| \quad \text{and} \quad \hat{\sigma}_- = |g\rangle \langle e| \quad . \qquad (8.9)$$

The third operator to complete the Pauli spin algebra is the inversion operator, i.e. the third component of the Bloch vector

$$\hat{\sigma}_3 = |e\rangle \langle e| - |g\rangle \langle g| \quad . \qquad (8.10)$$

Test yourself

3. Write the operators $\hat{\sigma}_+$, $\hat{\sigma}_-$ and $\hat{\sigma}_3$ in matrix form.

Jaynes-Cummings-Model

Now we put everything together to the Jaynes-Cummings-model. Sometimes this model is also called 'dressed atom' model.[5,6,7,8]

[5] Rand, 2016, chap. 6.8.
[6] Gerry and Knight, 2005, chap. 4.5.
[7] Fox, 2007, chap. 10.4.
[8] Haroche, 2006, chap. 3.4.

We construct an Hamiltonian of three parts: atom, optical field, and light-matter interaction. The atom part is, using $\hbar\omega_0 = E_e - E_g$

$$\hat{H}_A = \frac{1}{2}\,\hbar\omega_0\,\hat{\sigma}_3 \quad , \tag{8.11}$$

where we have set the zero of the energy scale half way between ground and excited state. The optical field part is

$$\hat{H}_F = \hbar\omega\,\hat{a}^\dagger\hat{a} \quad , \tag{8.12}$$

with the optical frequency ω and the zero of the energy scale set to the vacuum energy. Light-matter interaction is given in the dipole approximation and neglecting terms that violate energy conservation by[9]

[9] Rand, 2016, chap. 6.7.1.

$$\hat{H}_I = -\boldsymbol{\mu}\,\boldsymbol{E} = \hbar g\,(\hat{\sigma}_+\,\hat{a} + \hat{\sigma}_-\,\hat{a}^\dagger) \quad . \tag{8.13}$$

Absorption of a photon ($\hat{a}$) excites the atom ($\hat{\sigma}_+$) and the other way round. The coupling constant g is given by

$$g = \frac{\mu_{eg}\,E_{vac}}{\hbar} = \mu_{eg}\,\sqrt{\frac{\omega}{2\hbar\,\epsilon_0\,V}} \quad , \tag{8.14}$$

where μ_{eg} is the projection of the transition dipole moment on the polarization direction of the light field. In total we have thus

$$\hat{H} = \frac{1}{2}\,\hbar\omega_0\,\hat{\sigma}_3 + \hbar\omega\,\hat{a}^\dagger\hat{a} + \hbar g\,(\hat{\sigma}_+\,\hat{a} + \hat{\sigma}_-\,\hat{a}^\dagger) \quad . \tag{8.15}$$

The idea of the Jaynes-Cummings-Model is to find eigen-states of this Hamiltonian. This is the same idea as in a coupled pendulum: the atom is one pendulum, the light field another, and the spring connecting the pendula is the coupling constant g. The uncoupled eigen-states are $|g,n\rangle$ and $|e,n-1\rangle$, i.e. atom in ground or excited state, and either n or $n-1$ photons in the cavity. For these two states, the Hamilton operator reads in matrix form

$$\hat{H} = \hbar\begin{pmatrix} n\omega - \frac{1}{2}\omega_0 & g\sqrt{n} \\ g\sqrt{n} & (n-1)\omega + \frac{1}{2}\omega_0 \end{pmatrix} \quad . \tag{8.16}$$

The new eigen-states are linear combinations of the old, obtained by diagonalizing the Hamilton operator in matrix form. For the eigen-energy we get

$$E_\pm = \left(n - \frac{1}{2}\right)\hbar\omega \pm \frac{1}{2}\hbar\sqrt{\Delta^2 + 4|g|^2 n} \quad , \tag{8.17}$$

where $\Delta = \omega_0 - \omega$ is energy difference between the uncoupled eigen-states, or the detuning between atom and field. The square-root is called generalized Rabi frequency $\Omega_R = \sqrt{\Delta^2 + 4|g|^2 n}$. The new eigen-states are called dressed states $|D_\pm\rangle$ as the photons are 'dressing' the atom

$$|D_+\rangle = \sin\theta\,|g,n\rangle + \cos\theta\,|e,n-1\rangle \tag{8.18}$$

$$|D_-\rangle = \cos\theta\,|g,n\rangle - \sin\theta\,|e,n-1\rangle \tag{8.19}$$

with $\cos 2\theta = \Delta/\Omega_R$. On resonance, i.e. $\Delta = 0$, the two dressed states are the symmetric and anti-symmetric combinations of the uncoupled states.

Test yourself

4. Convince yourself that the Hamilton operators $\hat{H}_A$ and $\hat{H}_F$ indeed give the energy of atom and field.

5. Derive the matrix form of the total Hamilton operator, eq. 8.16, especially that the two off-diagonal element are the same.

6. Why and how is the interaction part of the Hamiltonian $\hat{H}_I$ *coupling* the two states? What is rotating with the angular frequency g? Compare to the spring between two pendula.

7. Play with https://demonstrations.wolfram.com/CavityQuantumElectrodynamicsWithBosonsEmissionSpectraInTheSt

Mollow Triplet

We now label the above dressed states by their characteristic photon number n as $|D_+^{(n)}\rangle$ and $|D_-^{(n)}\rangle$. This allows us to take into account also the two states $|D_+^{(n+1)}\rangle$ and $|D_-^{(n+1)}\rangle$. When $n \gg 1$ as in a laser field, we can assume that the Rabi frequency $\Omega_R = \sqrt{\Delta^2 + 4|g|^2 n}$ does not differ between these states. In this case, the four optical transitions that take out energy will lead to only three different lines in the spectrum. This is called the Mollow Triplet. The (degenerate) center line is at the laser frequency, the outer two separated by the Rabi frequency.

An example is shown in Figure 8.1. In fact, you do not really need a cavity, just a strong laser beam. In this experiment by Wrigge et al., single dye molecules (dibenzanthanthrene, DBATT) are dispersed in a matrix of other organic molecules (tetradecane) and cooled to a temperature of 1.4 K. At this low temperature, the molecules behave almost like a two-level system, emitting at a wavelength of about 590 nm. The line width is lifetime limited, i.e. as narrow as physically possible. A narrow-band laser is used to excite the molecule at resonance ($\Delta = 0$). The light scattered by the molecule is spectrally analyzed by a narrow scanning filter, a Fabry-Perot cavity. The resulting spectrum in Fig. 8.1 shows the central laser peak overlapping with one of the transitions of the Mollow triplet. The latter causes the two side peaks of lower intensity (note the logarithmic scaling). The splitting of the triplet depends on the laser power or the number n of photons in the cavity.
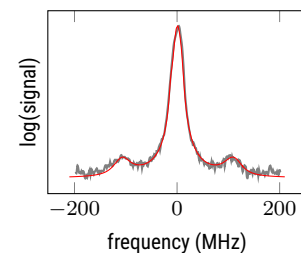

Figure 8.1: Mollow triplet in the light scattered at a single molecule at 1.4K. Data from Wrigge et al., 2008.

Test yourself

8. Draw a level scheme containing the uncoupled and the coupled states involved in the Mollow Triplet and the resulting spectrum. Which transition leads to which peak?

9. Play with https://demonstrations.wolfram.com/MollowTriplet

Vacuum Rabi Splitting and Photon Blockade

The splitting into dressed states $|D_+^{(n)}\rangle$ and $|D_-^{(n)}\rangle$ does only exist for a photon number $n \geq 1$. The uncoupled state $|g, n = 0\rangle$ cannot couple with the non-existing state $|e, n = -1\rangle$. The lowest state in the ladder does thus not split. From there we can reach two states, $|D_+^{(1)}\rangle$ and $|D_-^{(1)}\rangle$, by

absorbing a single photon in the system. These two states are at $\omega_0 \pm \hbar g$. (as $\omega_{cav} = \omega_{atom}$). This effect is called Vacuum Rabi Splitting, as it exists in the dark. The photon is only needed to detect its presence.

A consequence of this effect is the photon blockade. The first photon can be absorbed at $\omega_0 \pm \hbar g$, but not a second one! In this regime, we cannot neglect that the Rabi frequency depends on the photon number n. The second pair of states is at $2\omega_0 \pm \sqrt{2}\hbar g$, i.e., not at twice the energy of the first pair. Absorbing the first photon blocks this transition for any further absorption.

An example of an experimental realization is shown in Fig. 8.2. The authors used a InAs quantum dot embedded in a GaAs matrix, which behaves similarly to a two-level system at 930 nm wavelength. The cavity was a photonic crystal: air holes in the GaAs membrane lead to a bandgap for photons at this wavelength. Defects in the form of missing or shifted holes lead to a cavity with a high quality factor $Q \approx 10^4$. A resonant, spectrally narrow but pulsed laser ($f_{\text{rep}} = 80$ MHz) is reflected at the cavity plus quantum dot. The authors try to find two photons that arrive at two detectors simultaneously, a coincidence. For a laser beam obeying Poisson statistics, the probability of finding two photons with delay τ is independent of τ. With a pulsed laser, you will only find coincidences with delays $\tau = n\,T = n/f_{\text{rep}}$. Ideally, for a photon blockaed one should find no coincidences at $\tau = 0$. Here the authors were able to show a drop of about 10% due to background effects.
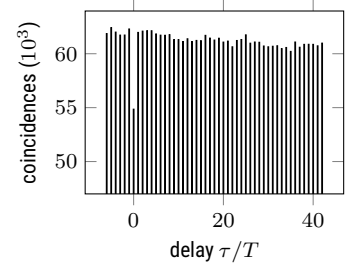

Figure 8.2: Photon blocked in the coincidence rate of a quantum dot in a cavity. Data from Faraon et al., 2008.

Test yourself

10. Draw a level scheme containing the uncoupled and the coupled states involved in Vacuum Rabi Splitting. Draw the absorption spectrum as seen by the first and by the second photon in the system.

Looking Back

In the last three chapters we discussed the coupling of systems in physics. After coupling, the original systems are gone. We can no longer say where an excitation is. New hybrid states emerge.

But is it justified to distinguish between systems according to classical physics, first or second quantization? After all, the correspondence principle holds, and we should be able to make the transition from quantum to classical by increasing some size parameter.

Test yourself

11. It is now up to you to revisit the examples given. How could we make the transition to classical physics? Which parameters do we have to change? Which effects would disappear? Which would remain and could be explained without quantum mechanics?

References

Faraon, Andrei et al. (2008). "Coherent generation of non-classical light on a chip via photon-induced tunnelling and blockade". In: *Nature Physics* 4.11, pp. 859–863. ⬀.

Fox, Mark (2007). *Quantum optics*. Oxford University Press.

Gerry, Christopher C. and Peter L. Knight (2005). *Introductory quantum optics*. Cambridge Univ. Press. ↗.

Haroche, Serge (2006). *Exploring the quantum. atoms, cavities and photons*. Oxford Univ. Press. ↗.

Rand, Stephen C. (2016). *Lectures on light. nonlinear and quantum optics using the density matrix*. Second edition. Oxford University Press. ↗.

Wrigge, G. et al. (2008). "Efficient coupling of photons to a single molecule and the observation of its resonance fluorescence". In: *Nature Physics* 4.1, pp. 60−66. ↗.

Chapter 9
Bloch Formalism [WIP]
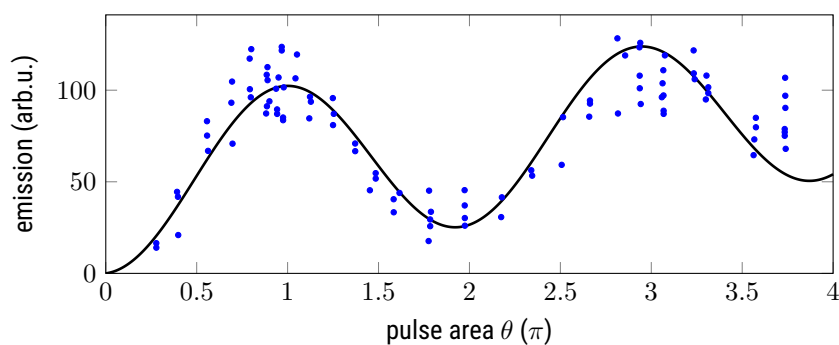
Markus Lippitz
November 7, 2025

Overview

Figure 9.1: Rabi oscillations in Rb atoms detected by fluorescence emission. The pulse area θ is proportional to the amplitude of the driving electric field. Data from Gibbs, 1973.

Many experimental realizations show Rabi oscillations. We will discuss them in terms of a two-level system interacting with an optical field, such as an atom in a vacuum or a molecule or quantum dot in a solid state at low temperature. But the same description applies to many other systems. In fact, a two-level system is equivalent to a spin $1/2$ system, such as an electron spin or a nuclear spin. So the same concepts are used in electron spin resonance or nuclear magnetic resonance experiments (ESR and NMR).

We shine a laser beam on an atom, a molecule, a quantum dot. The laser frequency is close to the optical transition. We measure the populations of the excited state, e.g. by fluorescence emission or tunneling of the electron out of this state. We turn on the laser for a given time t and measure the signal amplitude as a function of t. This somewhat indirect experiment is necessary because in many cases t is short compared to the emission or tunneling rate. Only in theory can we measure the population of the state as it evolves. We find periodic oscillations of the signal amplitude, the Rabi oscillations.[1]

[1] **Rabi1939**.

Density Matrix

We start by introducing the density matrix.[2] It is a tool in quantum mechanics

[2] Hamm, 2005; Parson, 2015; Rand, 2016.

to describe not only purely coherent states, but also statistical mixtures, as we will see below. The density matrix is a bit at the edge of the classical canon of quantum mechanics lectures.

When writing our wave function $|\psi\rangle$ in a basis $|n\rangle$ as

$$|\psi\rangle = \sum_n c_n \, |n\rangle \qquad (9.1)$$

then we can define a density operator $\hat\rho$ as

$$\hat\rho = |\psi\rangle \langle\psi| = \sum_{m,n} c_n c_m^\star \, |n\rangle \langle m| \qquad (9.2)$$

and the matrix elements of $\hat\rho$ are $\rho_{n,m} = c_n c_m^\star$ or

$$\rho = \begin{pmatrix} \rho_{00} & \rho_{01} \\ \rho_{10} & \rho_{11} \end{pmatrix} \quad . \qquad (9.3)$$

The density matrix allows to calculate the expectation value of any operator $\hat A$ as

$$\langle \hat A \rangle = \langle\psi|\hat A|\psi\rangle = \sum_{m,n} c_n c_m^\star \, A_{m,n} = \sum_{m,n} \rho_{n,m} \, A_{m,n} = Tr(A\rho) \quad , \qquad (9.4)$$

where the trace sums over the diagonal elements

$$Tr(U) = \sum_n U_{n,n} \quad . \qquad (9.5)$$

The trace of the density matrix is one for normalized states

$$Tr(\rho) = \sum_n \rho_{n,n} = \sum_n c_n c_n^\star = 1 \quad \text{if normalized} \quad . \qquad (9.6)$$

The interesting thing comes when looking at pure and mixed states. Pure states are the 'conventional' states discussed in quantum mechanics, for example this superposition of states

$$|\psi\rangle = \sqrt{\frac{1}{2}} \, (|1\rangle + |2\rangle) \quad . \qquad (9.7)$$

In this example, the density matrix reads

$$\rho = \frac{1}{2} \begin{pmatrix} 1 & 1 \\ 1 & 1 \end{pmatrix} \qquad (9.8)$$

and its trace is one. But the density matrix also allows to describe new things, beyond pure states, namely statistical mixtures of states. We can describe an ensemble of two-level systems, of which half the ensemble is in state $|1\rangle$, the other half in state $|2\rangle$. This can *not* be written as $|1\rangle + |2\rangle$, but a density matrix description is possible. If the statistical probability of each pure state with density matrix ρ_i is p_i, then the density matrix of the mixed state is given by

$$\rho_{\text{mixed}} = \sum_i p_i \, \rho_i \quad . \qquad (9.9)$$

For a $50 : 50$ mixture of $|1\rangle$ and $|2\rangle$ we get

$$\rho = \frac{1}{2} \begin{pmatrix} 1 & 0 \\ 0 & 1 \end{pmatrix} \quad . \qquad (9.10)$$

We can distinguish between pure and mixed states by looking at the trace of the squared density matrix

$$Tr(\rho^2) \quad = \quad 1 \quad \text{pure state} \tag{9.11}$$
$$< \quad 1 \quad \text{mixed state.} \tag{9.12}$$

Mixed states can be used not only to describe an ensemble of systems in different states, but also to describe a single system that is in different states at different times. Even if we can do an experiment on a single quantum system, we have to repeat it very often to reduce the noise by averaging. But the experiment does not always follow the same path: either a photon is absorbed or not, but it will most likely not always be absorbed. The time average of such an experiment therefore needs a statistical mixture to describe it.

The diagonal elements of the density matrix describe the populations of the states, i.e. $|c_n|^2$. The off-diagonal elements describe coherence between states. 'Coherence' means 'constant phase relation' or 'possibility to interfere', as with coherent (laser) or incoherent (candle) light. When writing $|1\rangle + |2\rangle$ we have defined the phase between the states to be zero, as

$$r\,e^{i\phi} = \frac{c_1}{c_2} \quad \text{gives here} \quad \phi = 0 \quad . \tag{9.13}$$

In a statistical mixture there is no[3] coherence between the states, as one sub-ensemble is in one state, another in another state, and they don't know anything of each other.

[3] better: not enough

Test yourself

1. For which values of b is the following density matrix describing a pure state ?

$$\rho = \frac{1}{2} \begin{pmatrix} 1 + a & b^\star \\ b & 1 - a \end{pmatrix}$$

   where a is real and b could be complex.

2. Assume a normalized wave function $|\psi\rangle = c_1\,|1\rangle + c_2\,|2\rangle$. Calculate its density matrix and convince yourself that it describes a pure state.

3. Investigate the off-diagonal elements of a density matrix describing a $50 : 50$ mixture of $|1\rangle$ and $\sqrt{1/2}(|1\rangle + |2\rangle)$.

Liouville–von Neumann equation

We can construct a differential equation for the time evolution of the density matrix that is a direct analogue of the Schrödinger equation, just that is also takes mixed states into account.

The time-derivative of the density operator $\hat{\rho}$ is

$$\frac{d}{dt}\hat{\rho} = \frac{d}{dt}\left(|\psi\rangle\langle\psi|\right) = \left(\frac{d}{dt}|\psi\rangle\right)\langle\psi| + |\psi\rangle\left(\frac{d}{dt}\langle\psi|\right) \quad . \tag{9.14}$$

Making use of the Schrödinger equation

$$\frac{d}{dt}|\psi\rangle = -\frac{i}{\hbar}\,\hat{H}\,|\psi\rangle \tag{9.15}$$

we get the *Liouville–von Neumann equation*

$$\frac{d}{dt}\hat{\rho} = -\frac{i}{\hbar}\left[\hat{H},\hat{\rho}\right] \quad . \tag{9.16}$$

As an example, let us look at a two-level system with the eigen-energies $E_0 = 0$ and $E_1 = \hbar\omega_0$. The Hamilton operator is thus

$$H = \begin{pmatrix} 0 & 0 \\ 0 & \hbar\omega_0 \end{pmatrix} \quad . \tag{9.17}$$

The commutator becomes

$$\left[\hat{H},\hat{\rho}\right] = \begin{pmatrix} 0 & -\hbar\omega_0\,\rho_{01} \\ \hbar\omega_0\,\rho_{10} & 0 \end{pmatrix} \quad . \tag{9.18}$$

The diagonal elements of the density matrix ρ, i.e., the populations, remain thus constant in time, as expected for this Hamiltonian. The off-diagonal elements, the coherences acquire a phase-factor proportional to the energy difference, i.e.

$$\rho_{01}(t) = \rho_{01}(0)\,\exp\left(i\,\omega_0\,t\right) \quad . \tag{9.19}$$

Test yourself

4. Derive eqs. 9.18 and 9.19.

Optical Bloch Equations

Now we switch on light and add an interaction Hamiltonian $\hat{H}_I = -\boldsymbol{\mu}\,\boldsymbol{E}$ with the dipole operator $\boldsymbol{\mu}$ and the optical field $\boldsymbol{E}$. In total, the Hamilton operator reads[4]

$$\hat{H} = \begin{pmatrix} 0 & -\boldsymbol{\mu}\,\boldsymbol{E} \\ -\boldsymbol{\mu}^{\star}\,\boldsymbol{E}^{\star} & \hbar\omega_0 \end{pmatrix} \quad . \tag{9.20}$$

[4] Rand, 2016, chap. 3.8.

The differential equations for the density matrix become the *Bloch equations*

$$\dot{\rho}_{00} = -\frac{i}{\hbar}\left(\rho_{01}\boldsymbol{\mu}^{\star}\,\boldsymbol{E}^{\star} - \rho_{10}\boldsymbol{\mu}\,\boldsymbol{E}\right) \tag{9.21}$$

$$\dot{\rho}_{11} = -\frac{i}{\hbar}\left(\rho_{10}\boldsymbol{\mu}\,\boldsymbol{E} - \rho_{01}\boldsymbol{\mu}^{\star}\,\boldsymbol{E}^{\star}\right) \tag{9.22}$$

$$\dot{\rho}_{01} = -\frac{i}{\hbar}\left(-\rho_{01}\hbar\omega_0 + (\rho_{00} - \rho_{11})\boldsymbol{\mu}\,\boldsymbol{E}\right) \tag{9.23}$$

$$\dot{\rho}_{10} = -\frac{i}{\hbar}\left(+\rho_{10}\hbar\omega_0 + (\rho_{11} - \rho_{00})\boldsymbol{\mu}^{\star}\,\boldsymbol{E}^{\star}\right) \tag{9.24}$$

These are effectively only 3 differential equations, as the wave function has to stay normalized, i.e., $\rho_{00} + \rho_{11} = 1$. We can simplify things by skipping some algebraic transformations and introducing the *Bloch vector $\boldsymbol{S}$* with

$$\boldsymbol{S} = \begin{pmatrix} u \\ v \\ w \end{pmatrix} = \begin{pmatrix} \rho_{01} + \rho_{10} \\ i(\rho_{01} - \rho_{10}) \\ \rho_{00} - \rho_{11} \end{pmatrix} = \begin{pmatrix} 2\Re(\rho_{01}) \\ 2\Im(\rho_{01}) \\ \rho_{00} - \rho_{11} \end{pmatrix} \quad . \tag{9.25}$$

The density matrix elements are recovered by

$$\rho = \frac{1}{2}\begin{pmatrix} 1 + w & u - iv \\ u + iv & 1 - w \end{pmatrix} \tag{9.26}$$

With this we can write the system of differential equation as

$$\dot{\boldsymbol{S}} = \boldsymbol{M} \times \boldsymbol{S} \quad \text{with} \quad \boldsymbol{M} = \begin{pmatrix} -\frac{2}{\hbar}\,\Re(\boldsymbol{\mu}\,\boldsymbol{E}) \\ -\frac{2}{\hbar}\,\Im(\boldsymbol{\mu}\,\boldsymbol{E}) \\ \omega_0 \end{pmatrix} \quad . \tag{9.27}$$

The time evolution of the Bloch vector, and by this of the density matrix, can be described by the action of a torque vector $\boldsymbol{M}$.

These equations were derived by Felix Bloch for the magnetization of an ensemble of atomic nuclei in an NMR experiment. For nuclear or electronic (ESR) magnetic moments, the vector corresponds to the direction of the ensemble average of the magnetization, i.e. it is a real-space vector in the laboratory frame. In our case, $\boldsymbol{S}$ is a vector in an abstract 3d vector space describing the density matrix of an ensemble of two-level systems. So I use uvw instead of xyz, but the physics is the same. Also spin-1/2 systems like electron spins or nuclear spins in ESR and NMR experiments form a two-level system.

Without optical field, the Bloch vector rotates around its w axis, as seen in the phase oscillation of the coherences in the last section. With optical field, also the populations changes, and things become complicated. To simplify things, we assume that our optical field is a single mode with a slowly varying amplitude only, i.e.

$$\boldsymbol{E}(t) = \boldsymbol{x}\,E_0(t)\left(e^{i\omega_L t} + e^{-i\omega_L t}\right) \quad . \tag{9.28}$$

The time-dependence of $E_0(t)$ should be slow compared to ω_L. This is the slowly varying amplitude approximation (SVEA). We do the same with the off-diagonal elements of the density matrix

$$\rho'_{01} = \rho_{01}\,e^{-i\omega_L t} \quad \text{and} \quad \rho'_{10} = \rho_{10}\,e^{+i\omega_L t} = \rho'^{\star}_{01} \quad . \tag{9.29}$$

We thus factor out a phase oscillation with the laser frequency and keep only the slowly varying rest.[5] Inspecting the differential equations for the density matrix, this leads together with our definition of $\boldsymbol{E}$ to the following modifications

[5] The diagonal elements do not phase-rotate and remain unchanged.

$$\omega_0 \rightarrow \omega_0 - \omega_L \quad \text{and} \quad \boldsymbol{\mu}\,\boldsymbol{E} \rightarrow \mu\,E_0\left(1 + e^{i2\omega_L t}\right) \approx \mu\,E_0 \quad . \tag{9.30}$$

As we assumed the elements of ρ' to vary slowly, we neglect the term $\exp(i2\omega_L t)$, as it will average out. This is the rotating wave approximation (RWA). Effectively, we are going into a rotating frame. Our new coordinate system rotates around the w axis with the angular frequency of the laser ω_L. The optical frequency of the transition ω_0 is close to this laser frequency. We neglect terms of $\omega_0 + \omega_L$ and only keep terms of $\omega_0 - \omega_L$. In total we get[6]

[6] someone should check this!

$$\dot{\boldsymbol{S}}' = \boldsymbol{M}' \times \boldsymbol{S}' \quad \text{with} \quad \boldsymbol{M}' = \begin{pmatrix} -\mu E_0(t)/\hbar \\ 0 \\ \omega_0 - \omega_L \end{pmatrix} = \begin{pmatrix} -\Omega \\ 0 \\ \omega_0 - \omega_L \end{pmatrix} \tag{9.31}$$

with the (angular) Rabi frequency[7] $\hbar\Omega = \mu E_0(t)$ and $\mu = \boldsymbol{\mu}\,\boldsymbol{x}$ the projection of the transition dipole moment on the polarization direction of the light field. In the following, we stay in the rotating frame and leave out the prime symbols.

[7] Some definitions include a factor of 2 here, which is connected to the definiton of the electric field E.

Test yourself

5. Derive the Bloch equations 9.21 to 9.24 from the Hamilton operator eq. 9.20 and
    the Liouville-von Neumann equation.

Rabi Oscillations

Let us discuss the time evolution of the Bloch vector in the rotating frame.
Applying only a torque M, the length of the Bloch vector does not change.
It moves along the surface of a sphere, the *Bloch sphere*. The sphere has
a diameter of one when the density matrix describes a normalized pure
state. For mixed states, the Bloch vector is shorter. Below we will see how
dephasing and relaxation processes reduce the length of the Bloch vector.

A two-level system in the ground state is on the north pole of the sphere.
The state $|0\rangle + |1\rangle$ is on the equator, pointing along the u axis. All points
except the poles contain a coherence between the two levels.

The torque M rotates the Bloch vector around M with a angular fre-
quency $|M|$. A resonant laser field, i.e., $\omega_L = \omega_0$ rotates the Bloch vector
around the u axis. When this field acts continuously, the Bloch vector moves
from the north pole via the equator to the south pole and back to the north
pole and so on. The population of the state changes periodically from zero to
one:

$$\rho_{00} = \cos(\Omega t/2)^2 \quad . \tag{9.32}$$

These are the *Rabi oscillations*. In a laser pulse, the amplitude $E_0(t)$ of the
optical field varies, for example like a Gaussian. In this case, the instanta-
neous Rabi frequency Ω also varies and it is convenient to quantify the total
effect of a single pulse by the *pulse area* θ

$$\theta = \int_{pulse} \Omega(t)\, dt \quad . \tag{9.33}$$

A π pulse, acting on a system in the ground state, will thus lead to a system
in the excited state. A 2π pulse leaves the populations unchanged.[8]

When the laser is not fully resonant, the Bloch vector is rotated around an
axis in the u-w plane. Starting from the ground state at the north pole, it thus
does not reach the south pole anymore. The population of the excited state
will not reach one. At the same time, the phase oscillations of the two-level
system are not fully taken care of by the rotating frame anymore. A little bit
of rotation remains. In combination, this gives a complicated precession of
the Bloch vector S around the torque M with an effective Rabi frequency

$$\Omega_{\text{eff}} = \sqrt{\Omega^2 + (\omega_0 - \omega_L)^2} \quad . \tag{9.34}$$

We can observe these oscillations by any method that can determine the
population of the excited state, for example fluorescence emission, electron
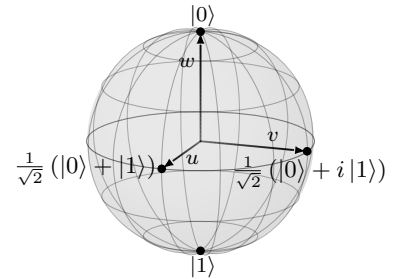emission or (transient) absorption.

Figure 9.2: Some Bloch vectors and their positions on the Bloch sphere.

[8] but has an effect on the phase

Figure 9.3: Rabi oscillations

Test yourself

6. Re-visit questions 1–3 from above and discuss the density matrix on the Bloch
    sphere.
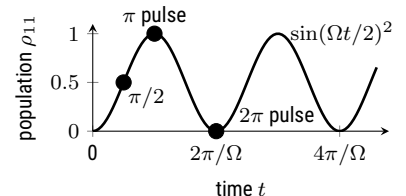
7. Write a computer program to calculate the trajectory of the Bloch vector in the rotating wave approximation, eq. 9.31. Use

$$\boldsymbol{S}'(t + \Delta t) \approx \boldsymbol{S}'(t) + \Delta t\, \boldsymbol{M}' \times \boldsymbol{S}'(t)$$

with a small enough Δt. The approximation holds when $|\boldsymbol{S}'(t)|$ remains close to one. Plot $\boldsymbol{S}'(t)$ in 3D on the Bloch sphere (Fig.9.2) and in 2D as function of time.

Damping and dephasing

In reality, both a coherence as well as the population of an excited state decays in the course of time. Without going into further detail, we can add these processes phenomenologically as Lindblad operator $\boldsymbol{L}$ to the Liouville-von Neumann equation

$$i\hbar\dot{\hat{\rho}} = [\hat{H}, \hat{\rho}] - \boldsymbol{L}\hat{\rho} \quad . \tag{9.35}$$

Excited state populations decay exponentially with a lifetime T_1. The coherence between two states decays with a time constant T_2 with

$$\frac{1}{T_2} = \frac{1}{T_2^\star} + \frac{1}{2\,T_1} \quad , \tag{9.36}$$

where $T_2^\star$ is called pure dephasing time. The T_1 time enters, as a decaying population also removes coherence. The prefactor of 2 is a consequence of effective spin-$1/2$-system. On the Bloch sphere, these processes let the Bloch vector move back to the north pole, but not along the surface of the sphere but with varying length of the vector.[9]

[9] In the original work of Bloch this scheme was applied to the magnetization of a spin-$1/2$ system which decays towards the center of the sphere, as thermal energy leads to almost equal population of both states.

References

Gibbs, Hyatt M (1973). "Incoherent resonance fluorescence from a Rb atomic beam excited by a short coherent optical pulse". In: *Phys. Rev. A* 8.1, p. 446. ⬀.

Hamm, Peter (2005). *Principles of Nonlinear Optical Spectroscopy: A Practical Approach or: Mukamel for Dummies*. ⬀.

Parson, William W. (2015). *Modern optical spectroscopy*. Springer. ⬀.

Rand, Stephen C. (2016). *Lectures on light. nonlinear and quantum optics using the density matrix*. Second edition. Oxford University Press. ⬀.

Part III

Example: All Together

Chapter 10
Lattice of plasmonic particles

Markus Lippitz
December 1, 2023

Overview

Now we combine everything. We have three ingredients: the plasmonic resonance of a small silver particle, a periodic arrangement of these particles in a two-dimensional lattice, and the narrow optical resonance of the TDBC dye. The particles hybridized with each other, combining the plasmon hybridization of Chapter 6 with lattice modes, as in a chain of masses and in solid-state physics in general. As we will see below, this results in an X-shaped dispersion relation, which we measure using Fourier optics.

In a second step, this lattice plasmon mode hybridizes with the optical transition of the dye, leading to characteristic anti-crossing features in the dispersion relation, where the X crosses the horizontal dye dispersion. Microscopically, we can model the influence of the dye by taking into account the refractive index of the medium.

This chapter is based on the master thesis of Simon Durst[1]. All figures are taken from his thesis, sometimes slightly modified.
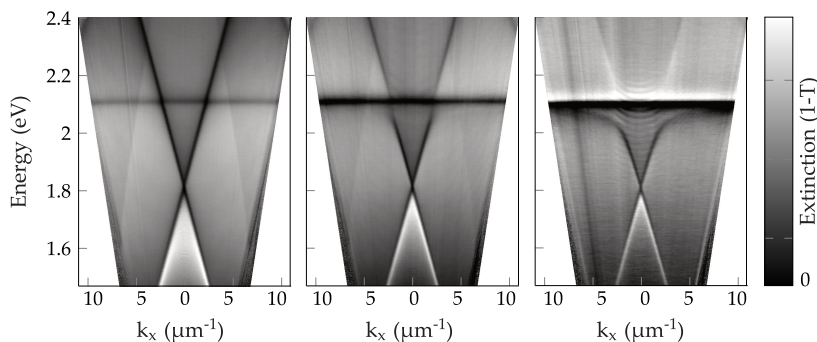
[1] Durst, 2021.

Figure 10.1: Dispersion relation of a lattice plasmon hybridized (X-shaped) with a dye (horizontal), for different concentrations of the dye (left to right: 1, 10, 60 weight %). The grey scale gives the extinction.

How this is measured

The samples consist of a rectangular lattice of silver particles on a glass substrate. It is fabricated by electron beam lithography. An electron sensi-

tive resist is exposed in a (slightly modified) electron microscope and then developed. At the exposed areas, the glass surface is accessible. The unexposed areas are still covered by the resist. A gold or silver film is deposited by thermal evaporation. When the resist is chemically removed, it takes with it the metal film on the unexposed areas. The metal remains only where it adheres directly to the glass surface. In this way, arbitrary two-dimensional structures can be fabricated with a resolution limited by the electron beam to about 50–80 nm in our case.

We have chosen a particle size of 80×80 nm. The lattice constant p_y is always 200 nm, p_x varies (see below). The lattice is coated with a polymer film containing the TDBC dye in variable concentration. Everything is covered with immersion oil ($n = 1.5$) and a second glass substrate, so that the particles are embedded in a homogeneous dielectric environment.

For a dispersion relation we need an energy E and a wave vector k. Since the sample is only two-dimensional, this is an in-plane wave vector, which we have chosen to be along the x-direction, i.e. k_x. The signal measured as the function of E and k_x is the transmission T or the extinction[2] $1 - T$. We measure transmission spectra for white light as a function of angle of incidence. Electron beam lithography results in a finite size lattice of 30×30 µm. It is difficult to keep the sample in the beam when rotating either the sample or the beam. So we keep everything fixed and measure all the angles at the same time. To do this, we illuminate the sample with a light cone with a large aperture angle (NA = 0.9, max. angle = $64°$). The transmitted light is collected by a second microscope objective. Fourier optics tells us that the front focal plane is Fourier transformed into the back focal plane. We can no longer use a small angle of incidence, but an ideal imaging system must satisfy the Abbé-Sine condition that rays of equal angle of incidence θ intersect at the same point at a height h with

$$h = f \sin \theta \quad .$$

(10.1)

We image this back-focal plane (BFP) on the entrance slit of a spectrometer and thus get an image on the CCD camera which in one direction is angle of incidence, in the other wavelength of the light beam. This is converted into a E-k_x scale. As the maximum angle is fixed, but $k \propto E$, we observable region of the dispersion relation has a trapezoidal shape, i.e, the maximum value of k_x is lower at lower energy. The light beam is polarized before the sample such that we image the s polarization on the entrance slit of the spectrometer, i.e. along the x-direction of the sample coordinate system.
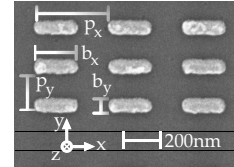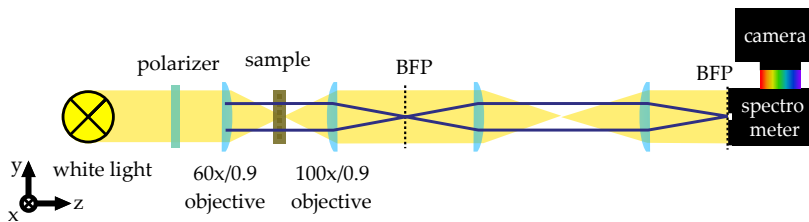

Figure 10.2: SEM micrograph of gold nanorods in a lattice. Indicated are the dimensions of the rods and the lattice constants.

[2] In this sample, not only absorption but also scattering leads to a reduced transmission. Therefore, we call it extinction and not absorption.
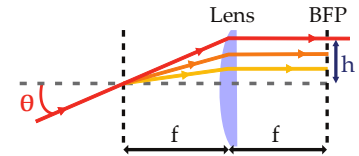

Figure 10.3: The back focal plane sorts rays by their angle in the front focal plane.

Figure 10.4: Setup to measure angle-dependent transmission spectra without moving parts.

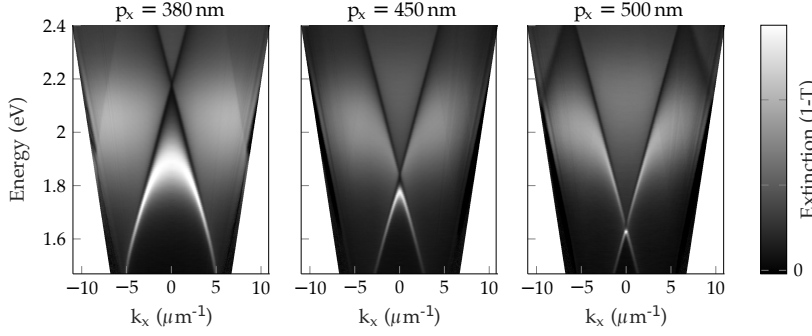## How to understand the dispersion relation (without dye)

Each panel in Fig. 10.5 shows a dispersion relation, i.e., the relation between (in-plane) momentum and energy. Two features combine: the particle plasmon resonance and a lattice resonance. The particle resonance is at a given eigen-frequency (or energy), spectrally rather broad, and independent of the angle of incidence or k_x, as the particles are rather spherical. This gives the broad, medium gray band around an energy of 2 eV. The second feature is the lattice resonance. An optical wave travels parallel to the interface. Its dispersion relation is

$$E = \hbar c_0 \ (k_x + m \cdot G) \tag{10.2}$$

where $G = 2\pi/p_x$ is the fundamental reciprocal lattice vector and m an integer. This results in the X-shaped feature for $m = \pm 1$. With varying p_x the crossing point, i.e., the energy E at $k_x = 0$ varies, as

$$E(k_x = 0) = m\frac{hc_0}{p_x} \quad . \tag{10.3}$$

In the right-most panel of Fig. 10.5 we see the second order $m = \pm 2$.

The eigenmode of the lattice resonance is spatially extended over the whole lattice and spectrally narrow. The interaction of a broad (particle) and a narrow (lattice) resonance leads to characteristic spectral features that are visible in Fig. 10.5 and could be described as Fano resonance[3]. But that is beyond the scope of this chapter. Here we follow a more microscopic approach. We calculate the extinction spectrum of an arrangement of many small particles at positions $\mathbf{r}_i$. Each particle is modelled as sphere with a polarizability α_i given by the material properties and the volume of the small particle.

[3] Ugo Fano, 1912–2001

Radiating electric dipole

Let us first look at a single electric dipole $\boldsymbol{\mu}$ at the position $\mathbf{r}_0$. Its field at the position $\mathbf{r}$ is given by[4]

[4] Novotny and Hecht, 2012, eq. 8.52.

$$\mathbf{E}(\mathbf{r}) = \frac{k^2}{\epsilon_0 \ \epsilon_{out}} \ \mathbf{G}(\mathbf{r}, \mathbf{r}_0) \ \boldsymbol{\mu} \tag{10.4}$$

with the length k of the wave vector in the medium of dielectric function ϵ_{out}. The Greens function $\mathbf{G}$ is given by[5]

[5] This follows Novotny and Hecht, 2012 eq. 8.55 and differs by $4\pi k^2$ from eq. 2 in Yurkin and Hoekstra, 2007

$$\mathbf{G}(\mathbf{r}, \mathbf{r}_0) = \frac{e^{ikR}}{4\pi \, k^2 \, R^3} \left[\left(k^2 R^2 + ikR - 1 \right) \mathbf{1} + \left(3 - 3ikR - k^2 R^2 \right) \frac{\mathbf{RR}}{R^2} \right]$$

(10.5)

with $\mathbf{R} = \mathbf{r} - \mathbf{r}_0$, $R = |\mathbf{R}|$, $\mathbf{1}$ the unity 3×3-tensor, and $\mathbf{RR}$ the outer product of $\mathbf{R}$ with itself, i.e.

$$\mathbf{RR} = \begin{pmatrix} R_x R_x & R_x R_y & R_x R_z \\ R_y R_x & R_y R_y & R_y R_z \\ R_z R_x & R_z R_y & R_z R_z \end{pmatrix} \quad .$$

(10.6)

This is a convenient method to describe the full vectorial field emitted by a dipole at position $\mathbf{r}_0$ everywhere in space, including both near- and far-field components.

Test yourself

1. Convince yourself that eq. 10.5 agrees with the other commonly used form

$$\mathbf{E} = \frac{e^{i\,kr}}{4\pi\epsilon_0 \, \epsilon_{out}} \frac{1}{r^3} \left\{ (kr)^2 \, (\hat{\mathbf{r}} \times \boldsymbol{\mu}) \times \hat{\mathbf{r}} + (1 - ikr) \, (3\hat{\mathbf{r}} \, [\hat{\mathbf{r}} \cdot \boldsymbol{\mu}] - \boldsymbol{\mu}) \right\} \quad .$$

(10.7)

Scattering sphere

We need to know the oscillation amplitude of the emitting dipole $\mathbf{p}$ to use eq. 10.5. As in chapter 7, it is related by the polarizability α to the incoming optical field $\mathbf{E}_{inc}$

$$\mathbf{p} = \epsilon_0 \, \epsilon_{out} \, \alpha \, \mathbf{E}_{inc}$$

(10.8)

with the dielectric function ϵ_{out} of the embedding medium. When we assume that the scattering nanoobject is a sphere, we can calculate

$$\alpha = 3V \, \frac{\epsilon_{in} - \epsilon_{out}}{\epsilon_{in} + 2\epsilon_{out}} \quad ,$$

(10.9)

where V is the volume of the sphere and ϵ_{in} the dielectric function of it. The sphere radiates a scattered field $\mathbf{E}_S$

$$\mathbf{E}_S(\mathbf{r}) = \frac{k^2}{\epsilon_0 \, \epsilon_{out}} \, \mathbf{G}(\mathbf{r}, \mathbf{r}_0) \, \mathbf{p}$$

(10.10)

$$= \frac{1}{4\pi \, \epsilon_0 \, \epsilon_{out}} \frac{e^{ikR}}{R^3} \, [\dots] \, \mathbf{p}$$

(10.11)

where the contents of the square brackets is the same as in eq.10.5 above. k is again the length of the wave vector in a medium with dielectric function ϵ_{out}.

Multiple particles

When we have more than one particle, each particle i sees the incident field $\mathbf{E}_{i,inc}$ at the position $\mathbf{r}_i$ plus the sum over all scattered fields $\mathbf{E}_{j,S}$ from all the other induced dipoles j

$$\mathbf{E}_{i,loc} = \mathbf{E}_{i,inc} + \sum_{j \neq i} \mathbf{E}_{j,S} = \mathbf{E}_0 \, e^{i\mathbf{k}\cdot\mathbf{r}_i} + \sum_{j \neq i} \frac{k^2}{\epsilon_0 \, \epsilon_{out}} \mathbf{G}(\mathbf{r}_i, \mathbf{r}_j) \, \mathbf{p}_j$$

(10.12)

with the dipole moment $\mathbf{p}_j$ of the particle at position $\mathbf{r}_j$. The position of the 'receiving' particle $\mathbf{r}_i$ takes the role of $\mathbf{r}$ in the Greens function; the position of the scattering particle $\mathbf{r}_j$ takes the role of the dipole at position $\mathbf{r}_0$ above.

The local field $\mathbf{E}_{i,loc}$ then induces a dipole moment again

$$\mathbf{p}_i = \epsilon_0 \, \epsilon_{out} \, \alpha_i \, \mathbf{E}_{i,loc} \quad . \tag{10.13}$$

Both equations together form a coupled equation system for the dipole moments $\mathbf{p}_i$

$$\mathbf{E}_0 \, e^{i\mathbf{k}\cdot\mathbf{r}_i} = \frac{1}{\epsilon_0\epsilon_{out}\alpha_i} \, \mathbf{p}_i \, - \sum_{j \neq i} \frac{k^2}{\epsilon_0 \, \epsilon_{out}} \mathbf{G}(\mathbf{r}_i, \mathbf{r}_j) \, \mathbf{p}_j \tag{10.14}$$

which can be written as

$$\mathbf{E}_{inc} = \mathbf{A} \, \mathbf{p} \quad , \tag{10.15}$$

where $\mathbf{p}$ and $\mathbf{E}_{inc}$ are column vectors containing the induced dipole moment and the incident field of all dipoles and $\mathbf{A}$ is an interaction matrix. Its elements are 3×3-sub-matrices given by[6]

$$\mathbf{A}_{ii} = \frac{1}{\epsilon_0\epsilon_{out}\alpha_i} \, \mathbf{1} \tag{10.16}$$

$$\mathbf{A}_{ij} = - \, \frac{k^2}{\epsilon_0 \, \epsilon_{out}} \mathbf{G}(\mathbf{r}_i, \mathbf{r}_j) \quad . \tag{10.17}$$

[6] This assume an isotropic polarizability. Otherwise, the diagonal elements should be $1/\alpha_{x,y,z}$ instead of $\mathbf{1}/\alpha$.

Some publications put the minus sign of the last equation into the Greens function.

The extinction cross-section can be calculated by the optical theorem from the interference of the forward-scattered wave with the incident wave. We get[7]

[7] Draine, 1988; Yurkin and Hoekstra, 2007.

$$\sigma_{ext} = \frac{k}{\epsilon_0\epsilon_{out} \, |\mathbf{E}_{inc}|^2} \, \sum_i \Im(\mathbf{p}_i \cdot \mathbf{E}_{i,inc}^{\star}) \quad . \tag{10.18}$$

The term $\Im(\mathbf{p} \cdot \mathbf{E}_{inc}^{\star})$ is very similar to the term for absorption, in which not the incident field $\mathbf{E}_{inc}$ but the local field $\mathbf{E}_{loc}$ would be used.

With this we have now everything at hand to calculate the extinction spectra of arrangements of small scattering spheres or dipoles. We solve eq. 10.15 for $\mathbf{p}$ and then calculate the cross-section. Depending on the community (and the distance between the dipoles) this is called discrete dipole approximation (DDA) or coupled dipole approximate (CDA).

Test yourself

2. Which size / dimension have $\mathbf{A}$ and $\mathbf{p}$ in eq. 10.15 ?

3. Sketch the interaction matrix $\mathbf{A}$ and its components.

Lattice sum

Things become easier when we are interested in infinite lattices of identical scatterers. As we are on a lattice, all lattice points are equal, especially in the amplitude and vectorial direction $\hat{\mathbf{n}}$ of the local field. It is then convenient to re-arrange eq. 10.12

$$\mathbf{E}_{i,loc} = \mathbf{E}_0 \, e^{i\mathbf{k}\cdot\mathbf{r}_i} \, + \sum_{j \neq i} k^2 \, \mathbf{G}(\mathbf{r}_i, \mathbf{r}_j) \, \alpha \, \mathbf{E}_{j,loc} \tag{10.19}$$

to

$$E_{i,loc}\, e^{-i\mathbf{k}\cdot\mathbf{r}_i} = \hat{\mathbf{n}} \cdot \mathbf{E}_0 + \sum_{j\neq i} k^2\, \hat{\mathbf{n}}\mathbf{G}(\mathbf{r}_i,\mathbf{r}_j)\hat{\mathbf{n}}\, \alpha\, E_{j,loc}\, e^{-i\mathbf{k}\cdot\mathbf{r}_i} \qquad (10.20)$$

so that we get

$$\hat{\mathbf{n}} \cdot \mathbf{E}_0 = E_{loc}\left(1 - \alpha \sum_{j\neq i} k^2\, \hat{\mathbf{n}}\mathbf{G}(\mathbf{r}_i,\mathbf{r}_j)\hat{\mathbf{n}}\; e^{i\mathbf{k}\cdot(\mathbf{r}_i-\mathbf{r}_j)}\right) = E_{loc}\,(1 - \alpha\, S) \qquad (10.21)$$

with the retarded lattice sum S. The induced dipole moment becomes

$$\mathbf{p} = \epsilon_0\, \epsilon_{out}\, \alpha\, \mathbf{E}_{loc} = \epsilon_0\, \epsilon_{out}\, \frac{\alpha}{1 - \alpha\, S}\, \mathbf{E}_0 \qquad (10.22)$$

or we define an effective (lattice) polarizability

$$\alpha_{\mathsf{lattice}} = \frac{\alpha}{1 - \alpha\, S} \quad . \qquad (10.23)$$

The extinction cross-section then becomes[8]

$$\sigma_{ext} = k\, \Im(\alpha_{\mathsf{lattice}}) \quad . \qquad (10.24)$$

The simulated dispersion relations agree well with the measured ones, as Fig.10.6 shows.

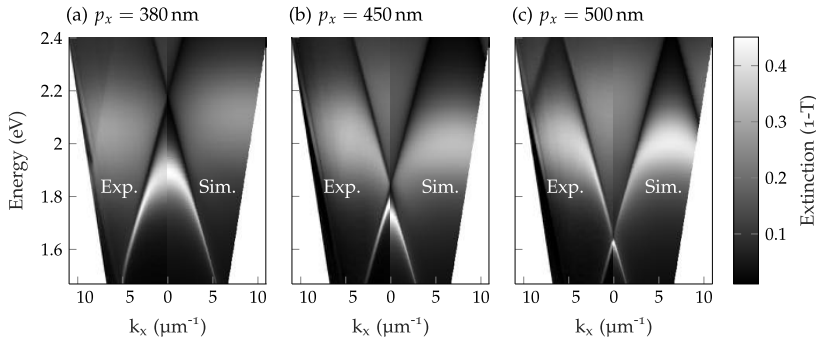(a) $p_x = 380\,\mathrm{nm}$ (b) $p_x = 450\,\mathrm{nm}$ (c) $p_x = 500\,\mathrm{nm}$

Figure 10.6: Simulations compared to experiment.

Coupling to a dye

Now that we have described the dispersion relation of the plasmonic lattice, we also include the TDBC dye. The dye molecules are embedded in the polymer film on top of the sample. The film covers the plasmonic particles and the area between them. The thickness of the film was chosen to be about 50 nm, roughly the height of the plasmonic nanostructure. The plasmonic near-fields are concentrated in a region of a few 10 nanometers around the particle. A film that is too thick would contain many dye molecules that are too far away to interact with the lattice plasmon.

The dye film leads to strong absorption around an energy $E \approx 2.1$ eV that is independent of the in-plane wave vector k_x. To better visualize the effect of the plasmon-dye coupling, we subtract the extinction of a dye film without plasmonic particles. This is shown in the figure 10.1 at the beginning of this

chapter. We see a reduced absorption at the dye resonance energy, i.e. a dark horizontal line in the dispersion plot. In the 'particle plus dye' sample, we have less dye because some volume is taken up by the particle. This effect reverses the sign of the dye feature at 2.1 eV.

Apart from the sign of the dye feature, we observe that the lattice plasmon feature changes from an X shape. When the lattice plasmon crosses the dye resonance, the lattice resonance bends away. This bending can be observed especially at the highest dye concentration (right panel). At higher energies, the lattice plasmon feature continues unperturbed.

We can model the coupling between the lattice plasmon and the dye using the usual coupled oscillator approach. The uncoupled oscillators have the eigenenergies

$$E_{\text{dye}} = \text{const.} \tag{10.25}$$

$$E_{\text{LP}}(k_x) = \hbar \ (k_x + m \cdot G) \quad . \tag{10.26}$$

With the coupling energy J we have to diagonalize the matrix

$$\begin{pmatrix} E_{\text{dye}} & J \\ J & E_{\text{LP}}(k_x) \end{pmatrix} \tag{10.27}$$

and get

$$E_{\pm} = \frac{E_{\text{dye}} + E_{\text{LP}}(k_x)}{2} \pm \sqrt{\left(\frac{E_{\text{dye}} - E_{\text{LP}}(k_x)}{2}\right)^2 + J^2} \quad . \tag{10.28}$$

This model for E_- is superimposed on the measured data in Fig.10.7. The blue symbols mark the minima of the extinction spectra at a given value of k_x to indicate the dispersion of the coupled mode.[9] Both agree well. We find coupling energies of 10, 40, and 86 meV, respectively.

[9] In a Fano resonance, the position of the resonance is close to, but not always at, the minimum, which is ignored here.
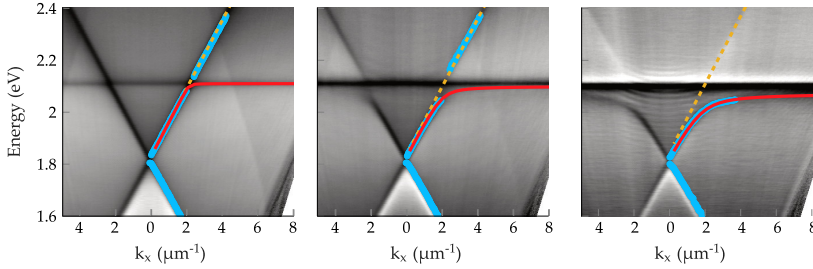

Figure 10.7: Anticrossing of lattice plasmon and dye. The data is a zoomed version of Fig.10.1. Superimposed are the lattice dispersion (green), the minima of the spectra (blue) and the coupled oscillator model (red).

Dielectric model

The model discussed above is fine, but we could look at this experiment from a completely different direction. We ignore all quantum mechanics, two-level systems, and coupling, and use only Maxwell's equations. We consider the TDBC dye and its polymer matrix as a dielectric material surrounding the plasmonic lattice. We get its index of refraction from the absorption spectrum, related to the imaginary part of the refractive index of the film.

The extinction coefficient α describes how the intensity of a beam decreases as it travels through absorbing media.

$$I(x) = I_0 T = I_0 e^{-\alpha x} \tag{10.29}$$

with the transmission T. It is wavelength depended and connected to the imaginary part of the index of refraction

$$\alpha(\lambda) = \frac{4\pi n_2(\lambda)}{\lambda} \qquad (10.30)$$

All together we get with a film thickness d

$$n_2(\lambda) = -\frac{\lambda}{4\pi\, d} \log T \qquad (10.31)$$

So we can measure $n_2(\lambda)$ and calculate the real part n_1 by a Kramers-Kronig relation. Then we set the dielectric function of the embedding medium $\epsilon_{out} = (n_1 + in_2)^2$ and again use the formalism that led to eq. 10.24. Of course, ϵ_{out} now depends on the dye concentration. The result of this simulation is shown in figure 10.8. It is in good agreement with the data. The depth of the horizontal pure dye absorption line is not fully recovered, which means that the ratio of interacting to non-interacting dye molecules in the model is wrong, or the reference film in the experiment differs a bit from the film at the plasmonic array.

The upper branch of the coupled mode has more contrast, is better visible in the simulation than in the experiment. In is not that it does not bend in the experiment, is just seems to fade out.[10] This is not fully captured by the model, but the model also in general shows sharper features than the experiment.
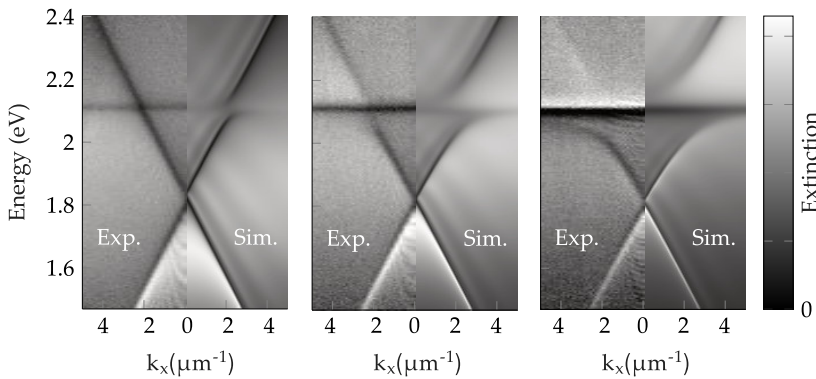
[10] See Wang et al., 2014 for an explanation.

Figure 10.8: The left half of each panel shows the same data as Fig. 10.1. The right half is calculated using the lattice sum and a wavelength dependent dielectric function describing the dye.

We do not need to use a coupling model to describe the bending of the lattice plasmon dispersion. Classical electrodynamics is good enough. The microscopic description of matter in terms of quantum mechanics and oscillating transition dipoles has to smoothly merge into the description of classical electrodynamics, as required by the correspondence principle.

References

Draine, B T (1988). "The discrete-dipole approximation and its application to interstellar graphite grains". In: *The Astrophysical Journal* 333, p. 848. ↗.

Durst, Simon (2021). "Excitonic Coupling to Surface Lattice Resonances : Experiment and Simulation". Bayreuth.

Novotny, Lukas and Bert Hecht (2012). *Principles of nano-optics*. 2. ed. Cambridge Univ. Press. ↗.

Wang, Wei et al. (2014). "Interplay between Strong Coupling and Radiative Damping of Excitons and Surface Plasmon Polaritons in Hybrid Nanostructures". In: *ACS Nano* 8.1, pp. 1056–1064. ⬀.

Yurkin, Maxim A and Alfons G Hoekstra (2007). "The discrete dipole approximation: an overview and recent developments". In: *Journal Of Quantitative Spectroscopy & Radiative Transfer* 106.1-3, pp. 558–589. ⬀.

Bibliography

Aizpurua, Javier and Rainer Hillenbrand (2012). "Localized Surface Plasmons: Basics and Applications in Field-Enhanced Spectroscopy". In: *Plasmonics*. Ed. by Stefan Enoch and Nicolas Bonod. Vol. 167. Springer series in optical sciences. ⬀.

Bohren, Craig F. and Donald R. Huffman (2007). *Absorption and Scattering of Light by Small Particles*. John Wiley & Sons, Ltd. ⬀.

Bransden, B. H. and C. J. Joachain (1996). *Physics of atoms and molecules*. Longman.

Butz, Tilman (2015). *Fourier Transformation for Pedestrians*. 2. ed. Springer. ⬀.

Cohen-Tannoudji, Claude, Bernard Diu, and Franck Laloë (1977). *Quantum Mechanics*. Wiley.

Czycholl, Gerd (2016). *Theoretische Festkörperphysik, Band 1*. 4. Aufl. Springer. ⬀.

Demtröder, Wolfgang (2013). *Molekülphysik. theoretische Grundlagen und experimentelle Methoden*. 2., überarb. und erw. Aufl. München: Oldenbourg, XVI, 487 S. ⬀.

Doicu, Adrian, Thomas Wriedt, and Yuri Eremin (2006). *Light Scattering by Systems of Particles-Null-Field Method with Discrete Sources-Theory and Programs*. Vol. 124. Springer series in optical sciences. Springer. ⬀.

Draine, B T (1988). "The discrete-dipole approximation and its application to interstellar graphite grains". In: *The Astrophysical Journal* 333, p. 848. ⬀.

Durst, Simon (2021). "Excitonic Coupling to Surface Lattice Resonances : Experiment and Simulation". Bayreuth.

Faraon, Andrei et al. (2008). "Coherent generation of non-classical light on a chip via photon-induced tunnelling and blockade". In: *Nature Physics* 4.11, pp. 859–863. ⬀.

Fox, Mark (2007). *Quantum optics*. Oxford University Press.

Friedrich, Thomas (2020). *Root-mean square parametrization*. ⬀.

Gerry, Christopher C. and Peter L. Knight (2005). *Introductory quantum optics*. Cambridge Univ. Press. ⬀.

Gibbs, Hyatt M (1973). "Incoherent resonance fluorescence from a Rb atomic beam excited by a short coherent optical pulse". In: *Phys. Rev. A* 8.1, p. 446. ⬀.

Gonser, Uli (1975). "From a strange effect to Mössbauer spectroscopy". In: *Mössbauer Spectroscopy*. Ed. by Uli Gonser. Topics in Applied Physics. Springer, pp. 1–50. ⬀.

Goodman, Joseph W. (2005). *Introduction to Fourier optics*. 3. ed. Roberts.

Hamm, Peter (2005). *Principles of Nonlinear Optical Spectroscopy: A Practical Approach or: Mukamel for Dummies*. ☑.

Haroche, Serge (2006). *Exploring the quantum. atoms, cavities and photons*. Oxford Univ. Press. ☑.

Horowitz, Paul and Winfield Hill (2015). *The art of electronics*. Third edition. New York, NY: Cambridge University Press.

Hunklinger, Siegfried (2014). *Festkörperphysik*. 4. aktualisierte Auflage. München: De Gruyter. ☑.

Jackson, John David (1999). *Classical electrodynamics*. 3. ed. New York [u.a.]: Wiley.

Johnson, Peter B and R.W. Christy (1972). "Optical constants of the noble metals". In: *Physical review B* 6.12, p. 4370. ☑.

Kalvius, Michael and Paul Kienle, eds. (2012). *The Rudolf Mössbauer Story*. Springer. ☑.

Klingelhöfer, G. et al. (2006). "Two earth years of Mössbauer studies of the surface of Mars with MIMOS II". In: *Hyperfine Interact.* 170.1-3, pp. 169–177. ☑.

Knapp, E.W. (1984). "Lineshapes of molecular aggregates, exchange narrowing and intersite correlation". In: *Chemical Physics* 85.1, pp. 73–82. ☑.

Köhler, Anna and Heinz Bässler (2015). *Electronic processes in organic semiconductors*. Weinheim: Wiley-VCH. ☑.

Moon, PB (1951). "Resonant nuclear scattering of gamma-rays: Theory and preliminary experiments". In: *Proceedings of the Physical Society. Section A* 64.1, p. 76. ☑.

Mössbauer, Rudolf L (1958a). "Kernresonanzabsorption von Gammastrahlung in Ir191". In: *Naturwissenschaften* 45.22, pp. 538–539. ☑.

– (1958b). "Kernresonanzfluoreszenz von Gammastrahlung in Ir191". In: *Zeitschrift für Physik* 151.2, pp. 124–143. ☑.

– (1961). "Recoilless nuclear resonance absorption". In: *Nobel Lecture*. ☑.

– (2000). "The discovery of the Mössbauer effect." In: *Hyperfine Interact.* 126. ☑.

Myroshnychenko, V et al. (2008). "Modelling the Optical Response of Gold Nanoparticles". In: *Chem. Soc. Rev.* 39.49. ☑.

Nolting, Wolfgang (2016). *Theoretical Physics 3 Electrodynamics*. Springer. ☑.

Novotny, Lukas and Bert Hecht (2012). *Principles of nano-optics*. 2. ed. Cambridge Univ. Press. ☑.

Parson, William W. (2015). *Modern optical spectroscopy*. Springer. ☑.

Potzel, W et al. (1992). "Gravitational redshift experiments with the high-resolution Mössbauer resonance in ^{67}Zn". In: *Hyperfine Interact.* 72. ☑.

Rand, Stephen C. (2016). *Lectures on light. nonlinear and quantum optics using the density matrix*. Second edition. Oxford University Press. ☑.

Renard, M. et al. (2004). "Pulse trains produced by phase-modulation of ultrashort optical pulses: tailoring and characterization". In: *Opt. Express* 12.3, pp. 473–482. ☑.

Saleh, Bahaa E. A. and Malvin C. Teich (1991). *Fundamentals of photonics*. New York, NY [u.a.]: Wiley. ☑.

Schatz, Günter, Alois Weidinger, and Manfred Deicher (2010). *Nukleare Fest-körperphysik*. 4., überarb. Aufl. Wiesbaden: Vieweg + Teubner.

Svensson, E. C., B. N. Brockhouse, and J. M. Rowe (1967). "Crystal dynamics of copper". In: *Physical Review* 155.3, p. 619. ⬀.

Träger, Frank, ed. (2012). *Springer Handbook of Lasers and Optics*. Berlin, Heidelberg: Springer. ⬀.

Valeur, Bernard and Mario Nuno Berberan-Santos (2012). *Molecular fluorescence*. 2. ed. Weinheim: Wiley-VCH. ⬀.

Wang, Wei et al. (2014). "Interplay between Strong Coupling and Radiative Damping of Excitons and Surface Plasmon Polaritons in Hybrid Nanostructures". In: *ACS Nano* 8.1, pp. 1056–1064. ⬀.

Wegener, Horst (1966). *Der Mössbauer-Effekt und seine Anwendungen in Physik und Chemie*. Mannheim: Bibliogr. Inst.

Wrigge, G. et al. (2008). "Efficient coupling of photons to a single molecule and the observation of its resonance fluorescence". In: *Nature Physics* 4.1, pp. 60–66. ⬀.

Yurkin, Maxim A and Alfons G Hoekstra (2007). "The discrete dipole approximation: an overview and recent developments". In: *Journal Of Quantitative Spectroscopy & Radiative Transfer* 106.1-3, pp. 558–589. ⬀.